DOCTORAL DISSERTATION

DIELECTRIC PHASE TRANSITIONS IN ROCHELLE SALT AND $SnCl_2(H_2O)_x(D_2O)_{2-x}$ AS STUDIED BY HIGH RESOLUTION HEAT CAPACITY MEASUREMENT

by

Masami TATSUMI

Department of Chemistry

Faculty of Science

Osaka University

1977

Doctoral Committee

Professor Syûzô Seki, Promoter

Professor Hideaki Chihara

Assistant Professor Hideko Kiriyama

Assistant Professor Hiroshi Suga

ACKNOWLEDGEMENTS

The author would like to express his sincere thanks to Professor Syûzô Seki and Assistant Professor Hiroshi Suga for introducing him to this field of study and for giving valuable suggestions in the course of this study. He also wishes to thank to Dr. Takasuke Matsuo for continuing guidance and encouragement as well as for his help in experiments throughout the course of this work. The auther is deeply indebted to Professor Wong for introducing him to the study of Raman scattering and for his help in analysis of Raman spectra. His gratitude is also rendered to Mr. Mitsuo Ohama for his assistance in taking Raman spectra. The author wishes to express his sincere thanks to Miss Keiko Ueda for excellent typewriting this thesis. Thanks are also extended to fellows of the Seki Laboratory for their assistance in preparing this manuscript. The author is deeply indebted to his wife Junko Tatsumi for her kind encouragement as well as for her assistance throughout the course of this work.

ABSTRACT

The heat capacity measurements of two hydrogen-bonded dielectrics, Rochelle salt and stannous chloride dihydrate [$SnCl_2(H_2O)_x(D_2O)_{2-x}$], were performed by an adiabatic high-resolution calorimeter. This calorimeter was specially designed for single crystal specimen. The calorimeter cell has a bank of thermistors for high-resolution measurements in addition to a miniature platinum resistance thermometer. The result of heat capacity measurements of benzoic acid as a standard material showed the inaccuracy of ± 0.1 % and the imprecision was confirmed to be less than ± 0.05 % between 50 and 275 K. The heat capacity of Rochelle salt was measured in the temperature range 190 to 310 K. At the both Curie points small positive anomalies were observed. The magnitudes of the anomalous heat capacity were 0.3 % of the total heat capacity at the both transition temperatures, which was consistent with the results calculated from the experiments on thermal expansion, electrocaloric and piezocaloric effects. The enthalpies and entropies of transitions at the two Curie points were found to be ΔH = 7.51 $J\,mol^{-1}$ and ΔS = 0.020 $JK^{-1}mol^{-1}$ at the lower Curie point and ΔH = 9.86 $J\,mol^{-1}$ and ΔS = 0.034 $JK^{-1}mol^{-1}$ at the upper Curie point, respectively.

The studies of the critical phenomenon were performed on solid solutions $SnCl_2(H_2O)_x(D_2O)_{2-x}$ (x=2.00, x=1.97, x=1.75, x=1.50, x=0.97, x=0.50, x=0.25 and x=0.03) by high-resolution heat capacity measurements. The critical temperature was found to increase on deuteration from 218 K(x=2.00) to 234 K(x=0.03).

The critical exponents characterizing the heat capacity divergence changed smoothly from 0.47 to 0.79 with the change of isotopic composition. In order to examine the annealing effect, we repeated the heat capacity measurements on x=0.96, x=0.50 and x=0.03 specimens. The anomalous heat capacity for x=0.96 increased by a factor of two and became sharper, whereas such a large change was not found in the heat capacity of the remainder. The small first-order components were observed in the pure hydrate and H_2O-rich solid solutions. The phase transition of the present system was considered to be the liquid-vapor type phase transition. The rounding phenomena were explained on the basis of the liquid-vapor type phase diagram.

CONTENTS

GENERAL INTRODUCTION

In recent years critical phenomena have been one of the most interesting fields in the phase transition problem which have been investigated from various points of view by many experimentalists and theorists [1,2,3,4]. Since Andrews first discovered the critical point of carbon dioxide in 1869 [5], the critical phenomena have been found in many systems; liquid-vapor systems, binary mixtures, paramagnetic-ferro-(antiferro-) magnetic transitions, paraelectric-ferro-(antiferro-) electric transitions, order-disorder transition, superfluid transition in ^{4}He, superconducting transition in metal, etc. As is well known in these systems, by varying temperature or other thermodynamic parameters (magnetic or electric field, pressure, etc.), the properties of two distinct phases can become more and more similar, and all differences vanish at the critical point. Above this point, only one homogeneous phase can exist and all changes are continuous. The critical phenomena described above differ from the first order transition, as can be seen at the melting or boiling point, in the point of the situation that the coexistence phases are in thermodynamic equilibrium at the latter point, while only one phase can exist stably at the former. The phase transitions at the critical point are characterized by strong critical fluctuations in the order parameters, so that we can find the singularities in the heat capacity, the magnetic (or electric) susceptibility, compressibility, etc. The central efforts have been directed toward the determination of the critical exponents, which characterize the singular-

ities of the thermodynamic quantities around the critical point, as well as verification of various relation expected to hold among them. Although a variety of experimental measurements have been reported for various thermodynamic quantities near the transition temperature, there are not too many measurements which can quantitatively elucidate the critical phenomena. In the past few years multicritical phenomena [6, 7], especially bicritical or tricritical phenomena, have been received much experimental and theoretical attention. At the tricritical point two critical lines and a first-order line terminate in the phase diagram. The existence of tricritical points has been demonstrated for multicomponent fluid mixtures, ^3He-^4He mixtures [8,9], metamagnet [10], NH_4Cl [11] and ND_4Cl [12] using density, magnetic field and pressure as external parameters. Furthermore, the observations of tricritical point have been very recently reported for liquid crystal [13], KDP [14] and SbSI [15]. Another recent advance on critical phenomena is on the study of the phase transition due to order-disorder of proton in the hydrogen bonded network in crystalline state. Though the ice and KDP models were proposed by Pauling in (1935) [16] and by Slater in(1941) [17], respectively, they can be applied to the only limited cases such as each species has precisely two near and two distinct protons, so that each species is electrically neutral. More recently in the sixth decade of this century this problem has made further progress and by relaxing the constraints of the ice condition, more general models are constructed for hydrogen bonded systems, *e.g.* staggered 6V-model [18] and 8V-model [19, 20]. 8V-model allows the creation of ionic species and

includes as special cases Ising model, the modified KDP model, dimer model and 6V-model. The model can be applied to the hydrogen-bonded systems with different lattices *e.g.* KDP [21], $NaH_3(SeO_3)_2$ [22], $SnCl_2 \cdot 2H_2O$ [23], $Cu(HCOO)_2 \cdot 4H_2O$ [24]. A number of heat capacity measurements have been reported for the phase transformations. However, most of them are not accurate enough, nor detailed enough, to allow evaluation of the critical exponents.

Excellent high resolution measurement of heat capacity has been first done by Buckingham, Fairbank and Keller [25] on the λ-transition in liquid ^4He. Voronel et al. have performed the precise determination of heat capacity on other fluid systems (Ar, Xe, O_2, C_2H_6) [26]. As for solids, the high resolution heat capacities on magnetics, dielectrics, metals etc. are reported by several authors, especially by Kornbit and Ahler [27], Reese and May [28], Schwartz [29], Landau [30], etc. Recently multicritical phenomena have been studied by heat capacity measurements in the systems of ^4He, ^3He-^4He mixtures [8,9] and DAG [10], where the other external parameter (pressure, composition or magnetic field) is changed in addition to temperature. Quite recently a number of results of the heat capacity in critical region have been reviewed by Grϕnvold [31] on the fluid, magnetics, dielectrics, superconductors and mixtures. The heat capacity is one of the most difficult properties to analyze in the critical region because of its weak divergence. Moreover, the approaching to the critical point is usually prevented by the rounding effect (phenomenon) due to the crystal imperfection and possible other causes and by the finite temperature

increments used in the determination of heat capacity. Generally liquid samples can be studied much closer to the critical point than solid samples. The main effort by experimentalist is to approach as close as possible to critical point without being disturbed by rounding. The exact study of critical phenomena by calorimetry requires the high-resolution measurements with high precision and high accuracy and the sample with high (physical and chemical) purity. There are two types of calorimeter used for high-resolution measurement which operate on different principles. One is the discontinuous heating method (the DC method) and the other the stationary state method (the AC method). Although the AC method has desirable features that the measurements can be made with smaller amount of the sample and easily operated automatically, it has the demerits: the specimens to be studied are limited to non-volatile substances and the absolute values of the heat capacities are very difficult to be determined. On the other hand, the DC method has no restrictions to the natures of specimens and yields the absolute value of heat capacities and is able to detect a minute first-order component which is sometimes accompanied by critical point. This last possibility is also important for characterization of the phase transition phenomenon.

We adopted the DC method, in view of the problem of the present interest. Our high resolution calorimeter is available for the study of a material with a slight excess heat capacity, as can be seen in the phase transitions of superconductors or Rochelle salt, as well as for the study of critical phenomena described above. The aim of the present work is

to investigate the phase transitions in two different systems (Rochelle salt and solid solutions between stannous chloride dihydrate and its dideuterate) by calorimetry, where the conventional calorimeter with ordinary resolution cannot give relevant data. These two substances exhibit the phase transitions associated with order-disorder of proton.

In the present thesis chapter 1 describes the outline and the improvement of the high resolution calorimeter of which the principle and the construction have been already reported [32]. In chapter 2, the heat capacity measurements on Rochelle salt between 190 and 310 K are presented. We can find the positive small anomaly at both the lower and the upper Curie temperatures. The excess heat capacities are 0.3 % of total heat capacity which is comparable with the imprecision of the ordinary resolution measurement. Capter 3 describes the results of the heat capacity measurements on six kinds of solid solutions between stannous chloride dihydrate and its dideuterate analogue and the result of Raman scattering on stannous chloride dihydrate. The present system exhibits the concentration dependence of the critical parameters and the order of the phase transition.

CHAPTER 1

HIGH RESOLUTION HEAT CAPACITY CALORIMETER

1.1. Outlines and improvements

The design and construction of the high resolution adiabatic calorimeter used in this work was described in detail elsewhere [32]. In order to avoid repetition, only a brief outline of the apparatus will be given here for the sake of convenient reference. Several improvements made since the previous publication of the apparatus will also be added here. The calorimeter consists of four major parts, viz., the cryostat, the adiabatic-control circuit, the temperature-measuring circuits and the energy supply and its measuring circuit (Fig. 1). The cryostat is of the typical one that is employed in the adiabatic calorimeter [33]. The calorimeter cell is a copper cylinder (50 mm high, 25 mm diam.) with a demountable lid and has a copper bobbin for loading a single crystal sample. The vacuum-tight closure of the cell was achieved by an indium O-ring seal inserted between the lapped faces of the flanges of the body and lid of the cell. Eight pairs of stainless steel screw (1.6 mm diam.) fixed the flanges. A thin layer of apiezon grease applied on the flange faces was helpful for effective sealing. (see below) The two types of thermometers are attached to the outer surface of the cell. One is a miniature platinum resistance thermometer (Model S 1059, the Minco Products, USA). The other is a bank of five glass-bead thermistors (Shibaura Denshi, model NSB) for the high resolution measurements. The former was used

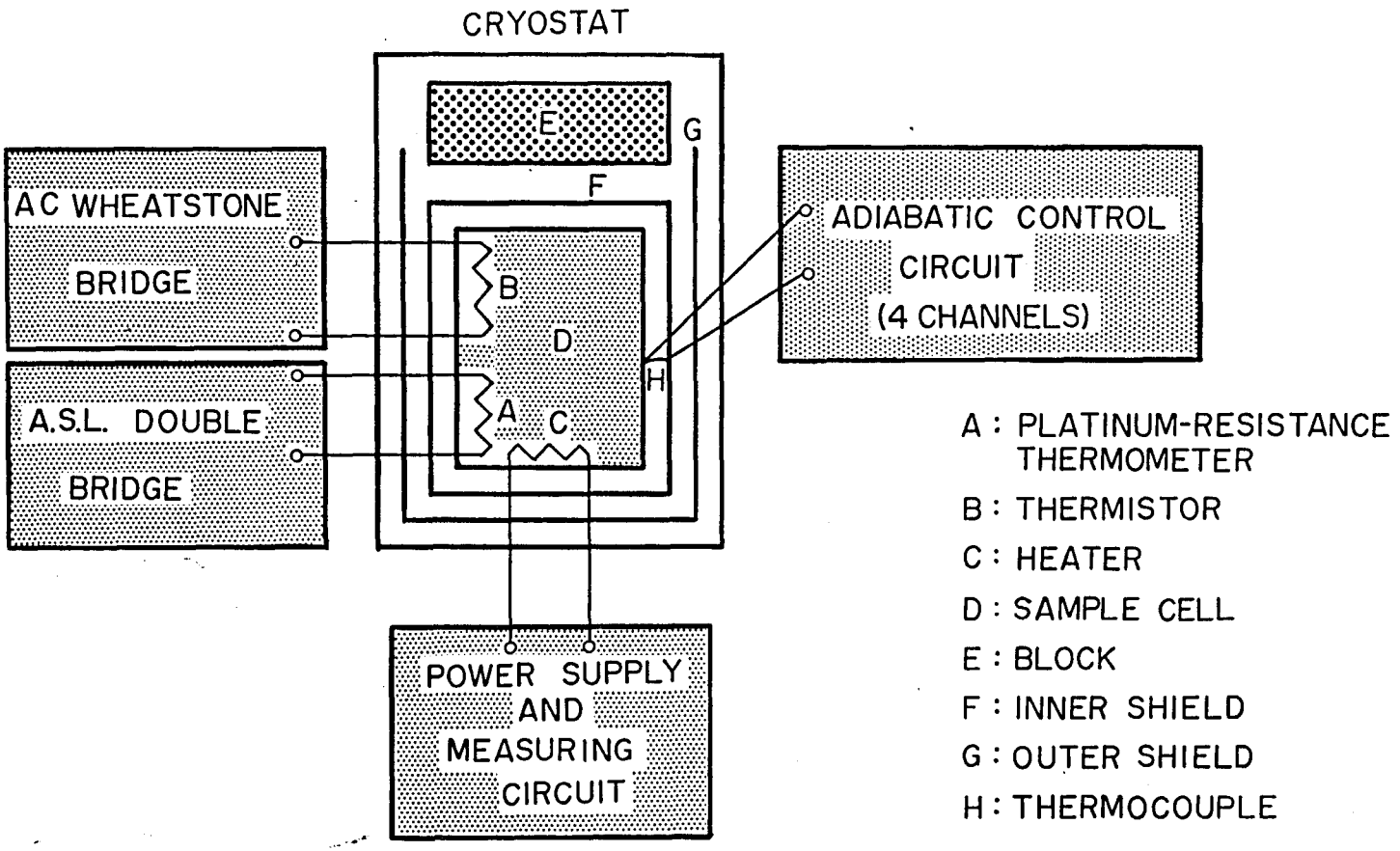

Fig.1 Block diagram of the calorimetric system.

for establishing an accurate temperature scale as well as for heat capacity measurement. The resistance was measured by the precision AC double bridge (Automatic System Laboratory Inc. Model H8) with inductively coupled ratio arms. The reading of the bridge gives the ratio (n_A) which is related to a resistance of the thermometer ($R(T)$) by the expression.

$$n_A \approx R(T)/\{R(T) + R_{std.}\},$$

where $R_{std.}$ is the resistance of the standard resistor. Three corrections had to be considered to this expression: effect of the impedance of the leads, effect of the self-heating and the inductance of the thermometer itself. The first correction was achieved by the connection of resistors in parallel with the inductive ratio arm in turn. The magnitude of this correction was less than 3/1000 K at any temperature studied. The second effect was eliminated in the following manner; a set of measurements with various bridge carrier valtages was plotted against the power dissipation and the value of n_A at zero power dissipation was determined by extrapolation. The last effect was taken into account by making the calibration of the Minco thermometer at a fixed frequency, while the standard thermometer was measured with DC current.

The Minco thermometer was calibrated at a fixed carrier frequency (390 Hz) against the laboratory thermometer (L&N Pt-thermometer) certified at the US National Bureau of Standards according to the IPTS-68. In the high-resolution measurements, AC Wheatstone bridge was used to measure the thermistor resistance. A lock-in amplifier (Princeton Applied Research Corp. Model 124) was employed as a highly sensitive

detector. We could reduce noises from various sources to an extent of thermal noise. The temperature was typically measured to ±5μK, and in a favorable instance the sensitivity increased to ±2μK. The maintenance of adiabaticity of the calorimeter cell was conducted by 4-channels-adiabatic controllers which regulated the temperature of three jackets (inner cylinder and upper cone, inner bottom cone, outer jacket) and a tempering block. The electric energy to the calorimeter heater was supplied by a regulated constant-voltage power source and measured with a five place digital voltmeter in conjunction with a thermostated 100Ω standard resistor.

Several improvements of the apparatus made since the earlier publication are as follows.

i) Use of an indium O-ring facilitates the vacuum-tight closure of the calorimeter cell.

ii) In order to ease the procedure of assembling the calorimeter cell especially in the dry-box, two gold electric connecters were attached to the hermetic seal as the terminal for the calorimeter-heater-leads.

iii) In order to decrease the heat transfer to the calorimeter cell by conduction along the leads, one of the thermocouple junctions, which was previously located between the calorimeter cell and bottom cone, were fixed to the inner jacket. The copper leads of two thermometer were replaced by the constantan leads with smaller thermal conductivity.

iv) The significant errors were caused by the drift of stray E.M.F. induced at the terminal of thermocouple-lead especially in high resolution measurement. The stray E.M.F. was reduced

by decreasing the number of binding-post placed between the calorimeter and the microvolt amplifier.

v) The ASL AC double bridge works adequately when the resistance ratio (n_A) is between 0.2 and 0.8. Previously, we used two home made standard resistors (6.238453 Ω and 0.390430 Ω) and a commercial one of 100 Ω (Shimadzu Electrical Measuring Instruments Co., Ltd.). The first resistors were replaced by three General Radio Company card-type precision resistors (10, 1, 0.1 Ω) resulting in ample overlap between the intervals of the recommended ratio value. This modifications did not influence the temperature scale because the new resistors were calibrated against the 100 Ω resistor which remained as before.

vi) The maximum temperature coefficient of the card-type standard resistor has been stated by the manufacturer, ±20ppm/K. The improved thermostat was constructed, which consisted of the double-walled-aluminium box temperature-regulated by a proportional controller. The temperature was kept constant within ±50mK.

vii) The effect of the self-heating is corrected more reproducibly by monitoring the accurate power dissipated at the thermometer. For this purpose the bridge carrier voltage was measured by an AC voltmeter (Yokogawa electric works LTD).

viii) Temperature constancy of the bridge components was found to be essential for the high resolution measurement especially in the vicinity of critical points where thermal equilibrium is reached very sluggishly. In order to stabilize the temperature of the bridge components (two 1 kΩ resistors for

the fixed arms and a seven-decade 111.11110 kΩ variable resistor) against the change of the room temperature, they were housed in an air thermostat. The temperature of the thermostat was regulated by a controller equipped with a thermistor to be ±0.1 K throughout a series of heat capacity measurements. Temperature gradient in the air thermostat was minimized by a fan driven by a remote motor through a flexible torque transmitter.

1.2. Determination of precision and accuracy of the apparatus

A series of heat capacity measurement was performed on the benzoic acid, a recommended standard reference material, prepared by the US National Bureau of Standards. The weight of the sample(*in vacuo*) was 12.6106 g(0.10318 mol). For this measurement the bobbin in the calorimeter cell was replaced by a similar container which had four interval fins soldered to the wall to promote rapid temperature equilibration for the powdered or polycrystalline samples. The weight of the empty cell was *ca.* 50 g. The fraction of the heat capacity of the sample to the gross one was 0.74 at 15 K, 0.33 at 100 K and 0.42 at 300 K. The experimental values of the molar heat capacity are given in Table 1. The data at the low temperature were corrected to the differential heat capacity by applying curvature correction. Figure 2 shows the deviations plots of our individual data from the smoothed heat capacity of benzoic acid recommended by the US Calorimetry Conference[34]. The data by Furukawa et al.[35] and Cole et al.[36] are also plotted. These data were originally based on the IPTS-48, while our measurements were performed on the basis of the new temperature

Table 1. Molar heat capacity of benzoic acid.

T/K	$C_p/JK^{-1}mol^{-1}$	T/K	$C_p/JK^{-1}mol^{-1}$	T/K	$C_p/JK^{-1}mol^{-1}$
12.51	3.95	53.56	42.03	180.96	94.90
14.17	5.29	56.72	44.07	184.91	96.57
15.54	6.47	60.18	46.17	188.83	98.11
16.63	7.58	63.66	47.89	192.71	99.71
17.56	8.55	66.93	49.62	196.56	101.35
18.38	9.44	70.03	51.23	200.36	102.84
19.14	10.27	72.99	52.65	204.39	104.67
19.82	11.04	75.82	54.00	208.65	106.44
20.47	11.73	78.56	55.14	212.85	108.27
21.12	12.42	81.20	56.32	217.04	110.11
21.87	13.22	84.19	57.62	221.17	111.90
22.64	14.01	87.89	59.14	225.27	113.64
23.36	14.83	91.87	60.77	229.31	115.46
24.16	15.76	100.55	64.19	233.34	117.33
25.05	16.55	104.86	65.98	237.31	118.89
25.89	17.65	109.09	67.49	241.39	120.73
26.70	18.48	113.15	68.98	245.57	122.58
27.50	19.38	117.14	70.42	249.73	124.55
28.24	20.18	124.85	73.27	253.86	126.50
28.96	21.01	128.59	74.70	257.93	128.27
29.90	21.97	132.28	76.04	261.97	130.13
31.18	23.23	135.99	77.52	265.98	131.89
32.54	24.68	140.02	78.98	270.10	133.89
33.95	26.13	143.91	80.44	274.17	135.80
35.54	27.65	147.73	81.89	278.22	137.34
37.32	29.34	151.81	83.42	282.56	139.26
39.16	31.02	156.14	85.06	287.00	141.23
41.12	32.67	160.41	86.68	291.24	143.35
43.19	34.43	164.62	88.37	295.44	145.22
45.34	36.12	168.78	90.06	299.62	147.07
47.82	38.00	172.89	91.65	303.75	148.97
50.61	39.96	176.94	93.30		

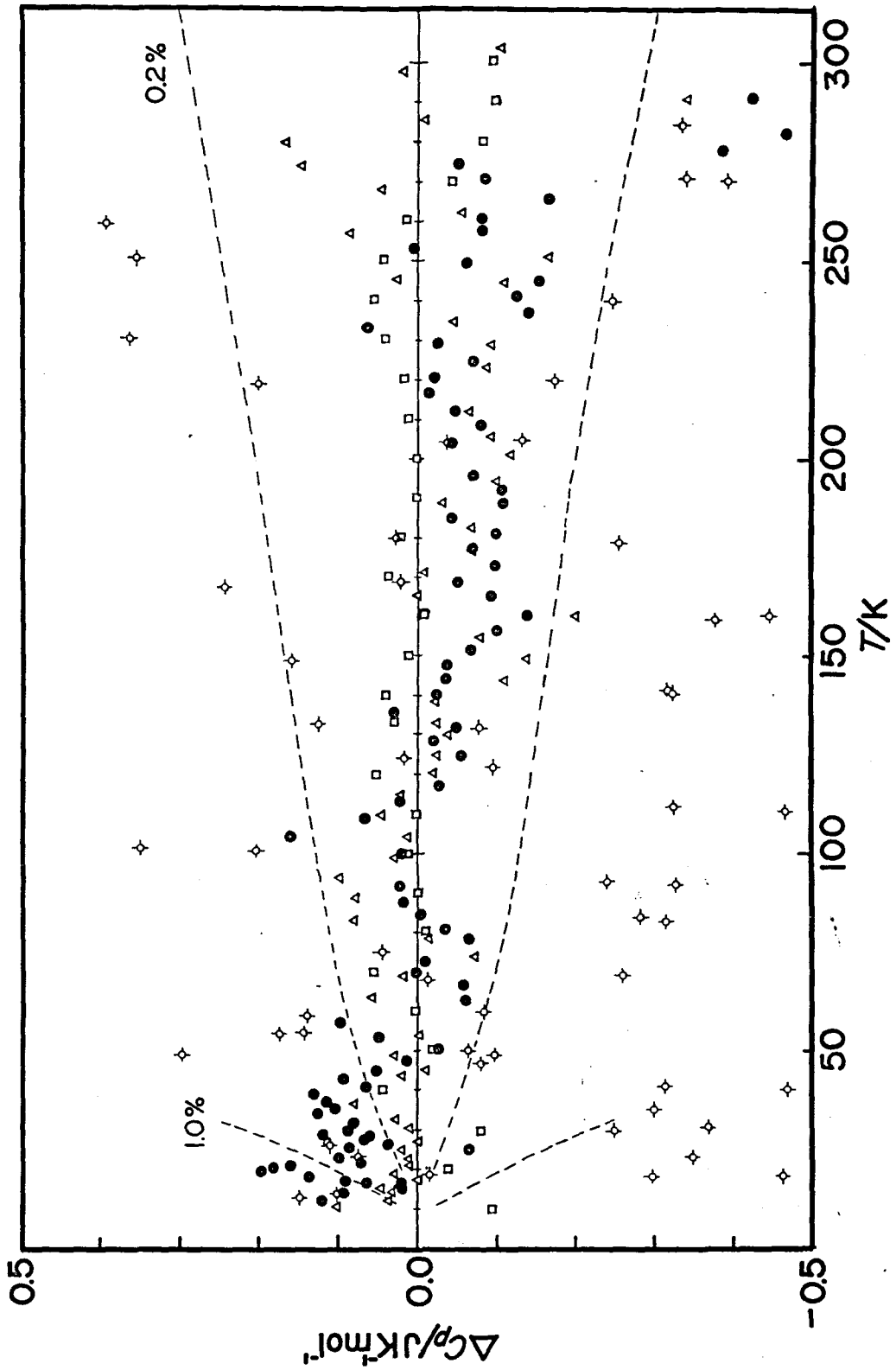

Fig.2 Deviation plot of the measured values for the heat capacity of benzoic acid. ● the present data; □ Furukawa etal.; △ Cole et al.; ⊖ Gorbunov et al.

scle(IPTS-68). In order to compare these data with ours, they were converted into IPTS-68[37]. Deviation of our heat capacity data from the smoothed curve is about 1 % of the total heat capacity at 20 K, 0.5% between 25 and 50 K($\Delta T \approx 1.5$ K) and 0.1% between 50 and 275 K($\Delta T \approx 4$K). It should be noted that the weight of the samples employed by the different authors are considerably different, *i.e.* 12.6106 g(ours), 100.99 g(Cole et al.) and 6.16 g(Gorbunov et al.)[38]. In view of the probable dependence of the precision and accuracy of the measurement on the amount of the sample, our data are quite satisfying.

1.3. Long term stability of thermistor resistance

The thermistor thermometer was calibrated against the Minco platinum thermometer in each series of the high resolution measurement. On determining the relation between the temperature and the resistance of the thermistor, the equation

$$T=\sum_{i=1}^{n} A^{i}(\ln R)^{i} \qquad (n= 2,3 \text{ or } 4)$$

was assumed and the expansion coefficients were determined by the least square fit. Nominal resistance of each thermistor is 4 kΩ at 0 °C. The connection of the five thermistors was changed so as to obtain the resultant resistance of 10~30 kΩ in the temperature interval of interest. Figure 3 shows some examples of the connection. These thermistors have been used already for four years and have experienced the liquid hydrogen temperatures more than ten times. In view of the highly stable apparatus used for the resistance measurements, this provides a rare case of a long term stability test of the thermistors at low temperature. Figure 4(a) shows an example of the ther-

mistor calibration, corresponding to the connections shown in Fig.3(c). An example of a least square fit resulted in the following expression for the temperature-resistance relation,

$$T=2.885683 \times 10^{2} - 2.477404 \times 10 \ln R + 1.640582 \times (\ln R)^{2} - 7.399469 \times 10^{-1} (\ln R)^{3}.$$

The deviation of the observed temperature from this equation was less than 10^{-3} K. The long term stability of the thermistors is shown in Fig.4(b), where the temperature at which the resultant resistance becomes 17 kΩ is plotted against the data of the observation. The scattering of the points is within ±15 mK and probably due to the fact that same of the all thermistors did not always occupy the same position in the configuration(Fig.3) in the different observations. From this plot it is found that thermistor thermometer can determine the absolute temperature within at least 15 mK.

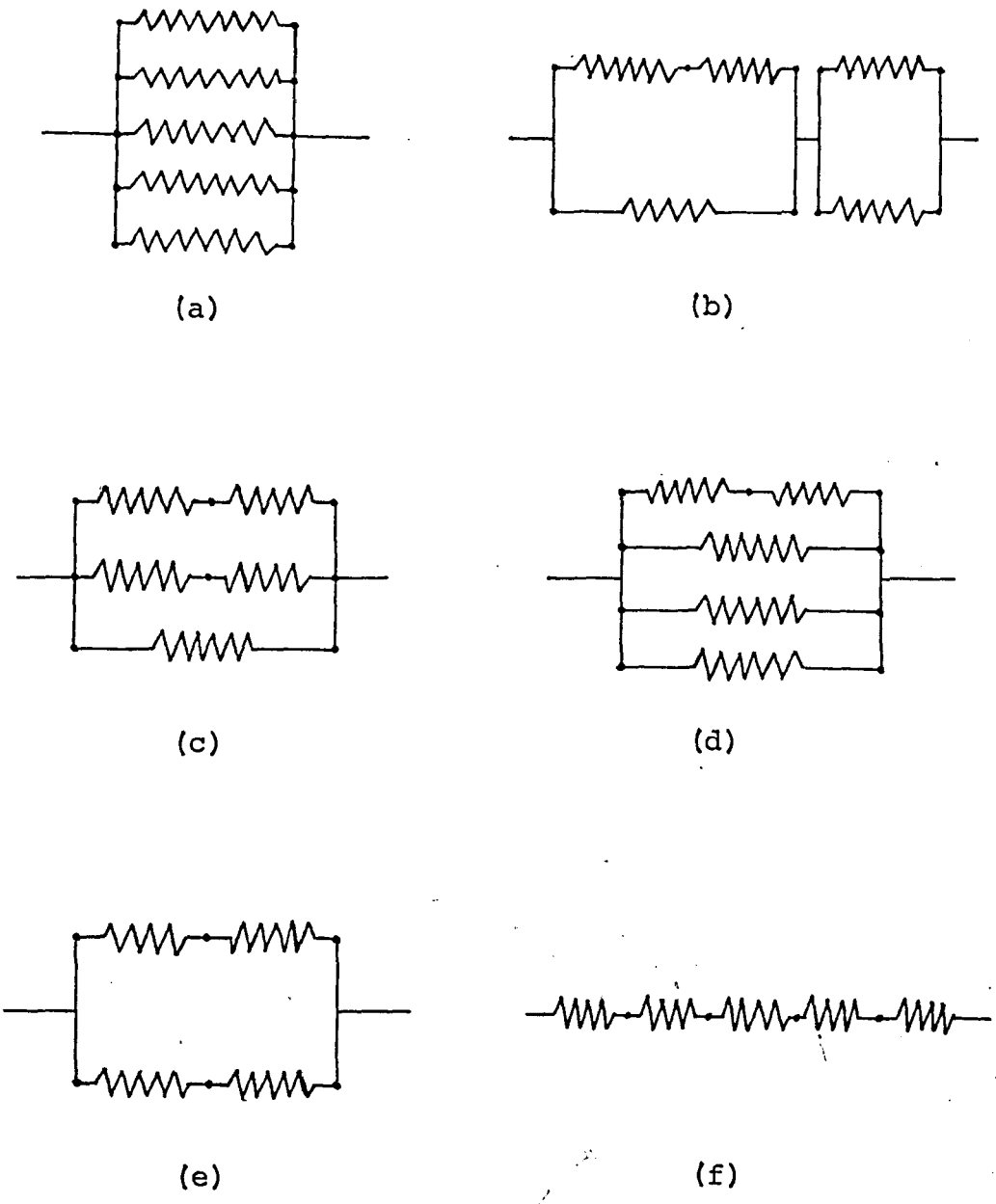

Fig.3. Example of the connection of thermistors.

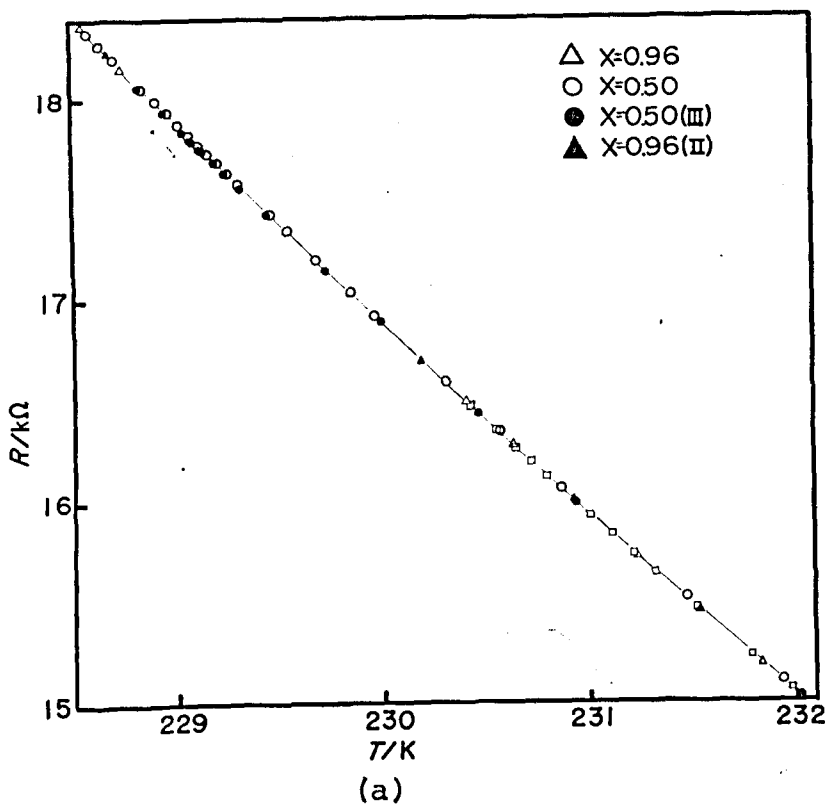

(a)

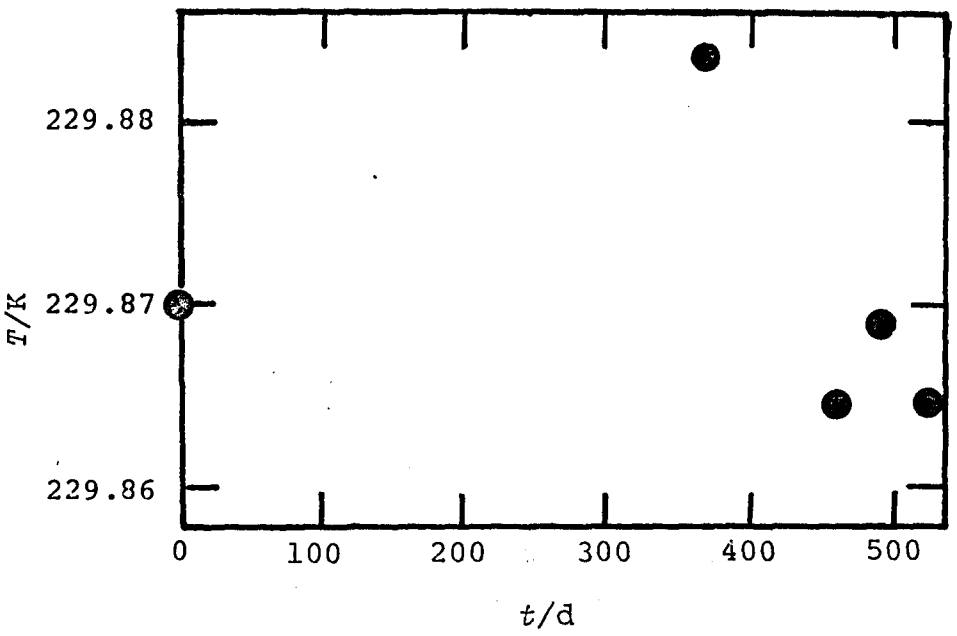

Fig.4 (a) Relation between the temperature and the net resistance of the five thermistors with connection shown in Fig.3(c).

(b) Long term variation of the thermistor thermometer(Fig.3(c)). The ordinate shows the temperature indicated by thermistor thermometer at 17 kΩ.

CHAPTER 2

PHASE TRANSITIONS OF ROCHELLE SALT AS STUDIED BY HIGH-RESOLUTION HEAT CAPACITY MEASUREMENT

2.1. Introduction

Rochelle salt (sodium potassium tartarate tetrahydrate, $NaKC_4H_6O_6 \cdot 4H_2O$) is the substance in which the phenomenon of ferroelectricity was first discovered by Valasek[39] in 1920. This crystal has several anomalous properties that earned it a unique position among now numerously known ferroelectic materials. It has two Curie points at 255 K and at 297 K. The ferroelectricity appears only at the intermediate temperature range between these two Curie points. The crystal symmetry[40] changes in an unusual way: the high temperature phase has the orthorhombic space group $P2_12_12_1$, while the intermediate phase the monoclinic space group $P2_1$. The low temperature phase has again the orthorhombic space group $P2_12_12_1$.

Physical properties of Rochelle salt have been studied by numerous authors[41] and cannot be conveniently cited here, but some of these relevant to the present study are: the dielectric constants[42], piezoelectric constants[41], the spontaneous polarization[42], the electro caloric[43] and piezocaloric properties[44] and the heat capacity.

Müller[45] developed a phenomenological theory of Rochelle salt and correlated these physical quantities with each other. Microscopic theories were advanced by Mason[46], Takahashi[47],

Devonshire[48], Mitsui[49] and Shukla and Blinc[50]. The recent theories assume two sublattice models in accordance with the space group mentioned above and more detailed structural data[51]. The problem which we are concerned with in the present study is the precise experimental determination of th heat capacity around the two phase transitions. As there seems to be a confusion as to the description of the shape of the anomalous heat capacity, a definition about the specification of the anomalous heat capacity is here in order. There are four possible types of the anomalous heat capacity of Rochelle salt, the difference among them being in the lower transition region (see Fig. 5). Anomaly of diverging type may be possible but is not relevant here. We say that curves (a) and (b) have positive anomalies at the two transitions and that curves (c) and (d) have a negative anomaly at the lower transition and a positive one at the upper one. The sign of the anomaly is thus defined as positive or negative according to whether the anomalous heat capacity is larger or smaller than the smooth back-ground heat capacity in the transition region. Another specification of the anomaly refers to the sign of the jump. We call the jump positive if the heat capacity increases discontinuously with increasing temperature. The negative jump is analogously defined with the discontinuous decrease of the heat capacity. Thus the curves (a) and (d) have a positive jump and curves (b) and (c) a negative jump at the respective lower transition. They all have a negative jump at the upper transition. We prefer the specification by

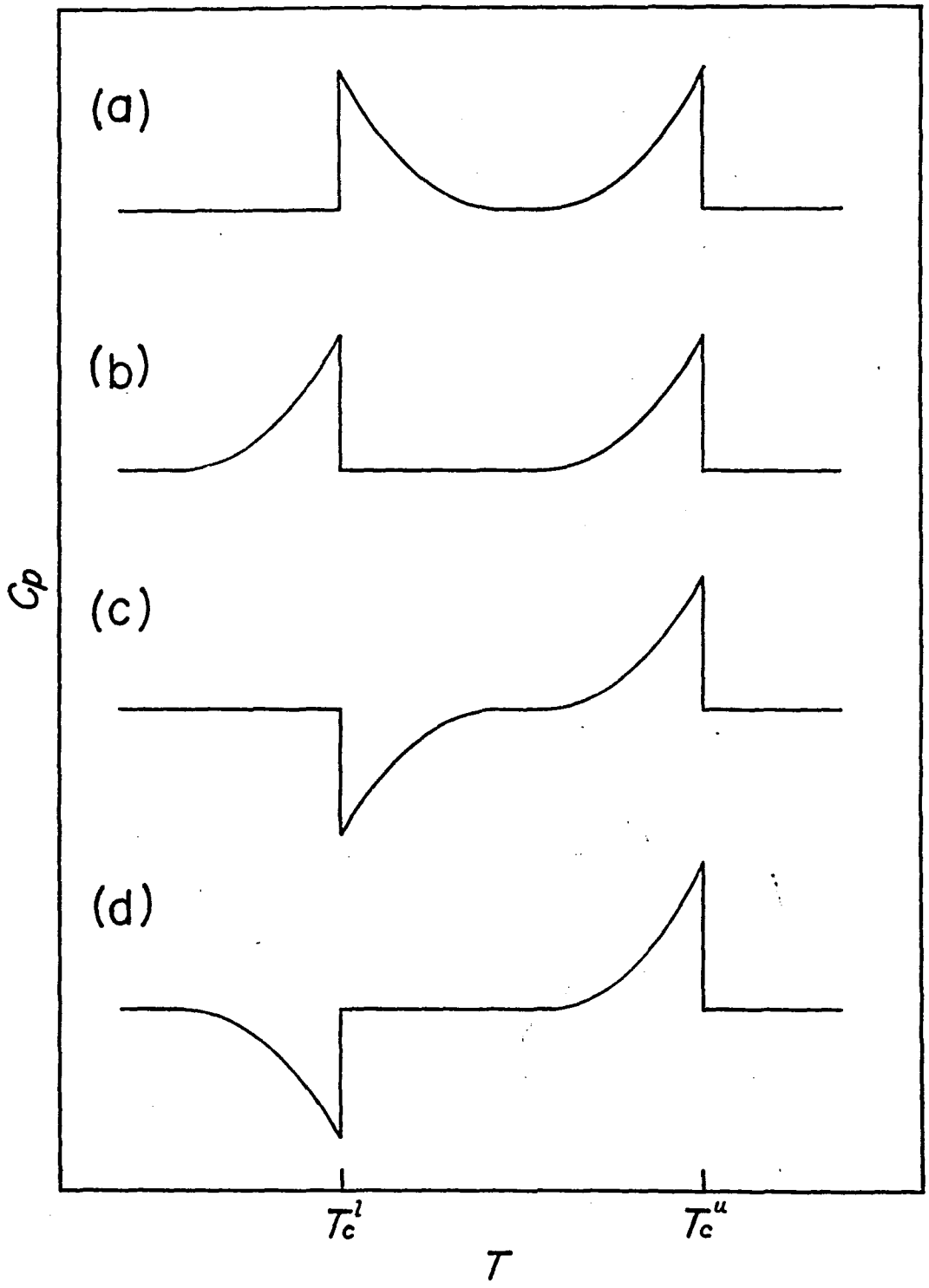

Fig.5 Four possible types of the anomalous heat capacity of Rochelle salt at the lower transition region.

the sign of the anomaly to the specification by the sign of the heat capacity jump because a clear-cut discontinuity is not always accessible calorimetrically. The "jump" specification may be appropriate in discussion of the electrocaloric and piezocaloric measurement or of the Ehrenfest relation of the phase transition lines.

There have been hitherto six investigations to detect the heat capacity anomalies in Rochelle salt. Rusterholz[52] found a sharp anomaly at the upper transition point by differential calorimetry amounting to five percents of the total heat capacity. This was not confirmed by Hicks and Hooley[53] who measured the heat capacity from 15 to 350 K. The latter's data are a smooth function of the temperature within the experimental imprecision of about 1% over the whole temperature range expect at the melting point. Wilson[54] paid particular attention to the transition points. In one series of measurements employing a single crystal he found no anomaly at the lower transition and small one at the upper. The significance of the latter was conceded by him as barely above the imprecision of the measurement. Wilson obtained a negative anomaly at the lower transition in another series by using small crystals. The heat capacity he obtained resembled the curve (c) or (d) in Fig. 5.

Hirakawa and Furukawa[55] measured the heat capacity of Rochelle salt over limited temperature ranges around the two transition points with what purported to be a conduction type calorimeter. They reported anomalies at both of the transition.

We share the surprize with them that they found first order transitions. Unfortunately, they did not give any informations about the precision and accuracy of the apparatus, and also the latent heats of transitions. Nor is it possible to obtain an order-of-magnitude estimate of the heat effect associated with the claimed anomalies described in their diagrams.

Reese and May's measurement[56] around the upper transition was not precise enough to detect any anomaly. At the lower transition point they treated the heat capacity data (114 measurements) statistically and obtained a negative jump by 0.6% of the heat capacity. They claimed that this was the first experimental observation of a heat capacity anomaly at the lower transition. More recently in 1976, Helwig[57] reported the heat capacity of single crystals of Rochelle salt and found a negative anomaly at the lower transition and a positive anomaly at the upper, both amounting to 1% of the heat capacity. His data behaves qualitatively as the curve (d) of Fig. 5, although the electrocaloric experiment by the same author appears to be more in line with the curve (a) or (b). The experimental situation is thus very confusing. It may be summarized as follows. Two authors[Wilson, Helwig] observed depression of the heat capacity at the lower transition point and one[Reese and May] a negative jump. Two authors[Hicks and Hooley, Wilson] found no anomaly there. At the upper transition, positive anomaly was found by three authors[Rusterholz, Wilson, Helwig], and no anomaly was found by three [Hicks and Hooley, Wilson, Reese and May]. Still

another author [Hirakawa and Furukawa] found first order transitions at both of the transition temperatures. Temperature dependence the claimed anomalies by different authors are also at variance with each other. In this paper we report yet another measurement of the heat capacity of Rochelle salt aiming at the final of the series of the reports. This work should be partly in reply to the challenges from Wiseman and Kuebler [43] who estimated the anomalous heat capacity derived from the electrocaloric effect, from Imai based on his piezocaloric effect and also from Blinc and Zeks [50] who expect to verify their theory by precision calorimetry.

2.2. Experimental

A large single crystal was prepared from an aqueous solution of Rochelle salt (Wako Pure Chemical Ind. Ltd.) by slow cooling in a temperature-controlled water bath. The crystal was shaped into a cylinder with the diameter of 25 mm and the height 40 mm, and placed in a close-fitting, thin wall copper bobbin around which the heater wire was wound. The crystal-bobbin-heater assembly was enclosed in a vacuum-tight copper cell with an indium O-ring seal of 0.5 mm diameter. The ferroelectric axis was perpendicular to the cylindrical axis. The copper bobbin should provide an approximate boundary condition for the zero electric field. The weight of the crystal was 36.1299 g. The heat capacity measurements were performed with a high-resolution calorimeter. This adiabatic-type calorimeter was equipped with two kinds of thermometer;

One is a platinum resistance thermometer calibrated in the International Temperature Scale-68, and the other is a thermistor-thermometer. The former provides the well-established temperature scale. The latter was calibrated in situ against the former thermometer and used for precise measurement of small temperature increments. The practical resolution of the thermistor-thermometer was 3 μK with the power dessipation of 100 nW. The thermistor-thermometer consists of five thermistors, the connection of which was changed so as to give a suitable resultant resistance for measurement by use of an A.C. Wheatstone bridge in the temperature interval of interest. In the present measurement the resultant resistance was adjusted to ca. 17 kΩ around the lower Curie point and readjusted to ca. 7 kΩ around the upper Curie point. The heat capacities were measured in the temperature range of 190∿310 K with an ordinary resolution ($\Delta T \simeq 1 \sim 2$ K) and in the vicinity of the Curie points with a smaller temperature step ($\Delta T \simeq 1/10$ K). The imprecision of the high resolution measurement was confirmed to be less than 0.05% [32]. A comment on the construction of the calorimeters is here in order. The earlier workers [Rusterholz, Hicks and Hooley, Wilson, Hirakawa and Furukawa] used thermocouples as thermometer. This limited the capability of their apparatus because of the lower sensitivity and stability of thermocouples than of the platinum resistance thermometer and thermistor. Another deficiency of the earlier calorimeters [Reese and May, Hirakawa and Furukawa, Helwig], which was particularly grave to the study of Rochelle salt,

is that the calorimeter cells were not vacuum-tight. This means that the space around the cell could not be evacuated because the evacuation would have dehydrated the crystal. Consequently the adverse heat leak between the cell and the surrounding could be considerably larger than in a typical vacuum adiabatic calorimeter. Also variation of the dehydration pressure of the crystal with temperature would limit the accuracy of the open-cell calorimeter: the crystal dehydrates or rehydrates as the temperature increases or decreases. This process would be accompanied by an endothermic or exothermic effect whose magnitude depends on how long the crystal is kept at a particular temperature. The dual thermometry and the vacuum-tight cell employed in the present apparatus are believed to be a significant improvement over the earlier calorimeters.

In a preliminary measurement of heat capacity a small anomaly was found at ca. 269 K due to melting of a surplus water occluded in the crystal. In order to remove the extra water the sample was taken out of the calorimeter cell and kept in a closed glass vessel along with a partially dehydrated Rochelle salt for a month. By this treatment the spurious peak, though not eliminated completely, become much smaller. The excess of the water was estimated to be ca. 1 mg from the enthalpy of melting. The excess water is believed to have little effect on values of the heat capacity expect in the temperature range of its melting.

After these measurement were completed, a short publi-

cation appeared in which Ushatkin, Meriakri and Poplavko[58] reported that they found an antiferroelectric transition in Rochelle salt at 212 K by measuring the reflectivity and transmission coefficient of the far infrared radiation and the linear tharmal expansivity. We measured the heat capacity between 190 and 230 K in order to see if the phase transition could be confirmed. We did not find any anomalous behavior exceeding 0.1% of the heat capacity[Fig. 6].

2.3. Results and Discussion

2.3.1. Comparison with the earlier heat capacity data

The data obtained in this study are presented in chronological order in Table 2. After the first measurements around the lower Curie point was over, the sample was taken out for the purpose of removing the surplus water. No difference was found in the values of the heat capacity between the first and the second measurements. Figure 7 shows our results together with the data by Rusterholz, Hicks and Hooley, and Wilson. The data by Rusterholz are unreasonably large and have a sharp peak at the upper Curie point. His results deviate appreciably from the others though the large anomaly at the upper Curie point was also reported by Kobeko and Nelidow[59] and by Bantle. The latter authors did not publish the data in a form that allows comparison with the others. All the remaining data are in agreement with each other within the experimental error of about 1%. Our data except in the temperature range of transitions are well represented by the straight line C_p=

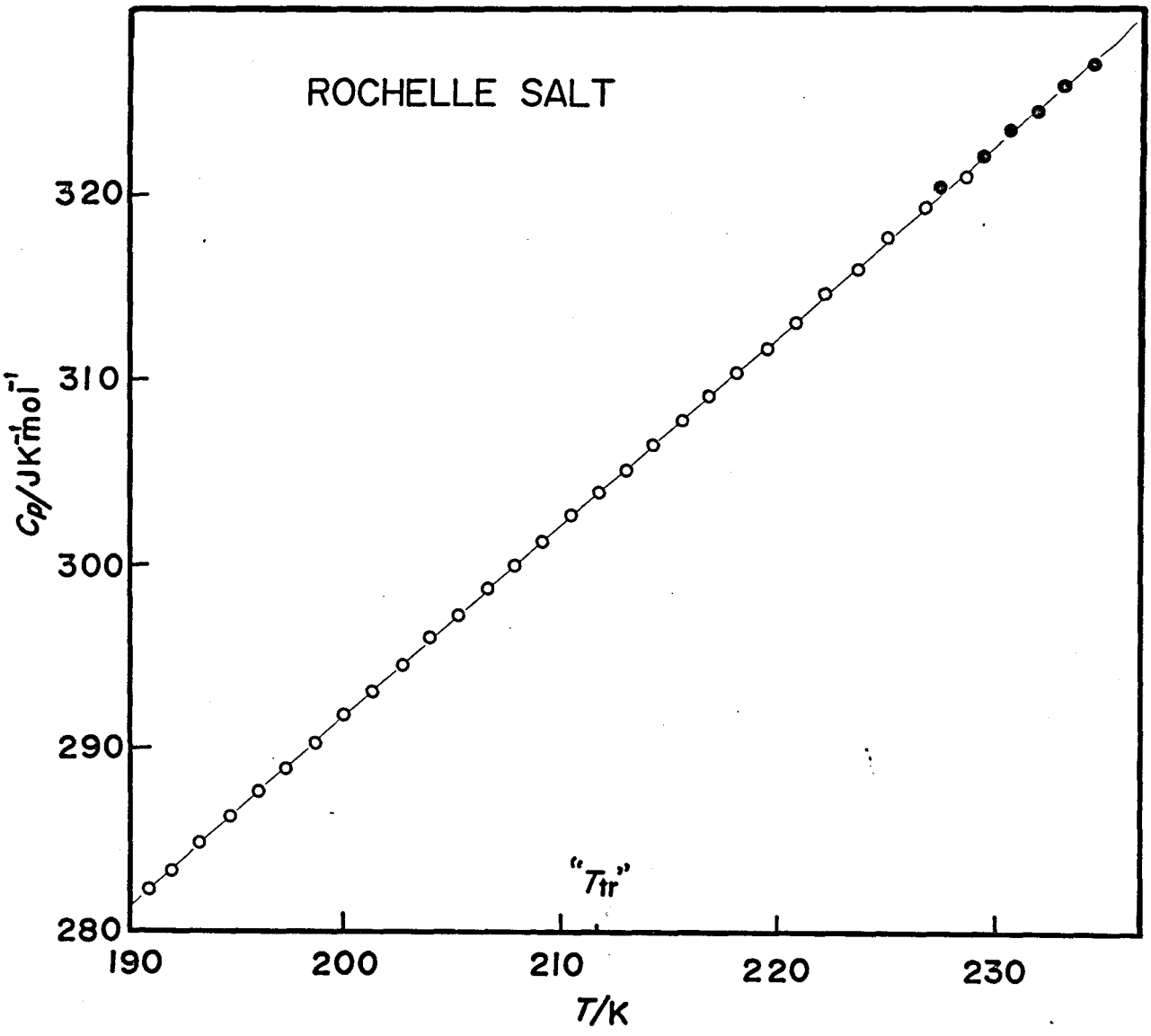

Fig.6. Heat capacity vs. temperature curve.
T_{tr} is the antiferroelectric transition temperature reported by Ushatkin et al.

Table 2. Molar heat capacity of Rochelle salt.

T/K	C_p/JK^{-1}mol^{-1}	T/K	C_p/JK^{-1}mol^{-1}	T/K	C_p/JK^{-1}mol^{-1}	T/K	C_p/JK^{-1}mol^{-1}	T/K	C_p/JK^{-1}mol^{-1}	T/K	C_p/JK^{-1}mol^{-1}
228.28	320.515	261.15	352.646	253.970	345.606	283.21	372.825	296.889	386.835	223.59	316.009
229.27	322.163	261.75	353.724	254.270	345.939	284.62	373.903	297.095	386.866	224.99	317.775
230.50	323.499	262.38	353.896	254.521	346.095	285.92	375.278	297.300	386.843	226.61	319.346
231.78	324.530	263.06	354.412	254.693	346.507	287.30	376.746	297.505	386.988	228.46	321.043
233.07	325.952	263.85	355.115	254.838	346.635	288.61	378.262	297.710	387.057		
234.36	327.093	264.63	356.185	254.982	346.882	291.23	380.941	297.916	387.228	193.79	284.947
235.70	328.553	265.42	356.802	255.126	346.795	292.33	382.207	298.121	387.393	195.41	286.894
237.10	329.936	266.28	357.607	255.271	347.513	293.21	383.199	298.326	387.607	196.32	287.417
238.48	331.210	267.22	358.474	255.415	347.822	294.07	384.340	298.532	387.850		
239.86	332.538	268.15	359.778	255.577	348.038	294.93	384.902	298.737	387.955		
241.19	333.983	269.07	364.536	255.757	348.159	295.78	385.512	298.941	388.118	258.79	350.900
242.46	335.139	270.00	361.122	255.937	348.577	296.63	386.308	299.146	388.190	259.77	351.659
243.72	335.912	270.86	361.724	256.117	348.740	297.47	386.472	299.350	388.532	261.23	352.276
244.99	337.397			256.297	348.851	298.32	386.816	299.555	388.608	264.89	356.278
246.21	338.412	268.61	360.825	256.476	348.995	299.17	388.027	299.759	388.918	265.63	356.450
247.39	339.631	269.15	359.427	256.656	349.158	300.02	388.933	299.976	388.962	267.00	357.841
248.39	340.717	269.70	360.091	256.835	349.237	300.97	389.996			268.56	360.913
249.17	341.303	270.32	360.591	257.015	349.403	302.03	390.800	298.48	387.597	269.91	360.561
249.96	342.178	270.94	361.489	257.194	349.837			299.42	388.472	271.26	361.851
250.75	342.811	271.56	361.849	257.373	349.557	270.72	361.028	300.45	389.300	282.52	372.200
251.53	343.646	272.20	362.458	257.553	349.655	272.55	362.700	301.58	390.183	283.97	373.528
252.27	344.428	272.86	363.841	257.732	349.863	274.45	364.231	302.70	392.074	285.61	375.350
253.00	345.068	273.54	363.505	257.911	349.979	276.34	365.997	304.02	392.253	287.22	377.061
253.67	345.764	274.22	364.356	258.090	350.151	277.87	367.583	305.50	393.519	288.83	378.679
254.26	346.014	274.99	365.411	258.269	350.392			306.99	394.956	290.44	380.368
254.73	346.381	275.83	366.411	258.446	350.521	274.08	363.685	308.47	396.245	291.76	381.829
255.14	347.185	276.75	366.989	258.625	350.725	276.07	365.427			293.03	383.127
255.54	347.990	277.79	367.942	258.804	350.761	278.05	367.895	294.53	384.316	294.23	384.401
255.86	348.717	278.85	368.715	258.983	350.860			295.37	385.285	295.41	385.479
256.12	348.607	280.08	368.895	259.175	351.110	281.96	371.504	296.22	386.340	296.59	386.277
256.50	348.771	281.48	371.208	259.380	351.486	282.69	371.879	297.07	386.988	297.78	387.004
256.63	349.474	282.90	372.332	259.585	351.408	283.52	372.567	297.91	387.574	298.96	388.238
256.88	349.677	284.32	373.817	259.790	351.648	284.37	373.247	298.75	387.832	300.14	389.395
257.14	349.693	285.72	375.114	259.995	351.807	285.32	374.309			301.32	390.490
257.40	349.849	287.13	376.590	260.200	351.941	286.54	375.645			302.68	391.842
257.78	349.302	288.55	378.012	260.438	352.345	287.93	377.278	190.96	282.290	304.25	393.616
258.16	349.935	257.57	350.224			289.32	379.301	192.01	283.361		
258.37	350.623	258.66	351.185	261.09	352.216	290.55	379.832	193.35	284.861		
258.74	350.388	259.87	352.638	262.11	353.341			194.69	286.331		
259.12	351.107	261.18	352.818	263.24	354.240	292.136	381.946	196.03	287.636		
259.50	351.388	262.52	353.974	264.37	355.247	292.362	382.301	197.37	288.981		
259.98	351.427	263.86	355.076	265.53	356.443	292.587	382.527	198.69	290.348		
260.52	352.193	265.20	356.294	266.86	357.575	292.813	382.781	200.02	291.818		
261.07	353.021	266.52	357.677			293.039	383.547	201.34	293.139		
261.70	353.154	267.84	359.013	265.48	356.404	293.264	383.298	202.66	294.593		
262.44	353.857	269.04	359.919	266.80	357.638	293.489	383.562	203.96	296.023		
263.18	353.638	270.09	360.692	268.10	359.325	293.715	383.855	205.26	297.266		
263.94	355.122	271.28	361.880	269.40	361.911	293.940	384.062				
253.17	345.295	272.58	363.138	265.77	356.341	294.165	384.286	206.56	298.766		
253.86	346.248			267.09	357.661	294.389	384.556	207.86	299.939		
254.55	346.545	244.90	336.944	268.39	360.333	294.614	384.841	209.14	301.299		
255.23	347.873	246.30	338.240	269.70	360.239	294.830	384.978	210.42	302.667		
255.92	348.372	247.49	339.725	271.03	361.536	295.035	385.254	211.70	303.980		
256.62	349.102	248.53	340.701	272.35	362.911	295.241	385.189	212.98	305.191		
257.30	349.834	249.57	341.475	273.57	363.888	295.448	385.464	214.24	306.481		
257.99	350.021	250.61	342.412	274.76	364.880	295.654	385.658	215.51	307.841		
258.68	350.763	251.65	343.537	276.05	366.403	295.860	385.890	216.77	309.185		
259.36	351.451	252.68	344.639	277.33	367.497	296.066	386.048	218.03	310.467		
260.06	352.123			278.62	368.770	296.272	386.458	219.40	311.796		
260.78	352.373	253.369	345.075	280.93	370.348	296.478	386.622	220.77	313.180		
261.51	352.927	253.669	345.343	281.99	371.528	296.684	386.825	222.08	314.704		

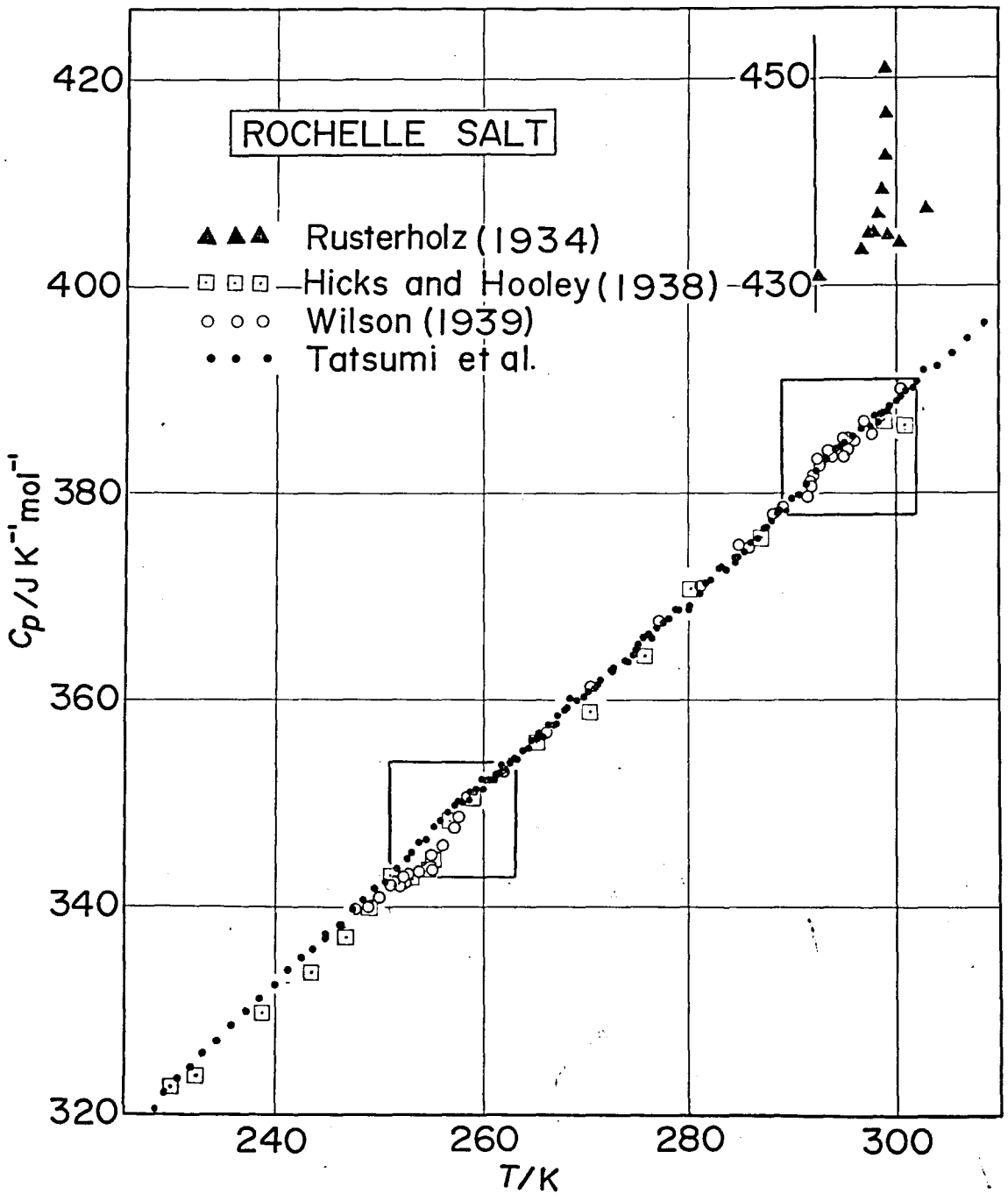

Fig.7. Heat capacity vs. temperature curve of Rochelle salt.

$0.924T + 110.638$ and agrees with the Wilson's data within 0.5%. In Figs. 8 and 9 our data are plotted in an enlarged scale in the neighborhood of the Curie points together with those by other authors.*) Evidently, there are positive anomalies at both of the Curie points in our experimental data. The excess heat capacities amount to 0.3% of the total. The negative anomaly claimed by Wilson is obscure in Fig. 8 because of the large scatter of his datum points. Reese and May's data are very limited in number and in the temperature range which they span. The discontinuity that they claimed to have found at the lower transition is also obscure. Their conclusion derived from independent averaging of the heat capacities below and above the transition does not appear to be persuasive because of the scatter of the data as large as 1%. Helwig's smoothed data are also shown in Figs. 8 and 9. The curve has a negative anomaly with a positive jump at the lower transition and is qualitatively different from ours. His measurement, though performed with a carefully specified electric boundary condition, is possibly not free from the two shortcomings of the open-cell type calorimeter namely, the heat leak and the sample dehydration.

A positive anomaly was found also at the upper transition as shown in Fig. 8 where earlier data are plotted together. Because the anomalous contribution is not very evident in the figure, in an attempt of better illustration of the anomaly,

---

*) Where only graphical presentation was given in the original paper, the numerical values were read off from a large-scale photoprint of the diagram.

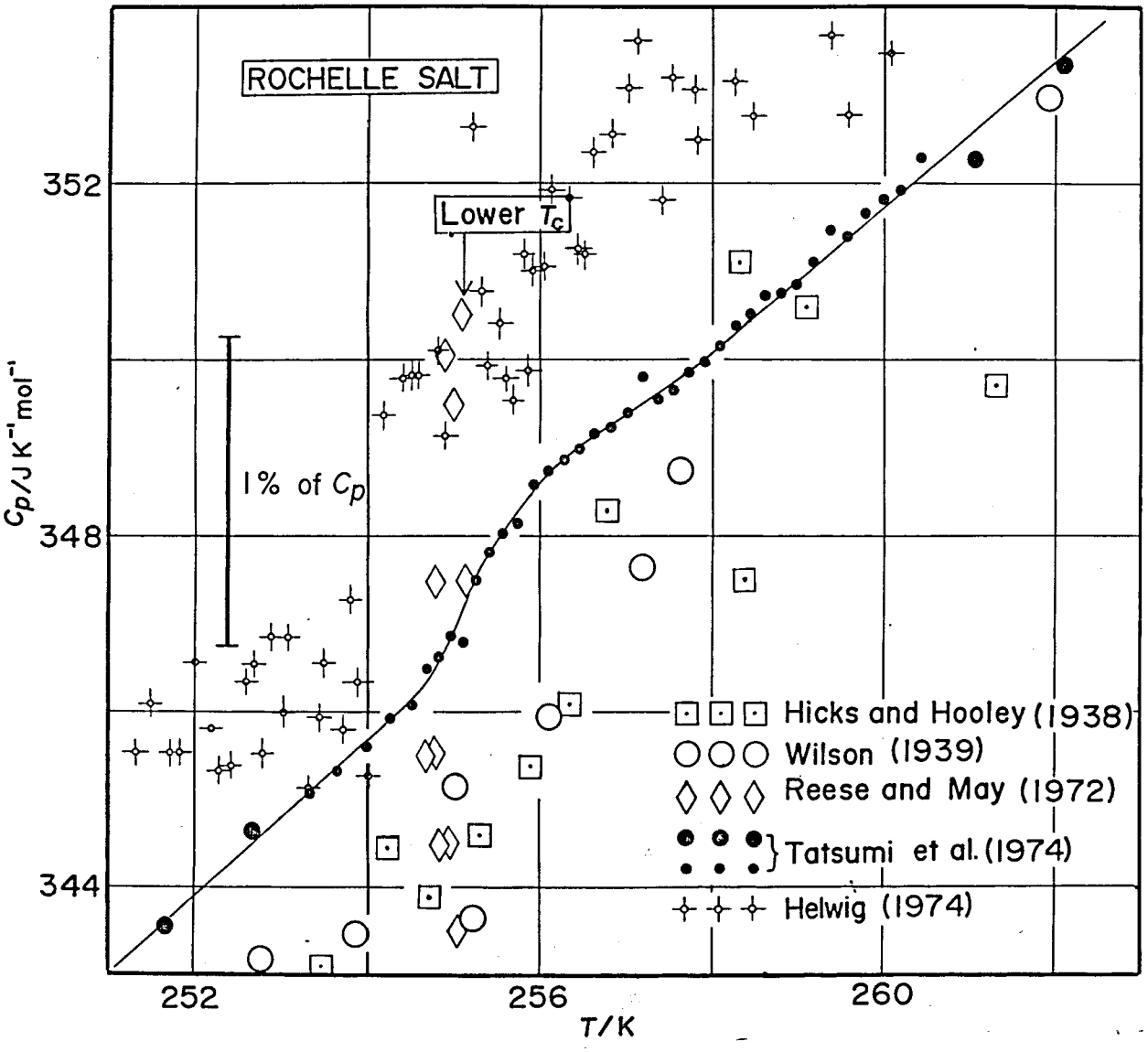

Fig.8. Detailed representation of C_p-T relationship around the lower Curie point.

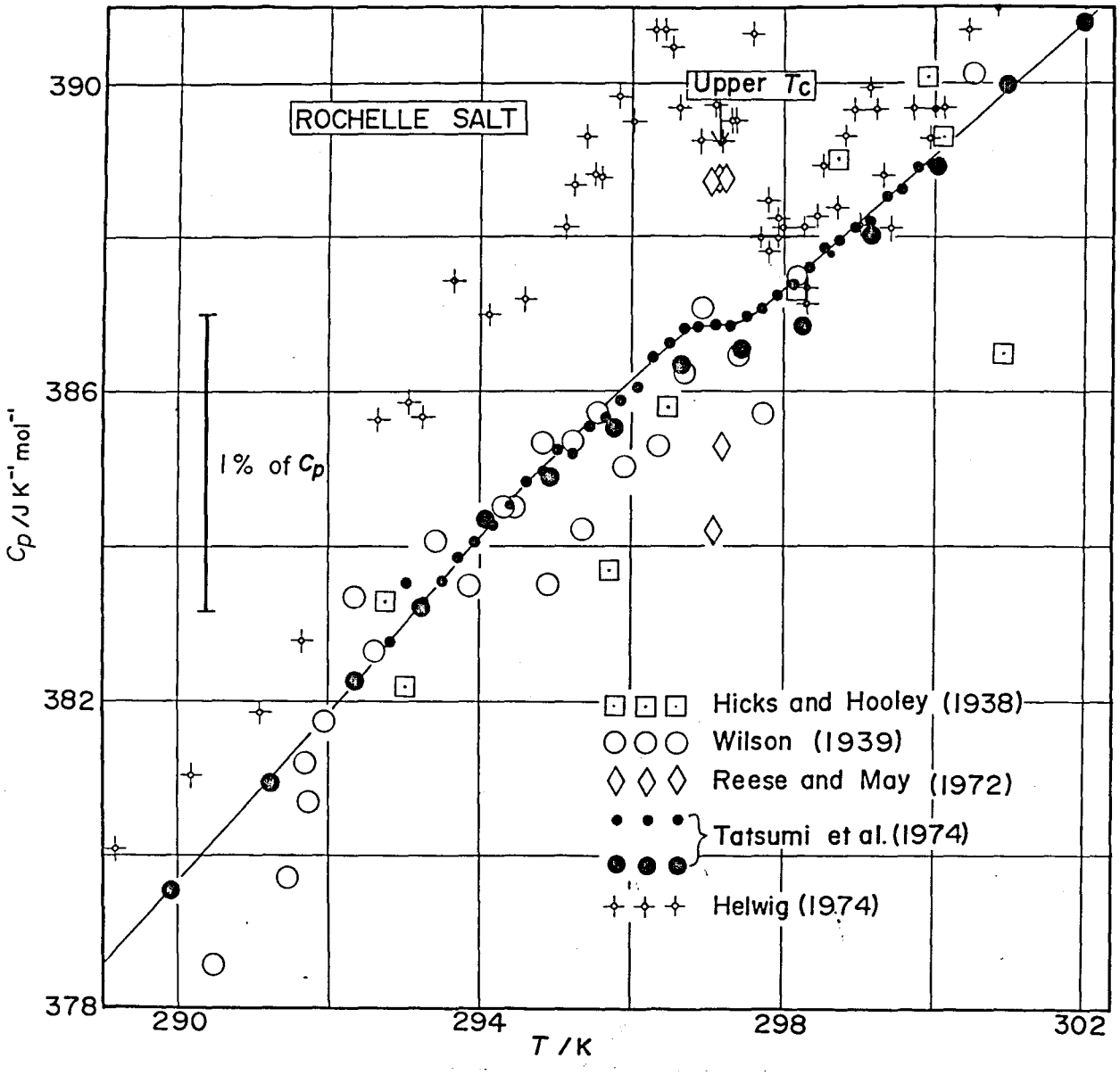

Fig.9 Detailed representation of C_p-T relationship around the upper Curie point.

$C_p/(T-T_o)$ is plotted against T in Fig. 10, where T_o=117.73 K was so chosen that the plot is flat in the temperature range. This presentation of the experimental data introduces little arbitrariness and is helpful in estimation of the background heat capacity. Fig. 11 shows the anomalous part of the heat capacity thus evaluated.

2.3.2. Relation among the calorimetric, electrocaloric, piezocaloric and dilatometric data.

According to the phenomenological theory of ferroelectrics, the elastic Gibbs energy G is given in powers of the polarization P:

$$G = G_0 + \frac{1}{2}\chi_0 P^2 + \frac{1}{4}\xi P^4 + \frac{1}{6}\zeta P^6,$$

where G_0 is the Gibbs energy of the unpolarized crystal, χ_0 the dielectric stiffness and ξ and ζ are appropriate higher order coefficients of the expansion. The excess heat capacity is given by:

$$\Delta C = C_E - C_P = -T(\partial\chi_0/\partial T)_P(\partial P_s^2/\partial T)_E,$$

where C_E and C_P are heat capacities at constant electric field and at constant polarization, respectively. Wiseman and Kuebler gave the temperature dependence of χ_0 and of spontaneous polarization P_s from the measurements of electrocaloric effect. From this equation ΔC was calculated as a function of temperature and plotted in Fig. 11. The excess heat capacity calculated from electrocaloric data takes the heat capacity at the constant polarization as the back ground value, while our back-ground heat capacity approximates the

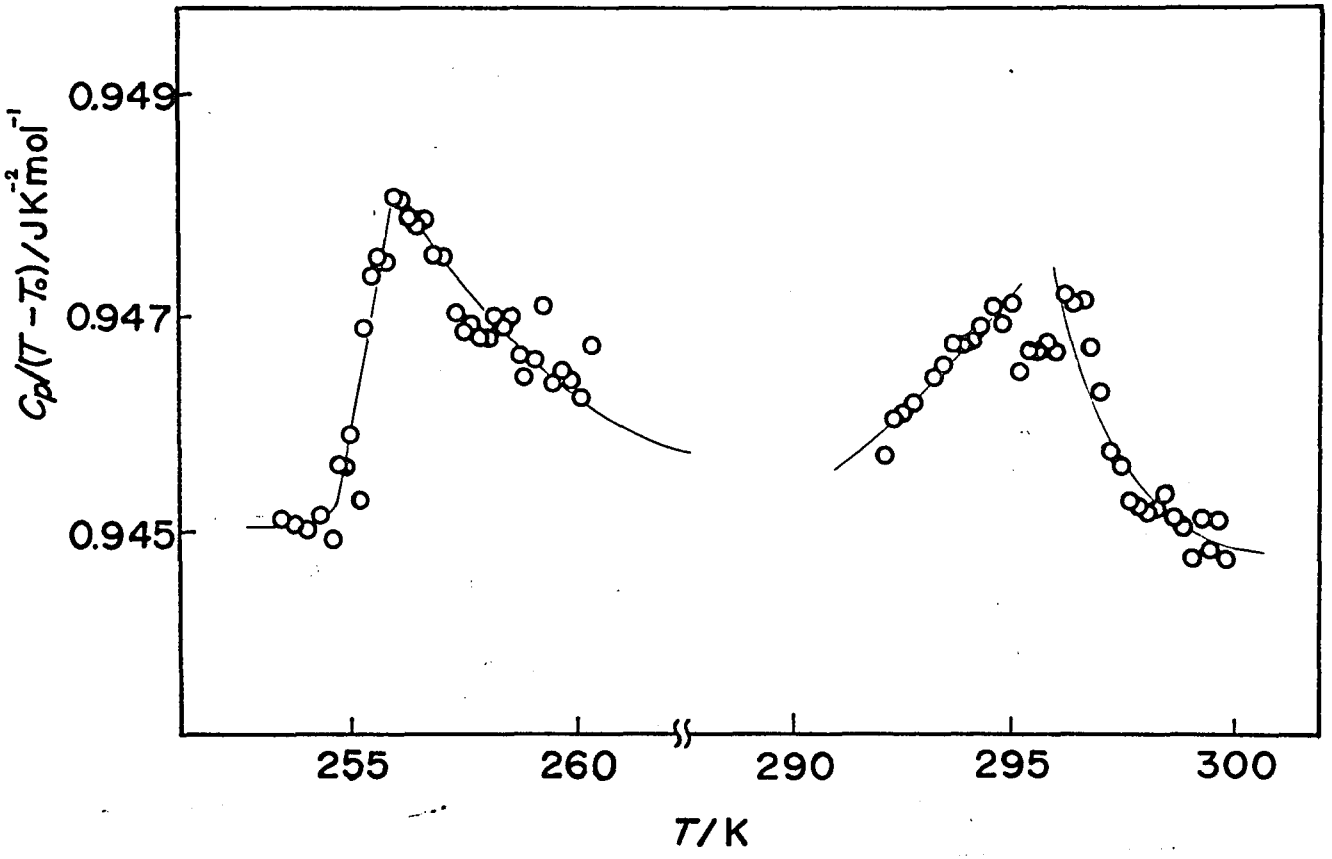

Fig.10. $C_p/(T-T_0)$ vs. temperature curve, where T_0 =117.73 K.

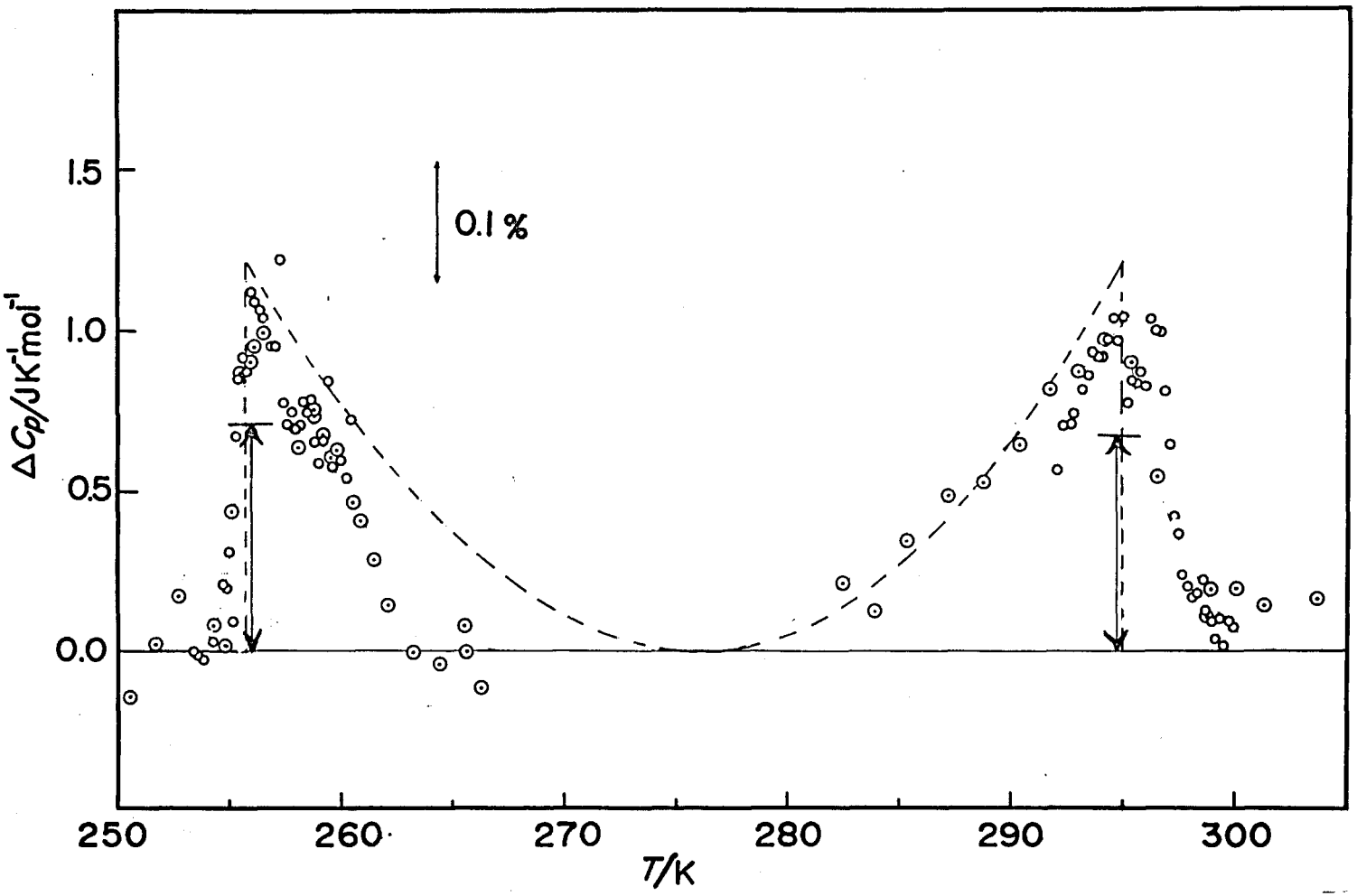

Fig.11. Anomalous heat capacity of Rochelle salt. The broken line is calculated from the result of electrocaloric effect. The arrows exhibit the jumps of C_p estimated from Ehrenfest relation.

heat capacity at the zero polarization. The difference between the two back-ground heat capacities is expected to be negligibly small at least near the transitions. Also shown in Fig. 11 is the amount of the heat capacity discontinuity at the transitions derived by Imai from his piezocaloric measurement. The consistency among the calorimetric, electrocaloric and piezocaloric measurements is thus satisfactory. In passing we should like to mention here that Helwig derived also the excess heat capacities at transition points by using his data on electrocaloric measurement. The heat capacity data obtained directly by his calorimetric measurement, however, are not in agreement with the derived data. It should be stressed that the heat capacity of the ferroelectric phase is larger than that of the non-ferroelectric phase, and that this is not because the latter have anomalously small heat capacity but because the former has anomalously large heat capacity in the vicinity of the transition regions. Our anomalous heat capacity behaves thus like curve (a) of Fig. 5 rather than like curve (d) as some of the earlier measurements(Wilson, and Helwig) suggested. In the cases of (b) and (c) in Fig. 5, the heat capacities in the ferroelectric region are smaller than the non-ferroelectric region at lower Curie point. In addition it should be pointed out that the electrocaloric and piezocaloric measurements alone are not sufficient for drawing this conclusion, because they tell nothing about the non-ferroelectric phases. In the same sense the Ehrenfest's relation for the second order

transition can only tell the jump height in the heat capacity curve. By use of this relation, Helwig estimated 1.97 J $K^{-1}mol^{-1}$ for the discontinuity at the lower transition and 0.28 $JK^{-1}mol^{-1}$ for the upper transition from the electrostrictive coefficients measured by other investigations. Recently a direct measurements of precise thermal expansion were performed by Imai[60] and he again calculated the magnitude of the jumps at both Curie temperatures by applying Ehrenfest relation. The jumps amount to 0.3%(1.20 JK^{-1} mol^{-1}) of total heat capacity at the lower Curie point and 0.2%(0.80 $JK^{-1}mol^{-1}$) at the upper Curie point. These values are in good agreement with our results. Integration of the anomalous heat capacity gives the enthalpy and entropy of transitions. They are 7.51 J mol^{-1} and 0.02 $JK^{-1}mol^{-1}$ for the lower transition and 9.86 J mol^{-1} and 0.034 $JK^{-1}mol^{-1}$ for the upper. They are defined as the corresponding quantities associated with the heat capacity in excess of the background value determined by the smooth interpolation of the normal heat capacity into the anomalous region. The definition should be kept in mind when a microscopic theory of the phase transition is compared with the experimental data.

2.4. Conclusion

We have described a precise measurement of the heat capacity of Rochelle salt from 190 to 310 K. The most important conclusion is that the anomalous heat capacity is positive at both of the Curie points. The anomaly, about

0.3% of the total heat capacity, is small enough to have been obscured in the scatter of the data obtained with less sophisticated calorimeter of the earlier authors. The signs and magnitudes of the anomalous heat capacities are consistent with the electrocaloric and piezocaloric measurement and with the Ehrenfest relation for the second order phase transitions. The general temperature dependence of the anomalous heat capacity coincides with the qualitative prediction based on thermodynamical consideration by Takahashi and behaves like the result of theoretical calculation by Blinc and Žekš based on the Mitsui's sublattice model. The deuterated Rochelle salt may be interesting to study in this respect, and the work is under way in the laboratory. We are thus approaching the ending of a long story of the anomalous heat capacity of Rochelle salt that has annoyed and delighted some of the chemists and physicists from time to time for the past forty years.

CHAPTER 3

CALORIMETRIC STUDY OF PHASE TRANSITIONS IN SOLID SOLUTIONS BETWEEN STANNOUS CHLORIDE DIHYDRATE AND ITS DEUTERATE AND RAMAN SCATTERING STUDY OF STANNOUS CHLORIDE DIHYDRATE

3.1. Introduction

The phase transition in stannous chloride dihydrate $SnCl_2 \cdot 2H_2O$ (abbreviated as SCD) was first discovered by Kiriyama et al. The complete crystal structure was determined by them from the study of the X-ray and neutron diffraction methods [62,63]. The crystal consists of the double layers, i.e. layers of stannous chloride molecules alternating with layers of water molecules. Two types of water molecules exist in the layer. One of water, designated as $H_2O(1)$, is coordinated to stannous ions and the other, $H_2O(2)$, is the water of crystallization. Each type of water molecules is linked to three others of different type in the same layer parallel to the (100) plane by hydrogen bonds. Figure 12(a) shows the crystal structure viewed along the a-axis and the deuteron-disordered arrangement is shown in Fig. 12(b). There are seven possible positions on which protons can occupy and the three kinds of hydrogen bond with different bond length. The O(2)---O(1') hydrogen bond differs from the other two in that its bond length increases anomalously below T_c, in contrast to the other two which show normal decrease in the bond length.

One should note another interesting property that SCD

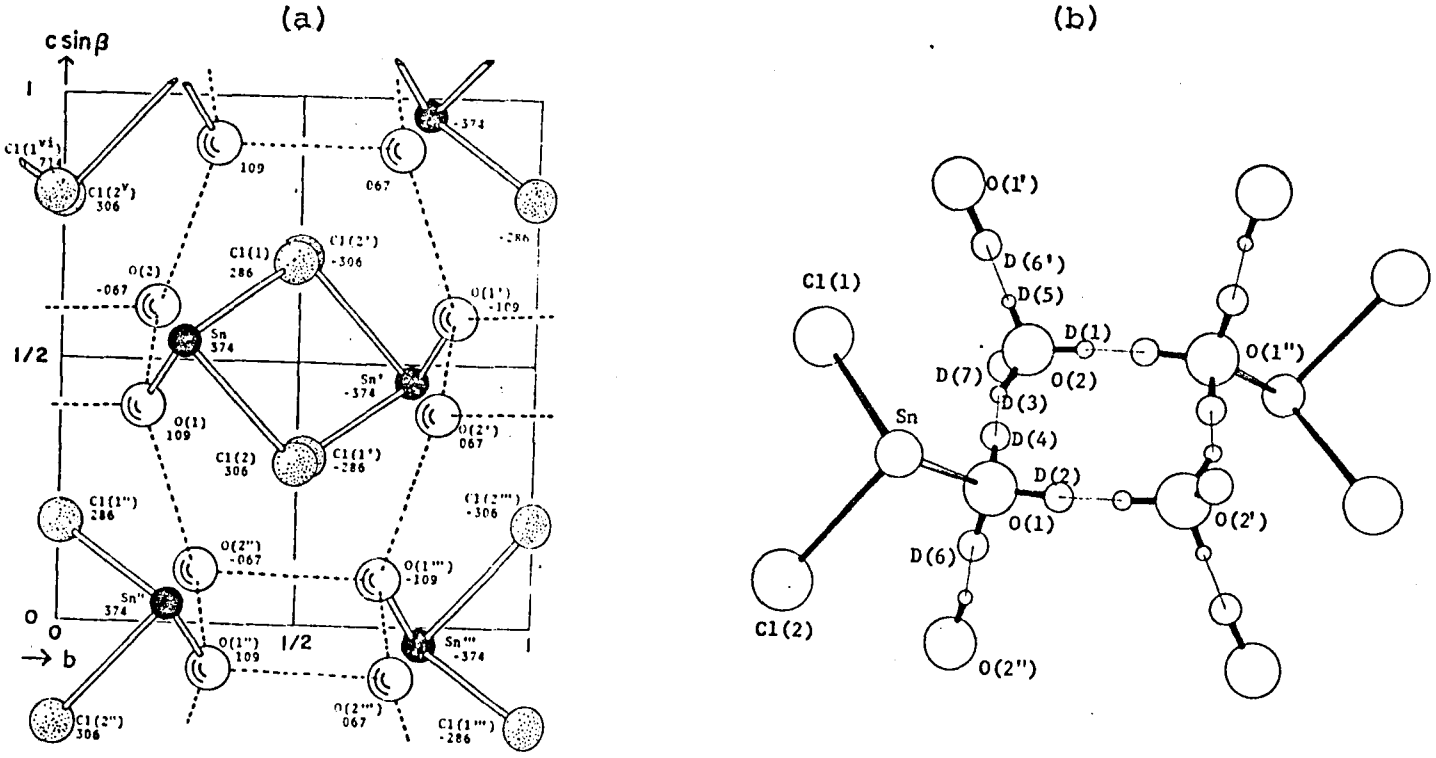

Fig.12. (a) The crystal structure viewed along the a axis.

(b) The deuteron-disordered arrangement in the high temperature phase of $SnCl_2 2D_2O$.

exhibits no change of crystal symmetry, monoclinic with space group $P_{2/c}$ - C_{2h}^5, with temperature variation through the phase transition region. Kiriyama *et al.* also investigated the phase transition in SCD by various experimental techniques, such as the dielectric constant [61], the d.c. conductivity [61], Raman scattering [64] and nuclear magnetic resonance [65]. The low-frequency dielectric constants along the b and c axes have high peaks at T_c and the d.c. conductivity along these axes shows sharper peak than that along the a axis. The deuteron NMR spectra suggested that the motion of water was the combined one of the 180° flip and the three-fold rotation about O(2)-D(7) and O(1)-Sn bonds. The heat capacity measurements were performed by Matsuo *et al.* [66] for SCD and its deuterated analog (DSCD). The heat capacity exhibited highly symmetrical peak at T_c, which was the trade mark of the two dimensional phase transition. The transition temperature increased on deuteration from 218 to 234 K. In addition to this, they found a glass transition phenomenon around 155 K. The state of aggregation realized below T_g was classified into a new type of glassy crystal in which the degree of freedom with long range order was frozen. From the results of these experiments, it has been pointed out that the phase transition is associated with the two dimensional ordering of the protonic positions.

Theoretically, Salinas and Nagle [67] proposed the dimer model on the basis of the crystal structure and gave its exact solution. They successfully predicted from their model

the ground state proton configuration and also obtained the highly symmetrical heat capacity at T_c. The proposed configuration was really confirmed by neutron diffraction taken at low temperatures. In the early study we performed the high resolution measurement of the heat capacity in SCD [68] and DSCD with interest in the highly symmetrical anomalous heat capacity. The significant differences were observed between them. In SCD a quasifirst-order component was found and the critical exponents were determined as $\alpha = 0.49$ below and above T_c. On the other hand, DSCD showed no first order component and the larger critical exponents i.e. $\alpha' = 0.73 (T>T_c)$, $\alpha = 0.78 (T>T_c)$. This situation is considered to contradict the universality hypothesis, since any difference of the fundamental properties cannot be found between SCD and DSCD. It is interesting to study how the critical exponents and the quasifirst-order component change with the variation of the concentration of the deuteron in water of crystallization. There is a possibility that the system of the solid solutions between SCD and DSCD has a tricritical point, at which the first order line changes to the critical line. Another possibility is that since the present two crystals do not associate with the changes of the crystal symmetry by the phase transitions, our system has a liquid-vapor type critical point as is found in Ce α-γ transition. For the purpose of studying the above problems, we performed the high resolution heat capacity measurement on the solid solutions with various deuteron concentrations. We also carried out the

Raman scattering experiment on SCD single crystal in order to understand more fully the mechanism of the phase transition due to the order-disorder of the positions.

3.2. Experimental and results

3.2.1. Sample preparation

The single crystals of solid solution of SCD and DSCD were prepared in the following manner. Commercial SCD (extra pure grade from Wako Pure Chemical Co., Ltd.) was first dehydrated by evacuation for a week. The extent of dehydration was determined by measurement of the weight loss. An appropriate amount of mixture of normal and 99.75% heavy water(E.Merck) having desired composition was added to the dehydrated crystal together with a small quantity of hydrochloric acid. The slurry obtained was heated up to about 45 °C in a closed glass vessel forming a clear solution and cooled slowly after seeding with a small piece of single crystal. The crystal was grown in the water bath thermostated by the proportional controller(within ±1/100 K) for a month. The sample for the calorimetry was cut from a large single crystal, shaped into a cylinder with dia. 25mm and height 40 mm, and enclosed in a calorimeter cell under atmosphere of helium. All the six single crystals having different isotopic composition were prepared in this manner. For the Raman scattering experiments, single crystal obtained from melt was used. Single crystals having good optical quality were selected and their surface was lapped by filter paper wetted with methanol. The lapped crystals were kept in sealed glass ampoules

to avoid dehydration. The anhydrous sample was prepared from the crushed dihydrate crystal by complete dehydration under high vacuum. The monohydrate containing only the coordinated H_2O molecules was prepared by keeping the dihydrate at 80 °C under one atmosphere of nitrogen for about ten hours[69]. The extent of dehydration was about 45 % which corresponds to the formula $SnCl_2$ $1.1H_2O$.

3.2.2. Determination of the isotopic composition of solid solution

The H_2O concentration in $SnCl_2(H_2O)_{0.96}(D_2O)_{1.04}$ was determined by means of the quantitative absorption intensity measurements of the proton magnetic resonance by use of the high resolution NMR spectrometer(Varian 60). Sevral mixtures of D_2O and H_2O having different mole ratio were used as standards for making the calibration curve. The isotopic mixture of water was collected into the NMR tube by vacuum distillation from the calorimetric crystal after completion of the heat capacity measurement. The error in the determination was found to be ±2 % from the scatter in the calibration of other solid solutions was equal to that of the melt. Though the effect of the hydrochloric acid to the content of proton was corrected, the ambiguity amounted to the maximum(±5 %) at the crystal with highest deuterium concentration of 0.875 mole%.

3.2.3. Heat capacity measurements

The heat capacity measurements were performed on crystals with six different compositions. Table 3 lists the concentra-

Table 3 Summary of solid solutions and aging period

abbreviation	formula	t/month*
x=2.00	$SnCl_2(H_2O)_{2.00}$	3
x=1.97	$SnCl_2(H_2O)_{1.97}(D_2O)_{0.03}$	4
x=1.75	$SnCl_2(H_2O)_{1.75}(D_2O)_{0.25}$	4
x=1.50	$SnCl_2(H_2O)_{1.50}(D_2O)_{0.50}$	7
x=0.96	$SnCl_2(H_2O)_{0.96}(D_2O)_{1.04}$	1
x=0.96(II)	$SnCl_2(H_2O)_{0.96}(D_2O)_{1.04}$	24
x=0.50	$SnCl_2(H_2O)_{0.50}(D_2O)_{1.50}$	4
x=0.50(II)	$SnCl_2(H_2O)_{0.50}(D_2O)_{1.50}$	10
x=0.25	$SnCl_2(H_2O)_{0.25}(D_2O)_{1.75}$	1
x=0.03	$SnCl_2(H_2O)_{0.03}(D_2O)_{1.97}$	1
x=0.03(II)	$SnCl_2(H_2O)_{0.03}(D_2O)_{1.97}$	48

* Time elapsed before starting the measurement after the preparation of the crystal.

tions and the time elapsed before starting the measurement after the preparation of the crystal. The abbreviated designations for each solid solution are also given there. Each measurement was carried out both with ordinary resolution(ΔT 1∿3K) from 11 to 300 K and with high resolution(ΔT 1/100 ∿ 5/100 K) in the vicinity of the transition temperature. Before the high resolution measurement, the transition temperature was apprximately determined by the measurement with ordinary temperature step. It took about fifteen minutes for all crystals to attain thermal equilibrium after switching off the heater current al-

though this period depended on the thermal contact between crystal and calorimeter cell. Longer time was required to determine the final temperature in the high resolution measurement. In all of the isotopic compositions studied, the heat capacity behaved anomalously in two temperature regions. One is around 220 ∿ 230 K region and is due to the order-disorder change in the hydrogen bonding network. The other is a relaxational anomaly around 150 K due to loss of equilibrium in rearrangement of protons in the hydrogen bonding network at the low temperature stage of ordering. Both anomalies change smoothly with the isotopic composition in their characters including the temperature and its interval of their occurence. Calorimetric details for each of the isotopic mixtures are descrived in the following. The numerical values of the heat capacity are given in from Table 4 to Table 10, and heat capacity curves are shown in from Fig. 13 to Fig. 18. The early results for x=2.00 and x=0.03 specimens are mentioned here briefly and the data are given in Ref.[70].

(i) x=2.00: The highly symmetrical shape of the anomaly was observed at 218.01 K with a quasi-isothermal absorption of energy amounting to 32.4 $J\,mol^{-1}$. It is very difficult to distinguish experimentally the small isothermal enthalpy increase (*i.e.* the quasi 1st order component) from the very large heat capacity. The first order component is calorimetrically detected by the discontinuous advent of large endothermic drift with long relaxation time and by the steep rise in the cumulated enthalpy or entropy as a function of temperature(see later).

Table 4. Molar heat capacity of x=1.97.

T/K	C_p/JK^{-1}mol^{-1}	T/K	C_p/JK^{-1}mol^{-1}	T/K	C_p/JK^{-1}mol^{-1}	T/K	C_p/JK^{-1}mol^{-1}
166.40	120.81	258.91	151.36	217.208	155.00		
167.41	121.28	260.41	151.80	217.236	155.15	1-st order region	
168.80	121.93	264.90	152.99	217.265	155.29		
170.34	122.58	266.39	153.55	217.294	155.59		
171.89	123.22	267.90	153.91	217.322	155.89		
173.41	123.91	270.98	154.88	217.351	156.02	218.234	246.46
175.03	124.61	198.39	134.89	217.379	156.54	218.248	222.16
176.76	125.32	199.80	135.71	217.406	156.82	218.263	208.24
178.46	125.99	200.99	136.27	217.431	157.10	218.277	201.15
180.17	126.78	202.03	136.91	217.455	157.36	218.293	195.25
181.85	127.52	203.05	137.32	217.480	157.58	218.308	190.33
183.54	128.23	204.08	137.94	217.504	157.79	218.324	186.79
185.21	129.35	205.11	138.26	217.528	158.13	218.340	183.52
186.79	129.61	206.13	139.31	217.552	158.58	218.357	180.67
188.45	130.39	207.14	139.78	217.576	158.91	218.373	178.06
190.09	131.25	208.14	140.84	217.598	159.27	218.389	176.30
191.74	131.81	209.15	141.13	217.619	159.70	218.406	174.69
193.37	132.57	210.44	141.78	217.638	160.06	218.424	173.28
194.99	133.29	210.961	142.61	217.657	160.67	218.441	172.00
196.62	134.08	211.653	143.21	217.676	160.45	218.459	170.76
198.23	134.90	212.342	143.78	217.695	161.12	218.477	169.87
199.85	136.04	213.029	144.55	217.714	161.39	218.494	168.63
201.43	137.10	213.678	145.31	217.733	161.85	218.512	167.69
203.02	137.27	215.266	147.81	217.746	162.02	218.530	166.94
204.60	138.69	215.559	148.31	217.765	162.70	218.548	166.15
206.17	139.35	215.726	148.75	217.783	163.09	218.566	165.80
207.73	142.73	215.840	148.90	217.802	163.62	218.584	165.11
209.26	141.17	215.931	149.31	217.820	164.17	218.602	164.30
210.81	142.28	216.013	149.44	217.838	164.56	218.620	163.58
212.34	143.68	216.086	149.59	217.854	165.21	218.638	163.36
213.86	145.45	216.158	149.87	217.871	165.90	218.657	162.83
215.37	148.05	216.231	150.13	217.887	166.30	218.678	162.27
216.84	153.26	216.305	150.31	217.904	166.79	218.698	161.74
218.15	202.19	216.370	150.51	217.920	167.32	218.719	161.32
219.47	154.13	216.427	150.76	217.937	168.02	218.740	160.73
222.43	147.20	216.478	150.91	217.953	168.87	218.762	160.31
223.93	146.12	216.517	150.96	217.969	172.32	218.783	160.05
225.43	145.53	216.552	151.10	217.985	170.75	218.805	159.54
226.93	145.26	216.587	151.26	218.002	172.35	218.826	158.93
228.43	145.18	216.623	151.45	218.018	173.29	218.848	158.74
229.93	145.29	216.659	151.53	218.034	174.97	218.870	158.48
231.43	145.48	216.694	151.86	218.049	176.24	218.893	158.19
232.93	145.68	216.729	151.85	218.065	177.58	218.915	157.84
234.45	145.89	216.764	152.02	218.081	179.71	218.939	157.58
236.01	146.19	216.798	152.32	218.096	181.98	218.963	157.24
237.57	146.52	216.831	152.49	218.112	184.51	218.987	157.13
239.12	146.86	216.864	152.62	218.127	187.52	219.012	156.67
240.66	147.02	216.897	152.84	218.143	191.36	219.037	156.54
242.21	147.31	216.930	152.91	218.157	195.86	219.062	156.35
243.75	147.69	216.962	153.27	218.172	201.68	219.087	156.07
245.29	147.90	216.994	153.45	218.186	210.22	219.112	155.53
246.78	148.20	217.025	153.62	218.200	221.87	219.138	155.47
248.31	148.60	217.056	153.86	218.212	253.45	219.164	155.39
249.84	148.91	217.087	153.97	218.222	415.61	219.190	155.42
254.40	150.10	217.118	154.01	1-st order region		219.216	154.60
255.90	150.46	217.149	154.43			219.243	154.79
257.41	150.91	217.179	154.62			219.270	154.22

(continued)

T/K	C_p/JK^{-1}mol^{-1}	T/K	C_p/JK^{-1}mol^{-1}	T/K	C_p/JK^{-1}mol^{-1}
219.298	154.11	41.24	37.09	143.12	107.85
219.325	154.02	42.75	38.63	145.07	108.73
219.353	153.40	44.05	40.14	147.00	109.59
219.381	153.54	45.46	41.70	148.94	110.33
219.410	153.24	47.04	43.41	150.86	111.05
219.438	153.20	48.65	45.17	152.78	111.84
219.468	152.77	50.35	46.92	154.66	113.42
219.498	152.78	52.05	48.73	156.51	116.29
219.528	152.64	53.68	50.43	158.35	117.29
219.559	152.52	55.33	52.13	160.22	117.99
219.591	152.32	56.99	53.56	162.11	118.97
219.624	152.19	58.61	55.07	164.00	119.57
219.658	151.95	60.19	56.88	182.71	127.87
219.692	151.84	61.14	57.40	184.28	128.52
219.727	151.67	62.65	58.72	185.84	129.21
219.762	151.57	64.23	60.11	199.75	135.66
219.799	151.24	65.84	61.15	201.33	136.37
219.840	151.17	67.55	64.38	202.95	137.23
219.883	150.87	69.33	64.42	204.57	138.13
219.927	150.74	71.05	65.85	206.18	139.32
219.973	150.67	72.85	67.32	207.76	144.69
220.020	150.49	74.73	68.80	209.33	141.20
220.078	150.40	76.56	70.23	248.09	148.54
220.202	150.02	78.35	71.56	250.00	148.79
220.401	149.48	80.13	72.87	251.65	149.28
220.690	148.99	81.93	74.18	253.14	149.68
11.24	3.27	83.71	75.43	262.04	152.12
12.21	4.00	85.51	76.69	263.51	152.47
13.66	5.38	87.27	77.86	271.32	155.09
15.09	6.74	88.95	78.98	273.60	155.60
15.99	7.71	90.61	80.04	275.55	156.15
16.81	8.55	92.33	81.20	277.47	156.69
17.60	9.35	94.09	82.29	279.40	157.11
18.32	10.22	95.87	83.39	281.31	157.72
18.99	10.99	97.62	84.51	283.22	158.23
19.71	11.88	99.38	85.55	285.14	159.20
20.48	12.73	101.17	86.65	287.02	159.81
21.29	13.63	102.93	87.69	288.93	160.47
22.12	14.61	104.66	88.72	290.81	161.24
22.88	15.45	106.39	89.68	292.69	161.78
23.67	16.82	108.30	90.76	294.71	162.66
24.46	17.39	110.39	91.91	296.87	163.45
25.22	18.30	112.47	93.02	299.18	164.61
26.10	19.34	114.51	94.11	301.33	165.87
27.13	20.59	116.53	95.17		
28.15	21.80	118.54	96.19		
29.15	23.07	120.60	97.25		
30.18	24.24	122.75	98.32		
31.32	25.68	124.86	99.34		
32.48	27.08	126.96	100.38		
33.48	28.26	129.04	101.33		
34.42	29.26	131.10	102.31		
35.38	30.43	133.16	103.23		
36.34	31.52	135.18	104.19		
37.34	32.68	137.19	105.11		
38.52	34.05	139.18	106.05		
39.82	35.48	141.15	107.00		

Table 5. Molar heat capacity of x=1.75.

T/K	C_p/JK^{-1}mol^{-1}
204.06	138.92
205.57	139.62
207.24	140.68
209.03	141.77
210.79	142.93
212.56	144.05
214.30	146.00
216.06	148.32
217.59	151.60
218.60	155.99
219.34	165.60
219.86	288.57
220.28	166.43
220.80	158.11
221.49	154.40
222.42	152.44
223.60	152.16
224.77	150.37
225.72	147.70
220.96	156.98
221.64	154.05
222.33	152.82
223.03	152.10
223.72	152.40
224.92	149.33
226.64	147.64
228.44	147.71
230.43	147.44
232.57	147.82
279.98	159.37
280.98	159.66
251.10	150.95
252.18	151.28
279.69	159.56
280.68	159.48
281.69	160.04
179.15	127.60
180.80	128.33
182.59	129.14
184.37	129.80
186.30	130.70
188.36	131.70
190.38	132.55
192.42	133.37
194.47	134.27
196.45	135.06
198.46	136.15

T/K	C_p/JK^{-1}mol^{-1}
200.46	137.15
206.33	140.21
208.25	141.23
210.18	142.37
212.12	143.92
214.03	145.68
215.94	147.96
217.82	152.09
219.20	160.79
219.85	261.86
220.33	171.12
221.23	156.06
222.76	154.12
224.59	148.81
226.46	147.96
228.34	147.02
230.29	147.34
232.28	147.36
234.26	147.53
221.47	154.22
222.35	151.50
223.10	150.11
223.85	149.02
224.61	148.78
225.46	148.16
226.56	147.70
227.98	147.39
219.47	190.30
221.00	158.80
222.21	152.21
224.09	148.88
224.82	148.18
225.86	147.91
207.03	140.57
208.66	141.52
210.16	142.44
210.156	142.50
211.177	143.22
212.127	143.99
213.073	144.78
213.937	145.61
215.453	147.20
216.137	148.20
216.733	149.15
217.157	149.99
217.495	150.75
217.793	151.32
217.986	151.98

T/K	C_p/JK^{-1}mol^{-1}
218.106	152.44
218.203	152.99
218.284	153.26
218.353	153.50
218.412	153.82
218.466	154.09
218.524	154.56
218.583	154.56
218.641	154.93
218.699	155.26
218.756	155.22
218.810	156.03
218.860	156.30
218.904	156.55
218.945	156.92
218.987	157.23
219.025	157.72
219.061	157.86
219.097	158.42
219.133	158.68
219.169	159.09
219.205	159.54
219.238	159.85
219.269	160.37
219.298	160.81
219.324	161.25
219.351	161.78
219.377	162.33
219.402	162.72
219.424	163.67
219.444	163.52
219.464	161.83
219.484	164.01
219.503	164.65
219.523	165.53
219.538	165.91
219.558	166.78
219.577	167.08
219.596	167.62
219.615	168.36
219.632	169.28
219.649	170.30
219.667	170.72
219.684	172.01
219.700	173.01
219.716	174.00
219.725	175.19
219.738	176.47
219.751	178.29
219.764	178.74
219.776	179.53
219.789	181.75
219.801	183.25
219.813	185.03
219.825	187.24
219.837	189.87
219.848	192.38
219.859	195.45
219.871	198.13

T/K	C_p/JK^{-1}mol^{-1}
219.882	203.46
219.893	209.05
219.903	216.25
219.914	225.35
219.924	237.31
219.933	254.78
219.942	285.35
219.950	328.41
219.956	457.50
	1-st order region
219.975	556.62
219.982	300.42
219.991	265.96
220.000	243.62
220.010	228.36
220.021	219.36
220.032	211.01
220.043	204.79
220.055	199.59
220.067	194.65
220.079	191.40
220.091	188.90
220.104	186.48
220.116	184.54
220.128	182.23
220.141	180.94
220.154	178.95
220.168	177.70
220.182	176.07
220.196	174.95
220.210	173.84
220.225	172.99
220.239	171.88
220.253	170.84
220.268	170.27
220.284	169.53
220.300	168.75
220.316	168.38
220.333	168.40
220.350	166.88
220.368	166.31
220.387	165.74
220.407	165.16
220.426	164.48
220.402	24.13
220.465	163.61
220.475	163.10
220.495	162.74
220.516	162.34
220.537	161.68
220.558	161.44
220.579	161.17
220.600	161.00

Table 6. Molar heat capacity of x=1.50.

T/K	C_p/JK^{-1}mol^{-1}	T/K	C_p/JK^{-1}mol^{-1}	T/K	C_p/JK^{-1}mol^{-1}	T/K	C_p/JK^{-1}mol^{-1}	T/K	C_p/JK^{-1}mol^{-1}
198.46	136.63	163.05	121.20	220.445	156.75	221.785	221.11	222.494	165.36
199.70	137.64	164.14	121.69	220.476	157.03	221.796	229.21	222.509	165.34
200.95	138.03	165.23	122.19	220.512	156.72	221.807	238.83	222.525	164.46
202.34	138.98	166.31	122.61	220.548	157.48	221.818	250.57	222.540	164.57
203.83	139.63	167.40	123.09	220.584	157.46	221.828	266.17	222.556	163.99
205.26	140.29	168.46	123.63	220.619	157.86	221.838	284.06	222.572	163.70
206.69	141.08	169.54	124.12	220.653	157.78	221.847	306.45	222.588	163.98
208.15	141.87	170.81	124.65	220.687	158.27	221.856	344.73	222.603	163.24
209.59	142.72	172.38	125.35	220.721	158.46	221.863	396.40	222.619	162.81
210.99	143.60	174.00	125.99	220.755	158.64	221.870	465.68	222.635	162.57
212.38	144.47	175.63	126.95	220.789	159.01	221.876	571.29	222.651	162.27
213.76	145.53	173.43	125.82	220.823	159.39	221.881	459.08	222.667	162.10
215.15	146.67	175.28	126.63	220.852	159.26	221.888	422.80	222.684	161.89
216.53	148.09	177.12	127.45	220.884	159.72	221.895	382.22	222.700	161.38
217.93	149.86	178.95	128.24	220.917	160.07	221.903	357.60	222.716	161.48
219.42	153.64	180.77	129.07	220.950	160.23	221.912	329.33	222.732	161.22
220.68	159.19	182.68	129.91	220.983	161.01	221.921	304.43	222.748	161.04
221.74	202.54	184.69	130.77	221.015	161.29	221.930	287.57	222.765	160.98
223.17	158.24	186.68	131.68	221.047	161.60	221.940	268.62	222.781	160.80
224.49	153.40	188.67	132.61	221.077	162.00	221.951	255.16	222.797	160.15
225.77	151.26	190.63	133.44	221.106	162.60	221.961	242.62	222.814	160.05
227.13	149.98	192.59	134.25	221.135	162.85	221.973	168.43	222.830	161.44
228.48	149.32	194.54	135.37	221.163	163.44	221.982	223.67	222.847	160.60
229.84	149.05	196.48	136.11	221.191	163.81	221.993	218.73	222.864	159.53
		198.40	136.95	221.219	164.27	222.006	214.50	222.882	159.62
		200.16	137.86	221.247	164.70	222.018	208.52	222.899	159.49
		201.74	138.73	221.273	165.54	222.030	203.10	222.917	159.00
125.50	101.07	203.15	139.34	221.297	166.06	222.043	200.24	222.935	159.19
126.55	101.57	204.40	139.93	221.314	165.84	222.056	195.20	222.953	159.09
127.64	102.12	205.64	140.54	221.334	166.39	222.069	193.12	222.967	158.42
128.82	102.67	206.79	141.30	221.353	167.38	222.082	190.70	222.986	158.40
130.19	103.27	207.85	141.89	221.372	167.75	222.096	188.47	223.004	158.39
131.36	103.96	208.89	142.43	221.390	168.63	222.109	186.51	223.023	158.24
132.60	104.52	209.87	143.09	221.409	169.32	222.123	185.04	223.042	157.63
133.83	105.09	210.78	143.45	221.426	169.89	222.133	182.32	223.058	157.84
135.06	105.66			221.444	170.50	222.147	181.06	223.078	157.88
136.28	106.25	215.583	147.06	221.461	171.10	222.161	179.74	223.098	157.97
137.50	106.78	216.128	147.60	221.478	172.00	222.175	178.39	223.118	157.91
138.71	107.39	216.593	148.11	221.495	172.80	222.189	178.27	223.139	157.53
139.91	108.38	217.046	148.62	221.512	173.89	222.202	176.64	223.162	157.25
141.12	108.59	217.470	149.16	221.528	175.26	222.217	175.98	223.184	157.52
142.32	109.13	217.845	149.39	221.543	176.12	222.231	174.95	223.206	157.16
143.50	109.43	218.144	150.07	221.559	176.07	222.245	174.39	223.228	157.15
144.70	110.21	218.399	150.52	221.573	177.77	222.259	173.32	223.252	157.00
145.89	110.77	218.640	150.96	221.588	178.44	222.273	172.35	223.278	156.75
147.08	111.28	218.867	151.46	221.602	179.83	222.288	171.91	223.303	156.68
148.25	111.80	219.075	151.83	221.616	181.38	222.302	171.58	223.329	156.51
149.44	112.26	219.276	152.36	221.630	183.55	222.317	170.58	223.355	156.61
150.62	112.83	219.468	152.83	221.644	183.52	222.331	170.10	223.382	156.06
151.81	113.27	219.652	153.42	221.658	185.32	222.346	169.22	223.409	156.25
152.98	113.77	219.813	153.90	221.671	187.52	222.360	169.08	223.438	155.86
154.15	114.31	219.950	154.27	221.685	189.57	222.375	168.17	223.468	155.97
155.30	115.45	220.062	154.74	221.698	192.24	222.390	167.94	223.498	155.63
156.42	117.98	220.141	155.12	221.711	194.54	222.404	167.49	223.528	155.85
157.54	118.87	220.205	155.43	221.724	197.79	222.419	167.25	223.558	155.30
158.64	119.21	220.260	155.57	221.736	200.65	222.434	166.41	223.588	155.43
159.75	119.71	220.311	155.94	221.749	204.78	222.449	166.43	223.619	155.28
160.86	120.38	220.357	156.20	221.761	212.19	222.464	166.04	223.650	155.15
161.96	120.74	220.402	156.51	221.773	214.91	222.479	165.03	223.682	155.15

(continued)

T/K	C_p/JK^{-1}mol^{-1}	T/K	C_p/JK^{-1}mol^{-1}	T/K	C_p/JK^{-1}mol^{-1}	T/K	C_p/JK^{-1}mol^{-1}
223.714	155.00	58.99	55.72	238.93	149.63	26.73	20.17
223.748	154.87	60.35	56.99	240.23	149.82	27.80	21.49
223.783	154.73	61.80	58.30	241.51	150.13	28.81	22.71
223.819	154.46	63.35	59.68	242.87	150.22	29.75	23.85
223.855	154.39	64.87	61.00	244.29	150.70	30.74	25.04
223.891	154.44	66.32	62.28	245.71	150.83	31.86	26.40
223.931	154.24	67.85	63.56	247.13	151.25	32.96	27.76
223.976	153.88	69.42	64.92	248.54	151.52	33.96	28.94
224.020	153.77	70.97	66.21	250.05	151.91	34.92	30.06
224.065	153.81	72.49	67.47	251.68	152.33	35.88	31.22
224.111	153.92	73.96	68.69	253.31	152.80	36.79	32.24
224.158	153.79	75.54	69.90	254.92	153.20	37.74	33.32
224.213	153.45	77.21	71.21	256.54	153.46	38.71	34.42
224.274	153.50	78.34	72.45	258.15	153.94	39.64	35.44
224.335	153.28			259.85	154.40	40.62	36.55
224.397	153.40			261.46	154.81	41.67	37.74
224.457	152.72	80.44	73.67	263.24	155.32	42.69	38.87
224.522	152.92	82.01	74.70	265.03	155.82	43.77	40.07
224.591	153.01	83.56	75.96			44.92	41.31
224.662	152.67	84.98	77.00			46.01	42.54
224.731	152.76	86.57	78.08	266.81	156.35	47.08	43.67
224.805	152.44	88.17	79.12	268.59	156.87	48.15	44.82
224.880	152.40	89.86	80.27	270.47	157.37		
224.931	152.69	91.52	81.42	272.53	158.08		
224.981	152.44	93.18	82.45	274.64	158.61		
225.081	152.30	94.79	83.56	276.75	159.30		
225.203	152.17	96.36	84.52	278.85	160.06		
225.325	152.10	97.92	85.58	280.93	160.56		
225.473	152.08	99.45	86.48	283.01	161.16	49.22	46.00
225.643	151.48	101.03	87.51	285.08	161.77	50.48	47.31
225.861	151.60	102.63	88.45	287.15	162.55	51.91	48.84
226.166	151.01	104.22	89.41	289.21	163.21	53.31	50.20
226.517	150.16	105.78	90.37	291.23	164.07	54.75	51.68
226.868	150.00	107.34	91.23	293.28	164.41	56.23	53.10
227.219	149.90	108.88	92.17	295.39	165.01	57.67	54.48
227.661	149.72	110.41	93.01	297.60	165.80	59.06	55.77
228.193	149.44	111.91	93.81	299.88	166.63		
228.771	149.27	113.42	94.71	302.24	167.64		
229.385	148.74	114.95	95.52				
229.992	148.95	116.54	96.28			130.04	103.22
230.608	148.95	118.09	97.24			131.70	104.06
231.240	148.89	119.63	98.04	13.14	4.87	133.51	104.89
231.967	148.85	121.18	98.83	13.75	5.48	135.41	105.80
232.774	148.89	122.70	99.66	14.32	6.00	137.29	106.67
233.581	149.00	124.22	100.38	15.18	6.88	139.22	107.53
234.388	148.99	125.72	101.20	16.35	7.97	141.19	108.43
235.195	149.04			17.18	8.94	143.15	109.37
236.001	149.21			18.00	9.85	145.15	110.38
236.801	149.22			18.77	10.74	147.08	111.26
237.605	149.36	227.43	149.82	19.46	11.54	148.99	112.08
238.409	149.62	228.84	149.34	20.19	12.40	150.84	112.96
		230.27	149.09	20.94	13.25	152.60	114.84
239.33	149.27	231.45	148.99	21.75	14.20	154.40	117.15
240.38	149.78	232.63	148.98	22.62	15.23	156.24	117.95
241.49	150.00	233.81	148.95	23.42	16.17	158.07	118.62
242.70	149.71	235.05	149.11	24.18	17.07	159.98	119.73
243.90	150.81	236.34	149.33	24.96	18.05	162.03	120.61
		237.64	149.38	25.77	19.07	164.24	121.63

Table 7. Molar heat capacity of x=0.96.

T/K	C_p/JK^{-1}mol^{-1}	T/K	C_p/JK^{-1}mol^{-1}	T/K	C_p/JK^{-1}mol^{-1}	T/K	C_p/JK^{-1}mol^{-1}	T/K	C_p/JK^{-1}mol^{-1}
11.60	3.53	74.45	69.58	180.41	131.05	136.69	108.12	216.792	149.10
12.34	4.13	76.29	71.07			138.88	109.23	217.281	149.43
12.94	4.67	78.34	72.59	182.29	131.97	141.04	110.30	217.673	149.69
13.47	5.18	80.22	74.11	184.25	132.83			218.021	149.96
13.95	5.66	82.42	75.72	186.20	133.71			218.379	150.20
14.40	6.10	84.94	77.55	188.12	134.60	143.01	111.30	218.715	150.62
14.82	6.52	75.41	70.34	190.31	135.60	144.80	112.12	219.028	150.88
15.20	6.92	77.70	72.20	192.03	136.44	146.66	112.97	219.342	151.16
15.60	7.32	79.96	73.87	193.56	137.01	148.34	113.75	219.639	151.47
16.09	7.83	82.39	75.75	195.06	137.84	150.11	114.45	220.573	152.33
16.67	8.47	84.78	77.50	196.57	138.46	151.87	115.22	220.884	152.63
17.24	9.05	87.33	79.33	198.07	139.13	153.65	115.99	221.188	153.15
17.78	9.63	89.82	81.04	199.57	139.78	155.43	116.91	221.497	153.67
18.35	10.30	92.06	82.55	201.06	140.47	157.19	118.61	221.806	154.05
18.98	11.02	94.24	84.03	202.55	141.22	158.94	120.89	222.114	154.50
19.56	11.70	96.37	85.46	204.03	141.92	160.67	121.71	222.581	155.46
20.14	12.49	98.48	86.84	205.49	142.67	162.39	122.82	222.897	156.20
20.79	13.15	100.55	88.18	207.08	143.40			223.069	156.55
22.07	14.63	102.59	89.48	208.64	144.20			223.205	157.02
22.69	15.38	104.56	90.69	210.23	145.01			223.305	157.32
23.29	16.10	106.54	91.91	211.81	145.91	193.62	137.04	223.405	157.75
23.94	16.89	108.50	93.08	213.40	146.80	195.10	137.75	223.508	158.04
24.69	17.78	110.51	94.25	214.96	147.79	200.84	140.36	223.605	158.37
25.52	18.73	112.56	95.45	216.53	148.84	202.49	141.15	223.690	158.13
26.28	19.72	114.57	96.61	218.09	150.03	204.13	141.88	223.769	158.66
27.06	20.68	116.57	97.72	219.63	151.38	205.76	142.66	223.836	159.06
27.94	21.75	118.55	98.84	221.16	153.12	207.38	143.50	223.893	158.89
28.86	22.86	120.51	99.85	222.68	155.69	208.98	144.37	223.938	159.11
29.78	24.05	122.45	100.92	224.17	161.22	210.55	145.19	224.028	159.56
30.69	25.25	124.36	101.93	225.55	189.83	212.07	146.08	224.064	159.50
31.62	26.31	126.26	102.94	226.92	169.89			223.983	159.32
32.68	27.61	128.15	103.88	228.37	158.16			224.092	159.63
33.80	28.95	130.07	104.89	229.84	155.45			224.118	160.19
34.86	30.13	132.06	105.90	231.33	154.32	253.56	156.16	224.162	160.47
35.94	31.44	134.02	106.84	232.83	153.73	255.28	156.68	224.192	160.58
37.12	32.81	135.97	107.78	234.34	153.45	257.46	157.05	224.236	160.44
38.36	34.19	137.90	108.73	235.84	153.28	259.85	157.91	224.280	160.98
39.62	35.67	139.82	109.63	237.35	153.31	262.24	158.38	224.325	161.21
40.97	37.01	141.74	110.70	239.53	153.41	264.62	158.97	224.366	161.60
42.14	38.45	143.63	111.59	241.17	153.70	266.99	159.68	224.403	161.69
43.54	40.00	145.51	112.45	242.80	153.93	269.30	160.24	224.441	162.20
45.08	41.72	147.38	113.34	244.43	154.25	271.65	161.03	224.478	162.61
46.61	43.38	149.23	114.15	246.05	154.52	274.00	161.63	224.509	162.55
48.06	44.95	151.08	114.92	247.71	154.77	276.34	162.32	224.536	162.73
49.53	46.55	152.92	115.75	249.36	155.02	278.69	162.97	224.564	163.21
51.05	48.19	154.73	116.85	251.00	155.79	281.06	163.66	224.591	163.43
52.59	49.87	156.53	118.18	252.67	155.92	283.47	164.59	224.619	163.75
54.08	51.39	158.29	120.61	254.37	156.41	285.88	165.25	224.646	164.02
55.59	52.98	160.04	120.71	256.06	156.98	288.27	166.07	224.673	164.16
57.16	54.57	161.78	122.06			290.74	166.82	224.701	163.90
58.72	56.25	163.52	123.24			293.22	167.66	224.728	164.84
60.30	57.62	165.28	124.47			295.78	168.37	224.755	165.42
61.95	59.18	167.02	125.17	133.97	106.78	298.42	169.24	224.782	165.53
63.66	60.80	168.89	125.83	135.81	107.70			224.808	148.22
65.33	62.31	170.76	126.63	137.82	108.66			224.836	166.18
67.03	64.24	172.61	127.55			214.343	147.53	224.863	166.59
68.87	65.08	174.51	128.44			215.064	148.01	224.890	166.91
70.79	66.82	176.51	129.31			215.691	148.32	224.917	167.24
72.66	68.01	178.49	130.14	134.50	107.06	216.238	148.67	224.944	167.77

(continued)

T/K	C_p/JK^{-1}mol^{-1}
224.971	168.13
224.998	168.58
225.024	169.22
225.049	169.56
225.072	170.18
225.095	170.71
225.118	171.48
225.141	171.80
225.164	172.40
225.187	172.97
225.209	173.64
225.232	174.16
225.255	174.92
225.276	175.53
225.297	176.25
225.318	177.04
225.338	177.66
225.359	178.78
225.379	179.56
225.400	180.13
225.421	181.11
225.441	182.15
225.461	183.03
225.481	184.54
225.501	185.44
225.521	186.64
225.541	187.40
225.560	188.77
225.580	190.30
225.599	191.64
225.595	191.62
225.617	193.41
225.636	194.23
225.656	197.13
225.673	197.99
225.689	199.59
225.705	201.05
225.720	202.03
225.736	203.52
225.751	204.49
225.767	205.90
225.782	207.60
225.797	208.49
225.812	210.06
225.827	210.43
225.843	211.93
225.858	213.34
225.873	213.72
225.887	214.53
225.902	214.63
225.917	214.38
225.932	214.83
225.947	213.82
225.962	213.81
225.977	212.97
225.992	212.24
226.007	211.20

T/K	C_p/JK^{-1}mol^{-1}
226.022	210.74
226.037	208.98
226.052	207.75
226.068	206.29
226.083	204.88
226.099	202.67
226.114	201.41
226.130	200.12
226.146	198.74
226.161	197.32
226.177	195.98
226.193	193.99
226.209	193.01
226.226	191.83
226.242	190.66
226.258	189.52
226.275	188.87
226.291	187.08
226.308	186.18
226.324	185.09
226.341	184.30
226.358	183.18
226.374	182.31
226.392	181.23
226.409	180.65
226.426	179.79
226.443	179.09
226.460	178.34
226.477	177.73
226.494	176.80
226.512	176.24
226.529	175.82
226.546	175.19
226.564	174.52
226.582	173.59
226.599	173.33
226.619	172.92
226.640	172.36
226.661	171.97
226.682	171.29
226.705	170.63
226.727	170.13
226.748	169.85
226.769	169.31
226.791	168.90
226.812	168.57
226.833	168.06
226.855	167.78
226.876	167.57
226.898	167.24
226.919	166.56
226.941	166.32
226.962	166.06
226.984	165.85
227.006	165.47
227.031	165.17
227.058	164.85

T/K	C_p/JK^{-1}mol^{-1}
227.085	165.46
227.112	164.38
227.139	163.98
227.166	163.62
227.194	163.44
227.221	163.29
227.248	163.02
227.276	162.82
227.303	162.58
227.330	162.39
227.358	162.10
227.385	162.02
227.413	161.66
227.440	161.40
227.468	161.36
227.495	161.15
227.523	161.03
227.555	160.77
227.592	160.65
227.629	160.50
227.666	160.30
227.703	160.18
227.740	159.99
227.777	159.80
227.815	159.63
227.852	159.51
227.889	159.27
227.926	159.18
227.963	159.32
228.000	158.97
228.056	158.77
228.131	158.51
228.205	158.26
228.289	158.03
228.383	157.85
228.481	157.54
228.583	157.42
228.686	157.12
228.791	156.92
228.923	156.69
229.073	156.34
229.230	156.11
229.415	155.88
229.626	155.63
229.837	155.44
230.056	155.16
230.284	154.94
230.513	154.81
230.772	154.61
231.074	154.40
231.377	154.21
231.680	154.14
231.982	154.05
232.286	153.97
232.640	153.74
232.995	153.64
233.349	153.62

T/K	C_p/JK^{-1}mol^{-1}
233.704	153.54
234.091	153.47
234.511	153.47
234.930	153.40
235.295	153.31
235.712	153.41
236.174	153.38
236.930	153.45
237.812	153.55
208.70	144.24
211.44	145.41
213.51	146.73
215.83	148.32
218.12	149.96
220.39	152.28
222.064	154.36
223.022	156.18
223.722	158.11
224.196	159.80
224.532	161.65
224.823	163.98
225.028	166.31
225.154	168.23
225.270	170.79
225.373	173.75
225.463	177.82
225.548	183.19
225.613	189.45
225.662	196.85
225.699	204.57
225.739	216.17
225.775	231.81
225.810	252.88
225.842	276.53
225.873	294.52
225.899	294.62
225.921	279.54
225.950	255.84
225.987	228.59
226.028	211.83
226.070	200.40
226.114	192.49
226.164	186.23
226.219	181.37
226.273	178.17
226.335	175.29
226.404	173.19
226.484	171.01
226.588	168.36
226.705	166.39
226.831	164.80
227.002	162.75
227.243	161.39
227.564	159.74
227.929	158.48
228.388	157.29
229.044	156.09

Table 8. Molar heat capacity of x=0.50.

T/K	C_p/JK^{-1}mol^{-1}	T/K	C_p/JK^{-1}mol^{-1}	T/K	C_p/JK^{-1}mol^{-1}	T/K	C_p/JK^{-1}mol^{-1}	T/K	C_p/JK^{-1}mol^{-1}
223.08	155.37	227.680	164.66	229.051	245.71	229.973	169.52	238.895	156.89
224.44	156.68	227.732	164.84	229.064	254.08	229.998	169.32	239.592	156.46
225.78	158.67	227.779	165.08	229.076	264.37	230.025	169.12	240.318	156.85
227.11	162.54	227.822	165.34	229.088	280.27	230.053	168.75	241.134	156.93
228.39	175.93	227.862	165.75	229.099	282.07	230.082	168.49	242.039	156.97
229.60	198.48	227.902	165.72	229.110	294.50	230.112	167.98	242.943	157.17
230.83	163.82	227.942	166.18	229.121	299.18	230.141	167.84		
232.14	160.52	227.979	166.71	229.131	304.81	230.170	167.87		
233.48	158.67	228.013	166.82	229.142	304.95	230.200	166.79	243.85	157.36
234.82	157.80	228.047	167.09	229.152	306.51	230.231	166.75	245.57	157.41
236.16	157.57	228.081	167.43	229.163	299.71	230.263	166.51	246.47	157.74
237.50	157.10	228.114	167.68	229.174	297.36	230.296	165.96	247.47	157.92
		228.138	167.98	229.185	288.20	230.327	166.34	248.55	158.22
		228.171	168.31	229.196	279.40	230.361	166.00	249.63	158.65
		228.203	168.55	229.208	267.57	230.395	165.58	250.70	158.97
199.67	141.58	228.235	168.90	229.220	257.11	230.429	165.51	251.90	160.26
201.14	142.20	228.265	169.59	229.232	247.19	230.466	165.28	253.20	163.30
202.60	142.78	228.294	169.77	229.245	240.05	230.506	165.13	254.68	160.64
205.49	144.44	228.323	170.18	229.258	230.38	230.546	164.85	256.34	160.08
206.93	145.10	228.351	170.61	229.271	224.25	230.587	165.14	258.00	160.39
208.35	145.95	228.379	170.44	229.285	216.71	230.630	164.55	259.66	160.81
209.78	146.60	228.407	171.03	229.299	212.76	230.675	164.14	261.49	160.79
212.63	147.96	228.433	170.92	229.314	207.75	230.731	163.92	267.65	162.03
213.93	148.79	228.457	171.69	229.328	203.90	230.786	163.64	269.77	162.49
215.10	149.40	228.481	172.70	229.343	200.36	230.840	163.62	271.89	163.15
216.26	150.12	228.503	172.79	229.358	197.89	230.901	163.49	276.88	165.30
217.28	150.73	228.525	173.13	229.373	194.08	230.969	163.16	278.17	165.95
218.14	151.28	228.546	173.75	229.388	192.79	231.037	162.77	280.34	166.66
219.00	151.73	228.567	174.53	229.404	190.91	231.106	162.62	282.64	167.31
219.86	152.60	228.588	174.81	229.420	188.76	231.181	162.38	284.93	168.00
220.633	152.92	228.607	175.34	229.436	190.68	231.264	162.18	287.17	168.75
221.315	153.59	228.627	176.24	229.452	185.71	231.346	161.87	289.40	169.50
221.954	154.19	228.645	176.64	229.452	187.59	231.429	161.72	291.63	170.03
222.474	154.68	228.663	177.31	229.485	183.61	231.504	161.41	293.84	171.57
222.920	155.08	228.681	178.17	229.502	182.44	231.628	161.18		
223.364	155.49	228.698	179.19	229.518	181.79	231.752	160.91		
223.733	155.87	228.715	178.86	229.535	180.68	231.876	160.69	296.10	171.93
224.028	156.23	228.732	180.67	229.550	179.58	232.021	160.50	298.39	172.74
224.322	156.57	228.749	180.80	229.567	179.43	232.188	160.16	300.84	173.73
224.616	156.96	228.766	181.78	229.584	180.56	232.364	159.86		
224.878	157.32	228.782	182.54	229.602	178.05	232.547	159.64		
225.108	157.65	228.799	183.43	229.619	177.37	232.741	159.40		
225.338	158.01	228.815	184.23	229.637	176.39	232.945	159.19	242.34	157.24
225.568	158.44	228.832	186.40	229.654	177.22	233.150	158.91	245.10	157.84
225.785	158.77	228.848	187.81	229.672	175.36	233.354	158.81	246.52	157.69
225.999	159.25	228.864	188.78	229.691	174.52	233.577	158.61	247.94	157.87
226.206	159.68	228.880	190.90	229.711	174.00	233.811	158.39	249.44	158.47
226.406	160.08	228.895	193.16	229.731	173.85	234.040	158.31	251.00	159.05
226.591	160.53	228.911	195.77	229.753	173.35	234.269	158.11	252.56	160.00
226.764	161.02	228.926	198.04	229.774	172.99	234.512	158.07	254.10	160.82
226.935	161.59	228.941	201.49	229.795	172.66	234.770	157.85	255.66	160.29
227.096	161.49	228.956	204.27	229.817	172.01	235.065	157.74	257.26	160.11
227.228	162.51	228.971	208.36	229.838	171.55	235.398	157.60	258.93	160.97
227.328	162.95	228.985	212.63	229.861	170.60	235.815	157.48	260.67	161.23
227.418	163.26	228.999	217.36	229.884	171.19	236.309	157.26	262.67	161.80
227.493	163.48	229.012	223.26	229.907	170.35	236.893	157.15	264.81	161.99
227.564	163.80	229.026	229.96	229.930	170.38	237.560	157.08	267.05	162.78
227.626	159.48	229.039	238.29	229.953	169.88	238.227	156.95	269.36	163.36

(continued)

T/K	C_p/JK^{-1}mol^{-1}
271.69	164.07
274.04	164.61
276.40	165.20
10.62	2.88
11.59	3.56
12.39	4.17
13.09	4.84
13.70	5.45
14.33	6.04
15.01	6.74
15.72	7.49
16.42	8.19
17.11	8.96
17.85	9.74
18.63	10.61
19.36	11.51
20.05	12.28
20.77	13.17
21.52	14.04
22.33	14.89
23.20	16.15
24.01	17.03
24.77	17.95
25.52	19.27
26.25	19.75
27.14	20.82
28.17	22.11
29.13	23.30
30.13	24.53
31.16	25.79
32.19	27.07
33.21	28.32
34.19	29.48
35.12	30.63
36.01	31.65
36.95	32.77
37.91	33.85
38.81	34.89
39.73	35.96
40.65	36.96
41.56	38.00
42.58	39.05
43.65	40.33
44.91	41.74
46.39	43.29
47.72	44.85
49.04	46.28
50.33	47.64
51.65	49.09
53.01	50.45
54.35	51.90
55.76	53.28
57.18	54.65

T/K	C_p/JK^{-1}mol^{-1}
58.55	56.02
59.89	57.27
61.20	58.50
62.70	59.86
64.30	61.32
67.78	62.67
67.23	63.91
68.72	65.24
70.24	66.54
71.74	67.81
73.31	69.16
74.98	70.54
76.62	71.86
78.22	73.16
79.79	74.26
81.34	75.55
82.96	76.76
84.66	78.05
86.34	79.30
87.99	80.44
89.61	81.63
91.21	82.73
92.79	83.83
94.35	84.95
95.88	85.97
97.40	87.00
98.91	88.03
100.39	88.93
101.86	90.00
103.42	90.90
105.08	92.07
106.71	92.96
108.32	94.02
109.91	95.01
111.48	95.98
113.05	96.78
114.60	97.70
116.14	98.64
117.66	99.52
119.17	100.36
120.67	101.18
122.16	101.95
123.66	102.82
125.17	103.64
126.68	104.44
128.24	105.26
129.64	105.99
131.01	106.75
132.57	107.54
134.14	108.35
135.63	109.15
137.07	109.83
138.26	110.38
139.44	110.91
140.65	111.64
141.85	112.25

T/K	C_p/JK^{-1}mol^{-1}
143.05	112.83
144.23	113.40
145.42	113.97
146.61	114.56
147.84	115.18
149.06	115.67
150.25	116.23
151.43	116.83
152.60	117.25
153.77	117.85
154.94	118.15
156.10	118.88
157.25	119.36
159.25	123.52
160.14	123.61
161.27	124.28
162.48	124.62
163.75	125.25
165.07	125.88
166.38	126.49
167.69	127.15
169.00	127.70
170.29	128.30
171.57	128.86
172.85	129.38
174.27	129.99
175.82	130.63
178.93	132.23
180.48	133.07
182.02	133.79
183.54	134.52
185.07	135.12
186.70	135.88
188.42	136.67
190.14	137.43
191.84	138.20
193.57	138.98
195.29	139.76
196.98	140.56
198.66	141.21
200.32	142.05
201.99	142.94
203.64	143.54
205.29	144.44
173.67	129.86
175.24	130.58
176.80	131.33
178.37	131.97
243.09	157.34
244.33	157.43
245.56	157.49
246.78	457.84
248.04	157.89
249.37	158.68

T/K	C_p/JK^{-1}mol^{-1}
250.71	159.02
252.09	159.94
253.44	162.82
254.88	160.17
256.42	160.24
257.97	160.64
259.57	161.06
261.50	161.33
263.74	161.80
265.90	162.39
228.969	207.31
228.984	212.22
228.998	217.34
229.011	222.77
229.024	230.41
229.038	235.43
229.051	243.69
229.063	254.37
229.075	263.92
229.087	275.22
229.099	284.49
229.110	293.39
229.120	301.73
229.131	303.62
229.142	308.36
229.152	306.75
229.162	272.06
229.173	299.28
229.184	286.81
229.196	278.97
229.207	268.89
197.26	140.77
198.56	141.42
200.23	142.01
202.11	142.90
204.25	143.80
206.64	145.06
209.46	146.53
212.70	148.17
216.89	150.02
219.05	151.97
221.44	153.62
222.94	155.25
224.181	156.59
225.170	157.96
225.929	159.25
226.493	160.54
226.974	161.63
227.330	162.99
227.570	164.12
227.808	165.41
227.985	166.74
228.103	167.64
228.220	168.87
228.336	170.29
228.452	172.26
228.561	174.57
228.657	177.59

T/K	C_p/JK^{-1}mol^{-1}
228.736	180.99
228.796	184.95
228.849	189.71
228.893	195.65
228.930	202.33
228.959	209.95
228.982	217.49
229.000	226.37
229.017	235.22
229.031	245.42
229.045	256.78
229.058	269.98
229.069	280.27
229.081	292.32
229.092	299.90
229.103	309.23
229.114	313.46
229.125	316.22
229.135	314.75
229.146	310.31
229.157	302.22
229.168	291.22
229.179	279.40
229.191	266.97
229.204	255.33
229.217	244.58
229.230	234.74
229.244	226.49
229.258	220.03
229.273	213.05
229.288	208.20
229.304	203.87
229.320	200.18
229.337	196.98
229.353	194.42
229.376	191.34
229.400	188.39
229.426	186.00
229.458	183.60
229.495	181.27
229.535	179.47
229.580	177.47
229.630	175.88
229.690	174.17
229.769	172.44
229.860	170.86
229.951	169.48
230.052	168.21
230.166	167.25
230.343	165.98
230.579	164.66
230.816	163.63
231.063	162.73
231.370	161.85
231.786	160.97
232.259	160.23
232.854	159.51
233.645	158.81

Table 9. Molar heat capacity of x=0.25.

T/K	C_p/JK^{-1}mol^{-1}	T/K	C_p/JK^{-1}mol^{-1}	T/K	C_p/JK^{-1}mol^{-1}	T/K	C_p/JK^{-1}mol^{-1}	T/K	C_p/JK^{-1}mol^{-1}	T/K	C_p/JK^{-1}mol^{-1}
196.76	141.48	231.31	184.85	162.64	125.66	229.784	169.39	231.146	198.49	14.04	5.82
198.17	141.98			164.39	126.44	229.859	169.86	231.163	196.20	14.66	6.54
199.85	142.86			166.21	127.30	229.926	170.42	231.180	193.96	15.26	7.04
201.68	143.72	55.62	53.40	168.20	128.30	229.990	171.04	231.198	191.66	15.82	7.61
203.53	144.55	57.84	55.59	170.17	129.24	230.054	171.77	231.217	189.70	16.40	8.18
205.41	145.32	62.05	59.51	172.12	130.06	230.116	172.18	231.222	188.57	17.05	8.86
207.32	146.48	64.02	61.29	174.06	131.05	230.164	173.64	231.243	187.30	17.81	9.70
209.17	147.37	65.91	63.41	175.99	131.79	230.207	174.79	231.263	186.08	18.53	10.55
211.10	148.39	67.76	64.60	177.91	132.97	230.247	174.43	231.284	184.76	19.22	11.30
214.97	150.31	69.55	66.20	179.81	133.72	230.285	175.86	231.305	183.54	19.88	12.07
216.91	151.36	71.29	67.71	181.67	134.78	230.323	177.60	231.326	182.38	20.50	12.87
218.81	152.48	73.00	69.15	183.55	135.37	230.360	178.78	231.349	180.72	21.08	13.56
220.72	153.68	74.79	70.68	185.43	136.28	230.398	179.47	231.372	179.61	21.64	14.20
222.63	155.21	76.65	72.21	187.34	137.19	230.433	181.77	231.394	179.07	22.25	14.92
224.40	156.90	78.48	73.67	189.27	137.93	230.467	182.03	231.417	178.10	22.99	15.82
226.02	158.64	80.37	75.18	191.20	138.96	230.500	184.56	231.440	177.50	23.77	16.70
227.63	161.19	82.34	76.67	193.13	139.78	230.529	186.17	231.467	176.89	24.51	17.71
229.21	166.72	84.27	78.14	195.04	140.62	230.552	188.00	231.500	175.83	25.24	18.56
230.86	201.92	86.14	79.50	196.92	141.46	230.573	188.18	231.535	175.05	26.18	19.70
232.14	169.43	87.98	80.84			230.593	190.13	231.561	174.11	27.26	21.03
233.70	162.67	89.79	82.14			230.612	192.17	231.598	173.40	28.32	22.37
235.30	160.79	91.57	83.43			230.631	194.98	231.637	172.79	29.48	23.77
236.90	159.70	93.27	84.55	210.65	147.98	230.648	197.15	231.676	171.93		
238.50	159.43	95.06	85.95	211.93	148.67	230.665	200.47	231.717	171.70		
240.11	159.10	97.19	87.35	213.22	149.20	230.682	203.54	231.761	170.92	30.71	25.31
241.37	159.06	99.27	88.76	214.49	150.27	230.699	205.12	231.809	170.33	32.02	26.94
243.38	159.18	101.34	90.22	215.77	150.63	230.715	209.49	231.857	169.77	33.38	28.61
247.21	159.90	103.37	91.45	217.03	151.39	230.722	210.23	231.905	169.26	34.66	30.13
249.91	160.06	105.36	92.78	218.28	152.11	230.738	215.03	231.953	168.74	35.87	31.59
251.91	160.35	107.31	93.99	219.55	152.90	230.753	219.86	232.001	168.42	37.06	32.94
253.90	160.74	109.32	95.18	220.76	153.65	230.767	226.03	232.057	168.05	38.37	34.49
255.94	161.18	111.38	96.52			230.781	231.54	232.122	167.56	39.75	36.05
258.00	161.74	113.40	97.73	221.849	156.32	230.794	236.16	232.186	166.95	41.14	37.63
260.07	162.20	115.42	98.86	222.777	156.66	230.807	242.31	232.254	166.61	42.56	39.24
262.23	162.79	117.45	100.08	223.574	156.99	230.820	245.36	232.324	166.24	43.97	40.81
264.48	163.21	119.50	101.20	224.342	157.40	230.832	251.57	232.395	165.72	45.34	42.36
266.74	163.94	121.53	102.38	225.050	157.92	230.845	256.67	232.456	165.51	46.67	43.82
268.97	164.63	123.52	103.47	225.619	158.43	230.857	260.19	232.527	165.09	48.24	45.57
271.20	165.16	125.51	104.59	226.029	158.63	230.869	264.73	232.604	164.95	50.05	47.55
273.42	166.05	127.47	105.65	226.445	159.10	230.880	267.34	232.686	164.70	51.77	49.45
275.62	166.55	129.41	106.66	227.259	160.26	230.890	267.82	232.769	164.28	53.42	51.24
278.19	167.26	131.32	107.70	227.638	160.88	230.902	268.86	232.862	163.99	55.09	52.88
281.08	168.04	133.22	108.55	227.985	161.60	230.913	269.34	232.965	163.73	59.20	56.82
283.99	168.93	135.11	109.45	228.247	162.08	230.925	268.50	233.069	163.40	57.05	54.75
286.88	169.85	136.99	110.57	228.457	162.76	230.937	266.52	233.164	163.11	61.46	58.98
289.76	170.77	138.89	111.55	228.640	163.27	230.949	264.71	233.294	162.89		
292.62	171.87	140.70	112.46	228.758	163.41	230.961	260.88	233.475	162.52		
295.47	172.37	142.53	113.38	228.830	163.92	230.973	256.62	233.683	162.14		
298.30	173.88	144.36	114.58	228.913	163.91	230.985	250.68	233.944	161.80		
301.12	174.94	146.13	115.22	229.002	164.53	230.998	245.29	234.256	161.40		
		147.82	116.13	229.081	164.80	231.010	238.98	234.618	161.00		
		149.27	116.88	229.160	165.18	231.025	230.70	235.028	160.62		
		151.13	117.59	229.238	165.47	231.038	225.84	235.492	160.38		
229.70	167.78	152.77	118.24	229.317	166.17	231.052	221.42	236.124	160.11		
229.95	170.30	154.42	118.99	229.395	166.75	231.066	217.12				
230.25	175.59	156.05	119.49	229.473	166.85	231.081	213.59	11.67	3.68		
230.54	184.13	157.67	120.61	229.551	167.85	231.096	209.69	12.26	4.12		
230.80	238.28	159.26	122.88	229.629	167.76	231.112	205.67	12.85	4.59		
231.04	231.43	160.88	124.62	229.707	168.27	231.129	200.35	13.45	5.37		

Table 10. Molar heat capacity of x=0.03.

T/K	C_p/JK^{-1}mol^{-1}	T/K	C_p/JK^{-1}mol^{-1}
222.69	156.27	234.618	228.64
223.56	156.87	234.634	227.56
224.44	157.48	234.651	228.42
225.30	157.36	234.668	230.76
226.21	158.70	234.684	231.73
227.15	159.51	234.785	221.27
		234.809	215.92
		234.838	213.97
		234.871	208.12
225.11	157.55	234.904	203.25
226.48	158.59	234.944	200.52
227.84	159.69	235.097	195.44
229.19	161.03	235.066	190.00
230.40	162.60	235.143	185.95
231.33	163.97	235.222	182.63
231.901	165.76	235.319	177.05
232.248	166.37	235.403	179.21
232.535	167.79	235.505	177.80
232.764	168.50	235.616	174.81
232.993	169.60	235.756	173.59
233.220	170.33	235.925	172.50
233.447	172.78	236.122	170.64
233.615	174.66		
233.728	175.78		
233.842	177.46		
233.939	179.46		
234.032	182.74		
234.120	186.51		
234.202	189.36	236.350	169.41
234.278	194.13	236.578	168.45
234.353	200.52	236.858	167.49
234.419	210.12	237.213	166.53
234.463	216.12	237.686	165.76
234.514	221.63	238.254	164.95
234.550	225.42	238.822	164.41
234.582	229.23		
234.602	230.67		

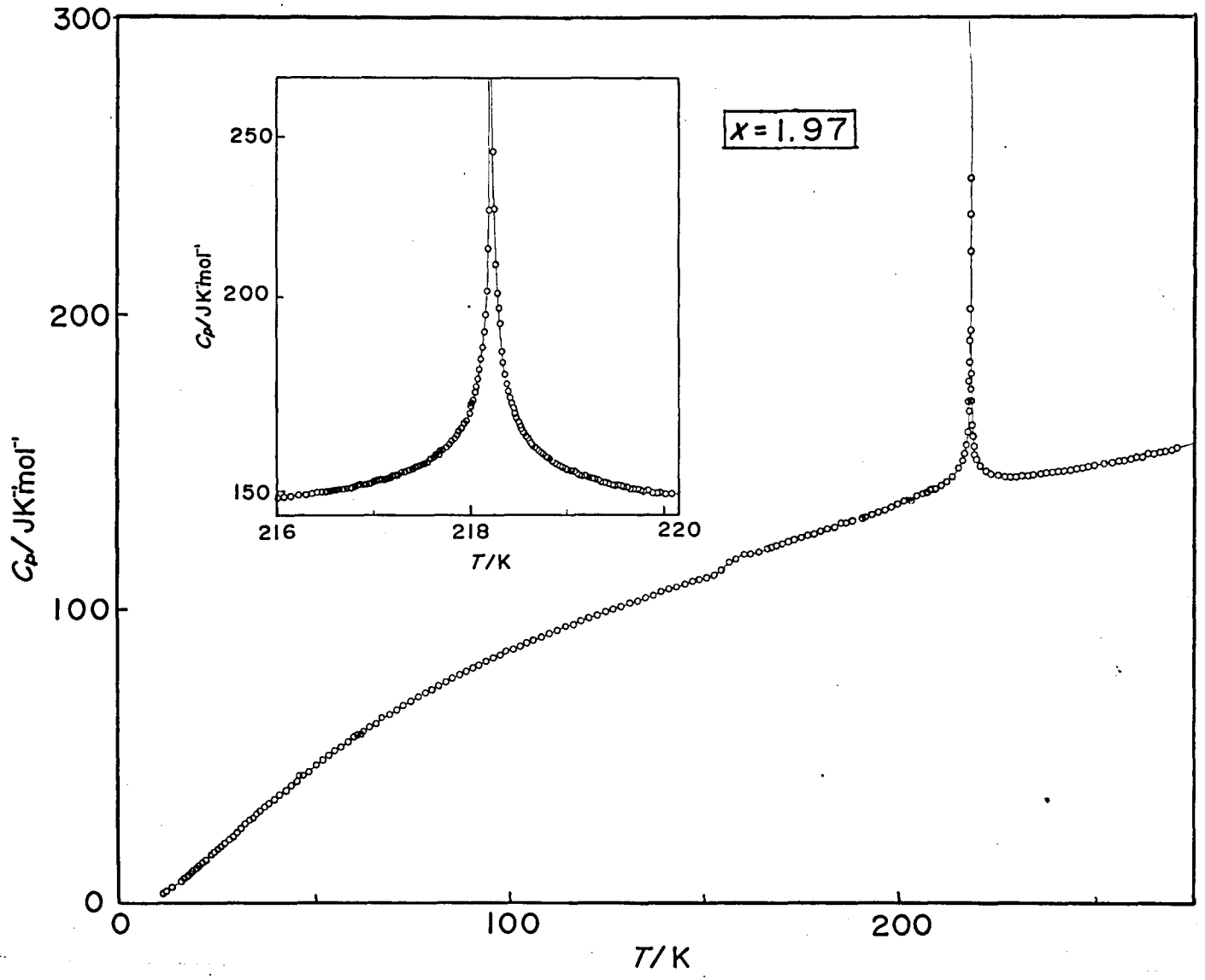

Fig.13. Molar heat capacity of x=1.97. The inset is an expanded view of the heat capacity curve near T_c.

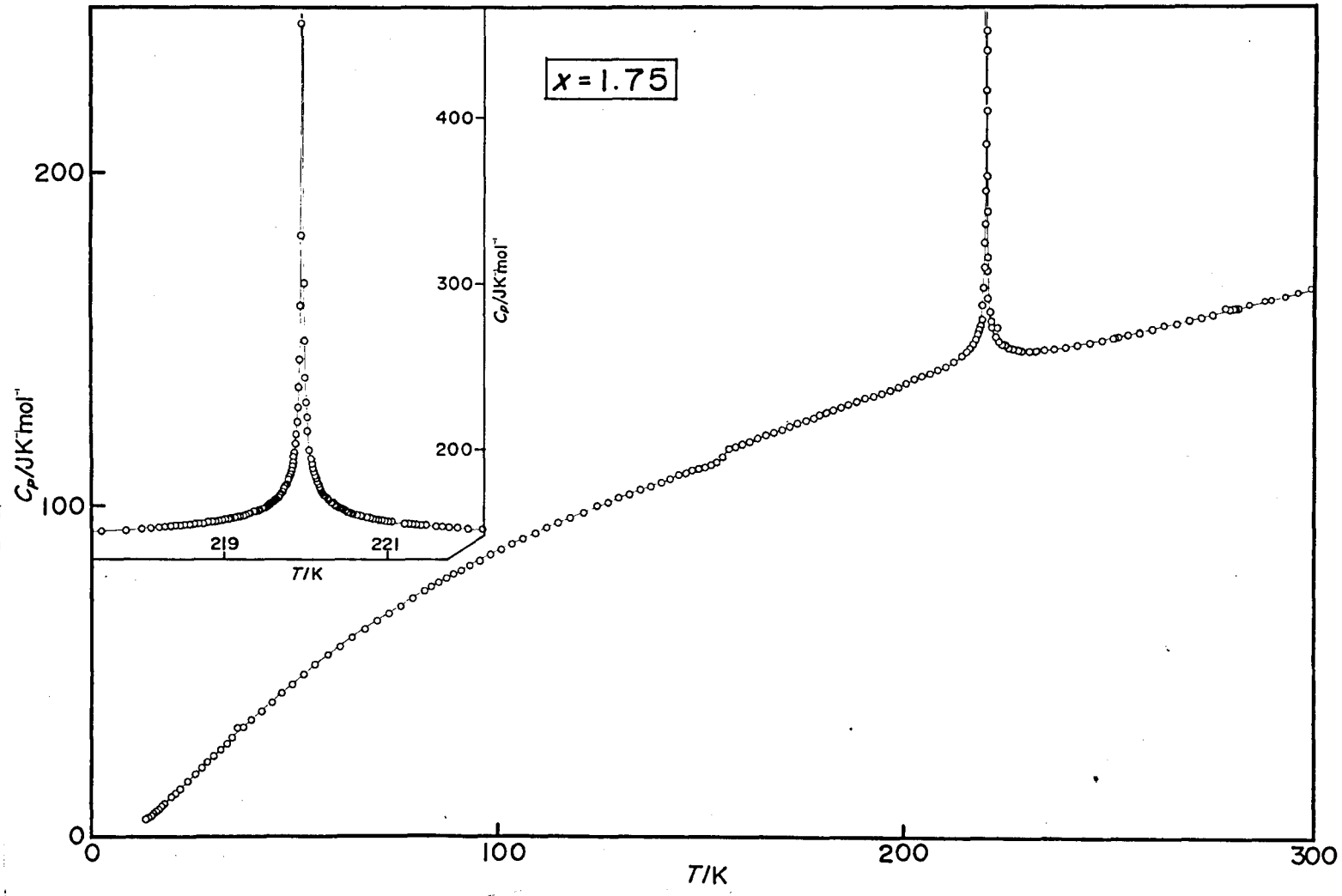

Fig.14. Molar heat capacity of x=1.75. The inset is an expanded view of the heat capacity curve near T_C.

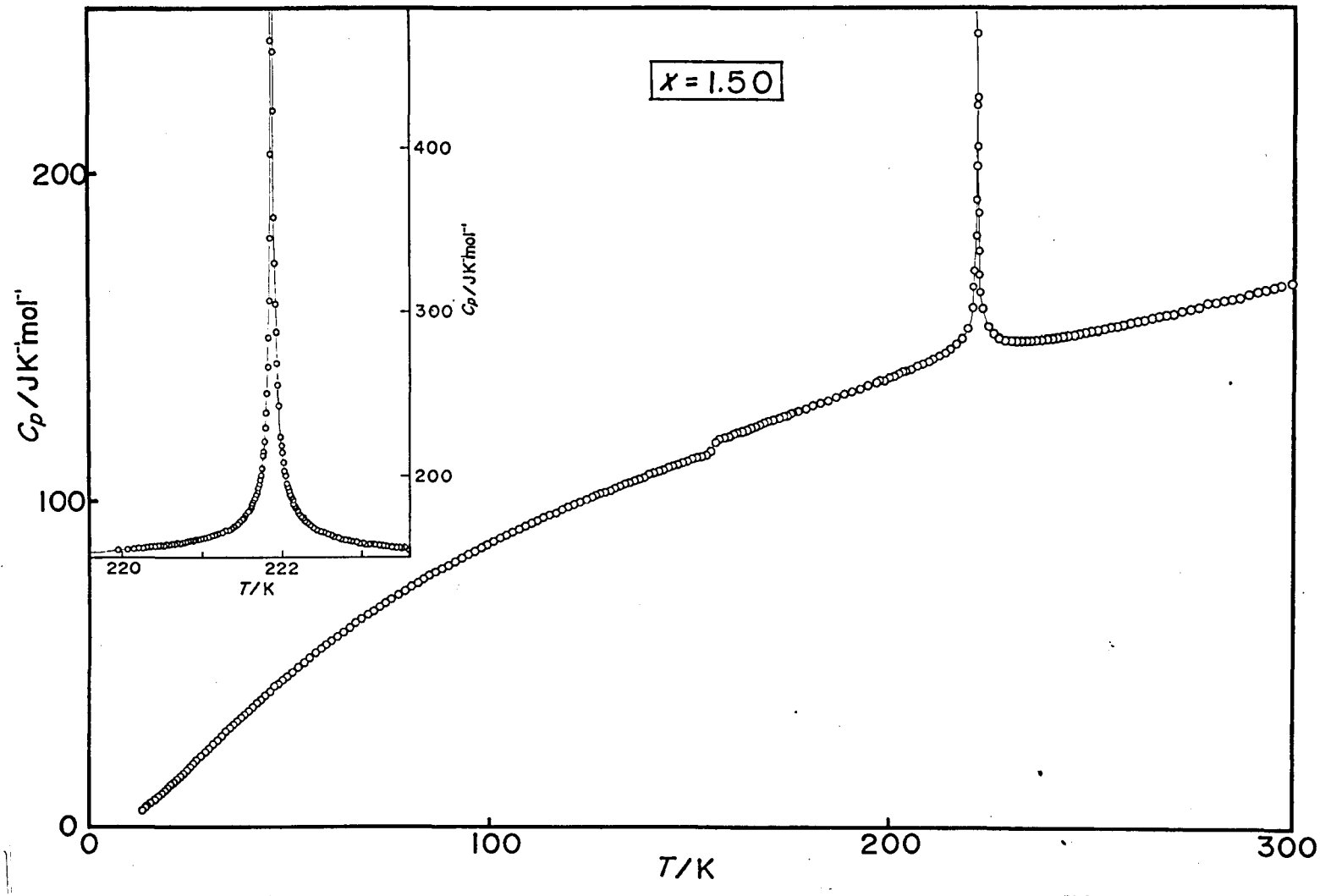

Fig.15. Molar heat capacity of x=1.50. The inset is an expanded view of the heat capacity curve near T_c.

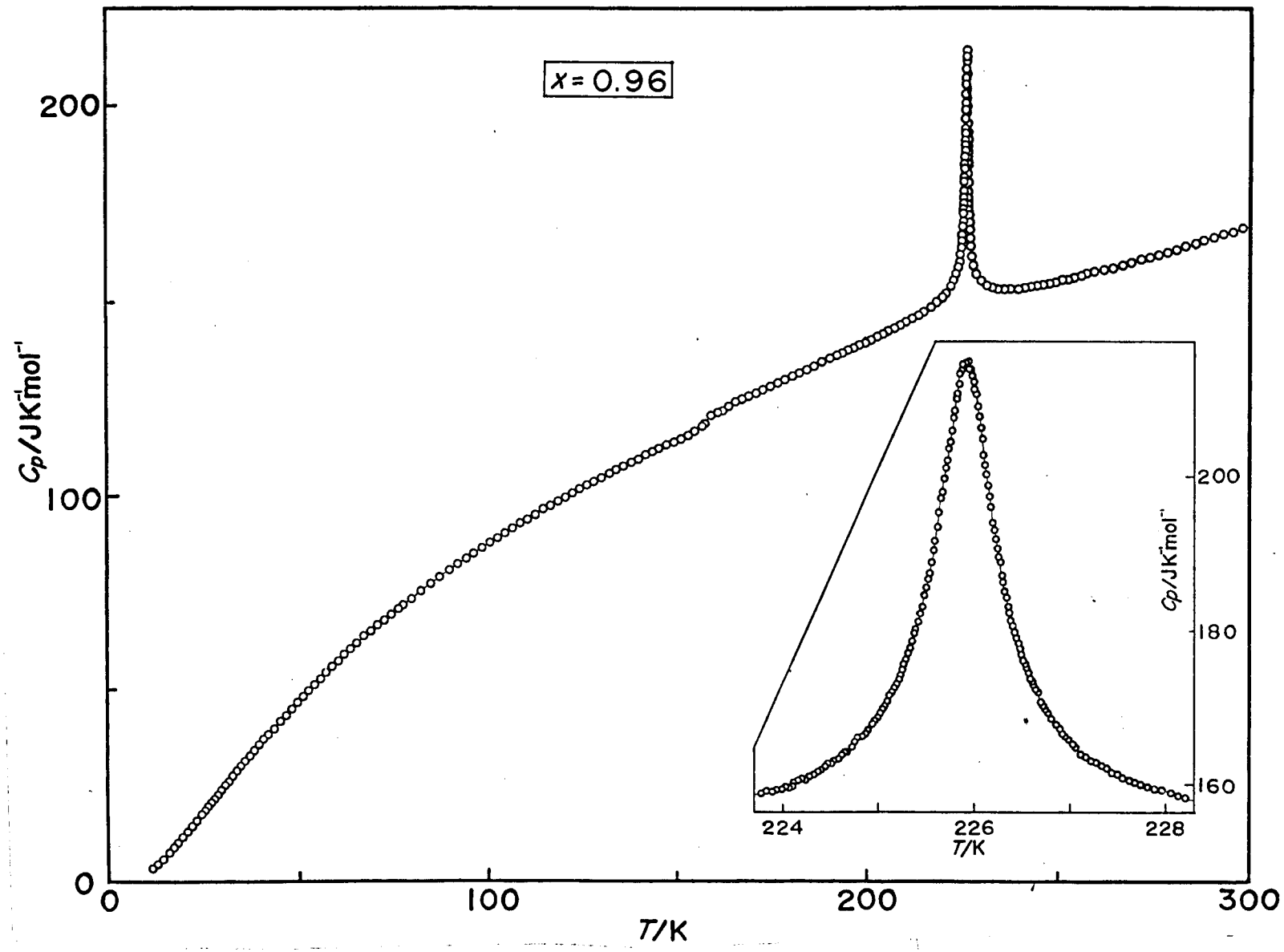

Fig.16. Molar heat capacity of x=0.96. The inset is an expanded view of the heat capacity curve near T_c.

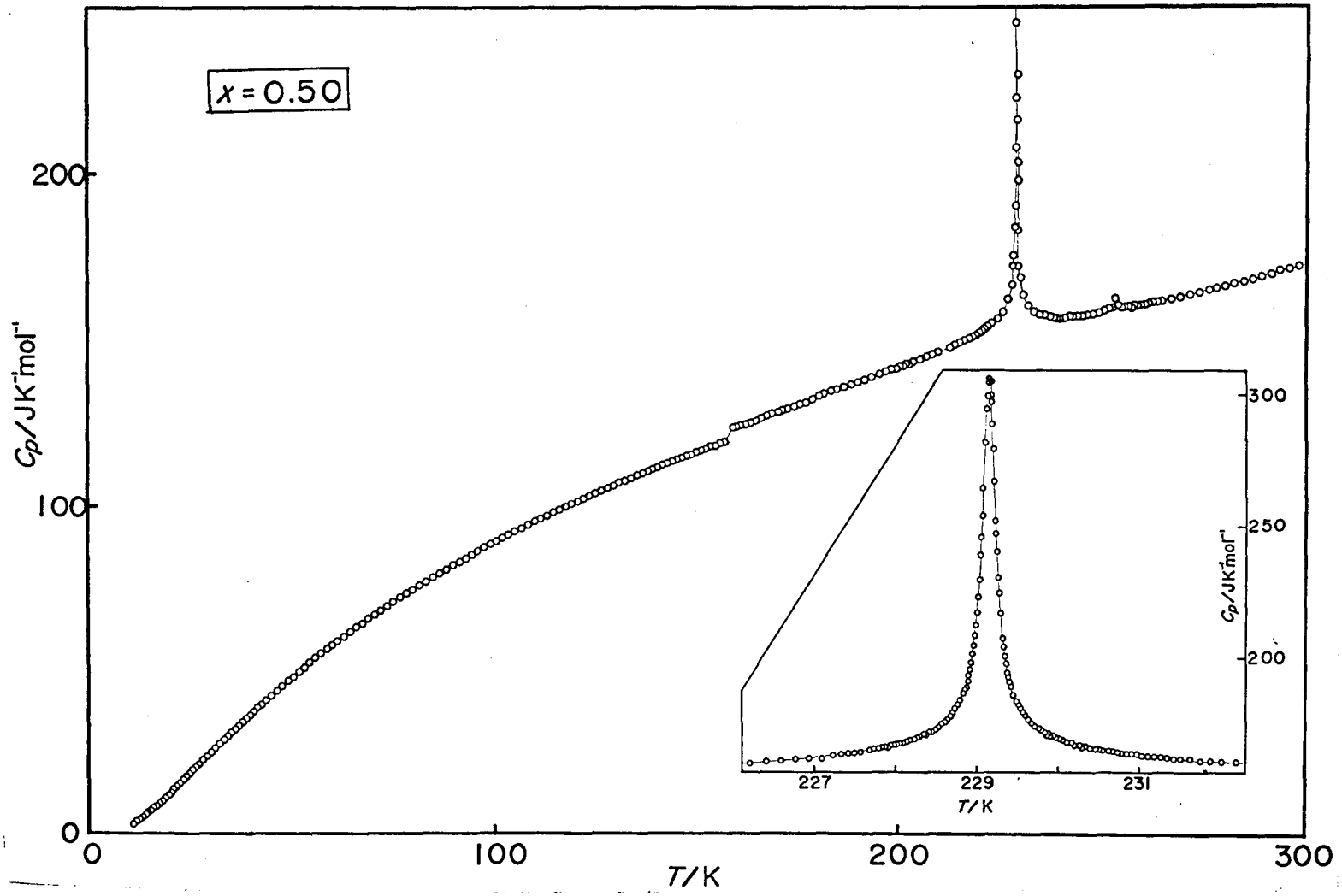

Fig.17. Molar heat capacity of x=0.50. The inset is an expanded view of the heat capacity curve near T_c.

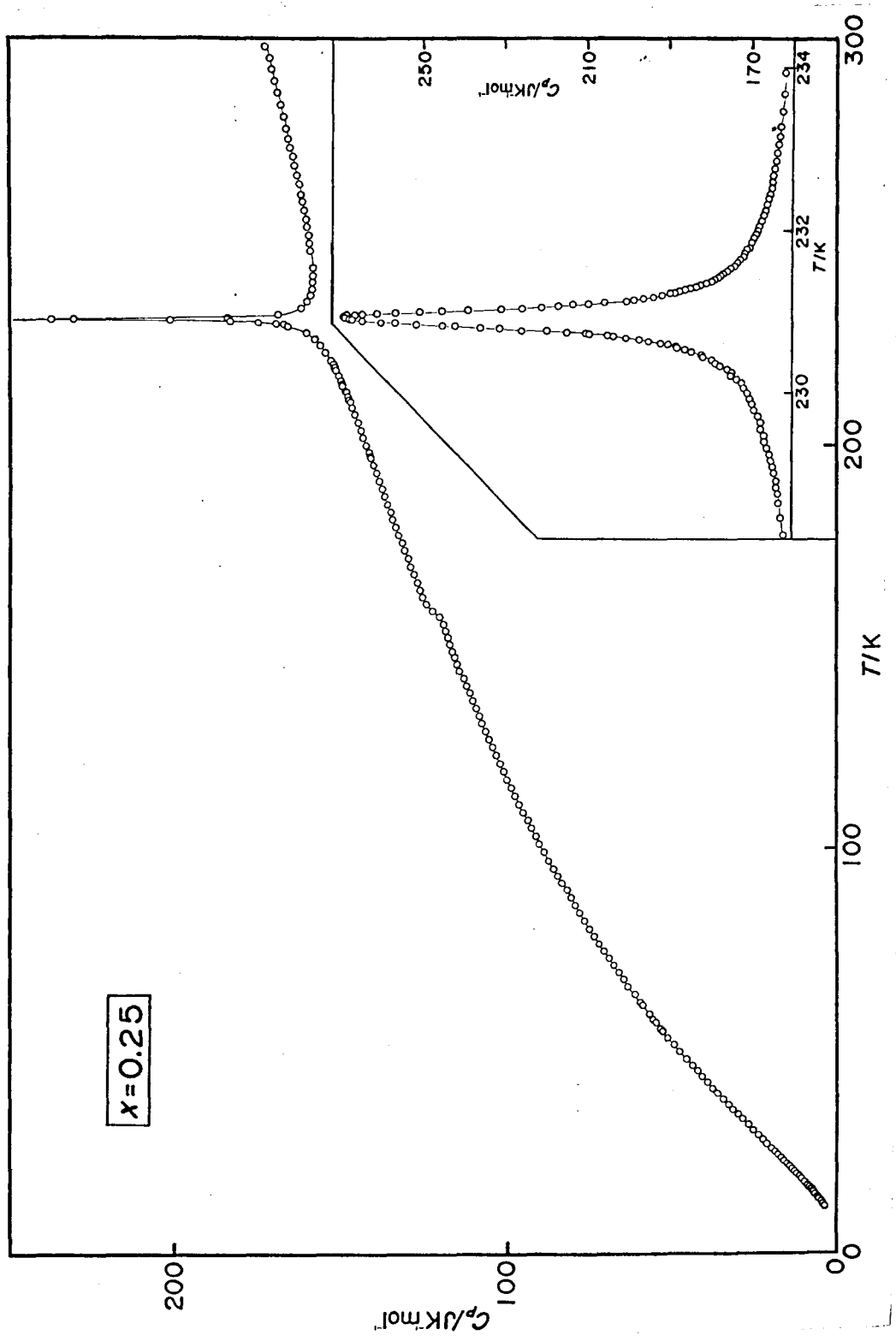

Fig.18. Molar heat capacity of x=0.25. The inset is an expanded view of the heat capacity curve near T_c.

To observe these phenomena requires the precise measurements with the minute temperature step. Our measurements are sufficient enough to detect the quasi 1st order component.

(ii) x=0.03: This crystal exhibited no 1st order component but a rounding phenomenon at the peak temperature(234.64 K). The shape of the anomalous heat capacity was broader than that found in x=2.00 and the maximum value of the peak was found to be 220 $J K^{-1} mol^{-1}$.

(iii) x=1.97: The phase transition occurred at 218.22 K. A small quasi-isothermal absorption of energy was found aroud ±1.5/100 K below and above the peak temperature. In this region the time for establishing the equilibrium became abruptly longer by the factor of 4∿6 with a sudden increase of the apparent heat capacity. The latent heat absorbed quasi-isothermally amounts to 33.12 $J mol^{-1}$. These phenomena are similar to those observed in x=2.00. The relaxational anomaly occurred at 150∿155 K.

(iv) x=1.75: The transition temperature is 219.96 K. The first order-component was again observed at the transition temperature. The latent heat of transition is 29.24 $J mol^{-1}$. In the first measurement a small hump was observed around 224 K, some 4 K above the phase transition temperature. In view of the reproducibility of the small peak, presence of impurity in the calorimetric specimen was suspected. Therefore, the heat capacity was measured on a crystal having the same composition but prepared from the stannous chloride dihydrate of a different commercial source. However in the newly prepared crystal the shoulder appeared at the same temperature(Fig.19).

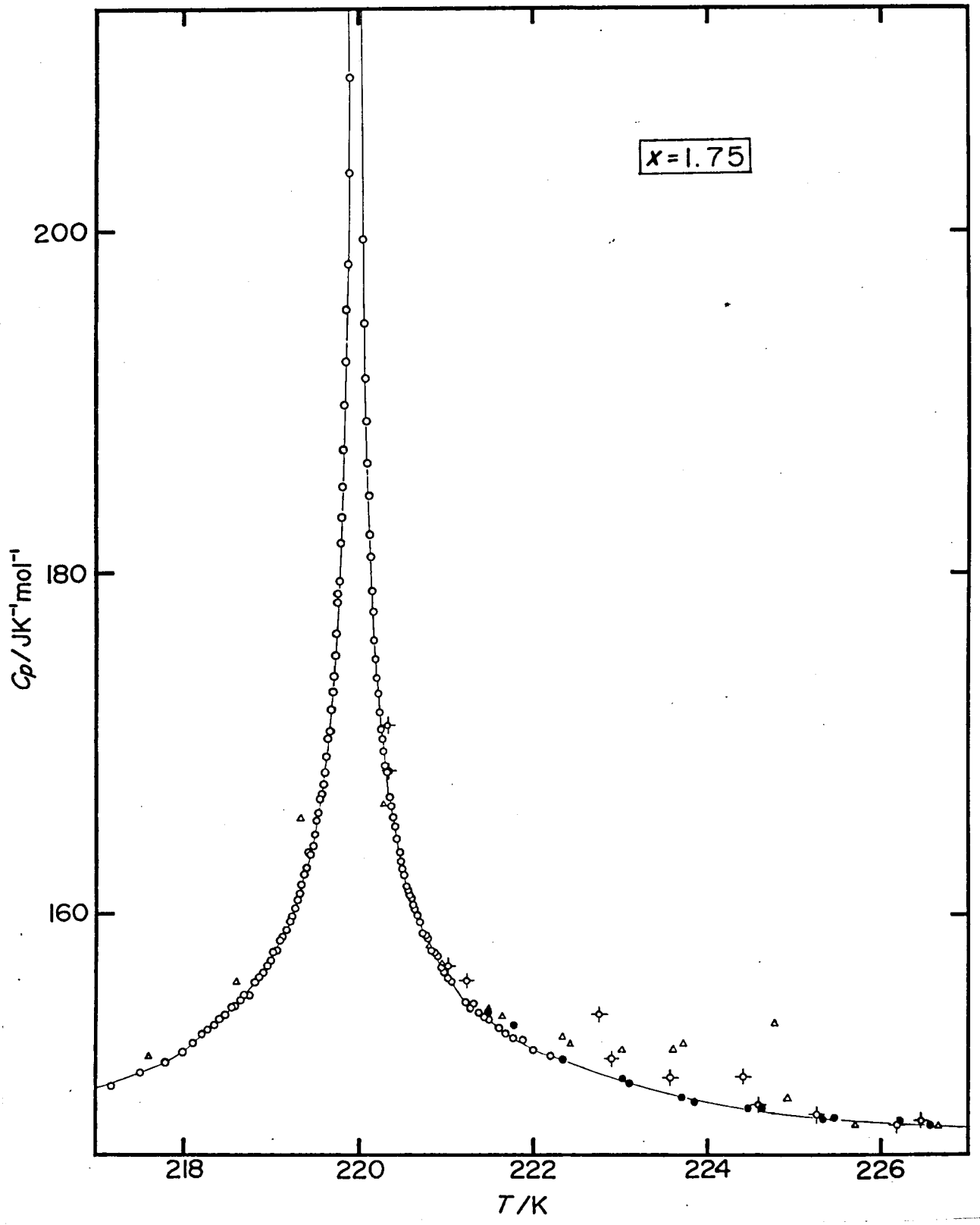

Fig.19. Pre-cooling effect on heat capacity of x=1.75
● cooled just 1 K above T_c; the others are
cooled below T_c.

Consequently it was concluded that this phenomenon was intrinsic in the crystal with the composition of x=1.75. In the temperature region of this anomaly, it took longer time(about 100 min.) to reach an equilibrium with the endothermic temperature drift of 3/10000 ∿ 6/10000 K during the drift time. The phenomenon was reproducible and depended on the pre-cooling condition. It was observed repeatedly when the crystal was cooled below the transition temperature prior to be measurement. When the measurement was started after cooling the sample crystal just 1 K above the transition temperature, the hump in the heat capacity and the associated endothermic effect were not observed.

(v) x=1.50: Although latent heat was not observed around the phase transition temperature 221.88 K, the crystal exhibited the highest peak of anomalous heat capacity(500 $JK^{-1}mol^{-1}$) among the crystals showing no first-order component, the time required for establishing the equilibrium gradually increased up to 90 minutes with increase in the heat capacity. Rounding of the heat capacity peak was not observed in the vicinity of the critical point. At 3 K above the peak temperature, the same phenomena as that found for x=1.75 appeared in the temperature drift but the heat capacity hump was not observed.

(vi) x=0.96: The anomalous heat capacity due to phase transition is located at 225.92 K and its maximum value is 220 $JK^{-1}mol^{-1}$ which is smaller than those of any other crystals. The peak was rounded within ±0.2 K of the transition temperature. The rounding region is slightly wider than those of other crystals. The magnitude and the shape of the heat capacity are

similar to those of x=0.03.

(vii) x=0.50: In this crystal the high resolution measurements were carried out twice before and after the cooling the crystal down to nitrogen temperature, in order to check the effect of thermal history. Reproducibility of the heat capacity was excellent in all respects including the transition temperature, the maximum value of heat capacity and the rounding region(Fig.20). Rounding phenomenon was found within ±2/100 K of the transition temperature(229.15 K) but the maximum of the heat capacity reached 290 $JK^{-1}mol^{-1}$ and is larger than that of x=0.96. This corresponds to the narrower region of the peak rounding at this compositions of the crystal.

(viii) x=0.25: The transition temperature is 230.92 K and the maximum of the peak is 260 $JK^{-1}mol^{-1}$ which is intermediate between those of x=0.96 and x=0.50. The rounding region is nearly the same as the case of x=0.50, and outside of this region the heat capacity due to phase transition is similar to that of x=0.50 in respect to the peak width and the sharpness. The measurement of x=0.03, x=0.25, x=0.50 and x=0.96 were performed within one month after the preparations of respective single crystals. In order to study any effect of aging of the crystals we repeated high resolution measuremants for these compositions near the transition temperatures. The sample crystal that had been measured before was used in the renewed measurement for x=0.50 and new single crystals of x=0.03 and x=0.96 were cut from the same ingot from which single crystals used in the earlier measurement were prepared. The time elapsed between the first and the second measurement were four years, ten

months and two years for the x=0.03, x=0.50 and x=0.96, respectively. The crystals had been kept in closed glass jars separately in the meantimes. For x=0.96 and x=0.50, the transition temperatures decreased by 3×10^{-2} K and 1×10^{-2} K. Considering the stability of the thermometers discussed earlier, one may attribute the shifts of the transition temperatures to change in the isotopic compositions. The amounts of the water are estimated from the change of the transition temperatures. They are calculated to be 14 mg/47 g and 6mg/60 g, respectively. It would be reasonable to assume that water of these amounts might well have been adsorpted on the inner surface of the glass jars when the ingots of the crystal were placed in them. The anomalous heat capacity in crystal x=0.96 increased by a factor of two and became sharper with the decrease of the rounding region (Fig.21). The peak height of x=0.50 increased 3 % in the rounding region but the heat capacity was in agreement with the previous results with 0.1 % outside the rounding region(Fig.20). In the crystal x=0.03 the anomalous heat capacity was reproduced(to 0.1 %) in both the temperatures as well as the shape of peak(Fig.22).

3.2.4. Raman scattering

The Raman spectra were observed for the single crystal and powder of SCD, monohydrate and anhydrate. The single crystal spectrum was measured at various temperatures between 80 and 295 K and the others were only at room temperature. The c-axis of the single crystal was determined by observing the

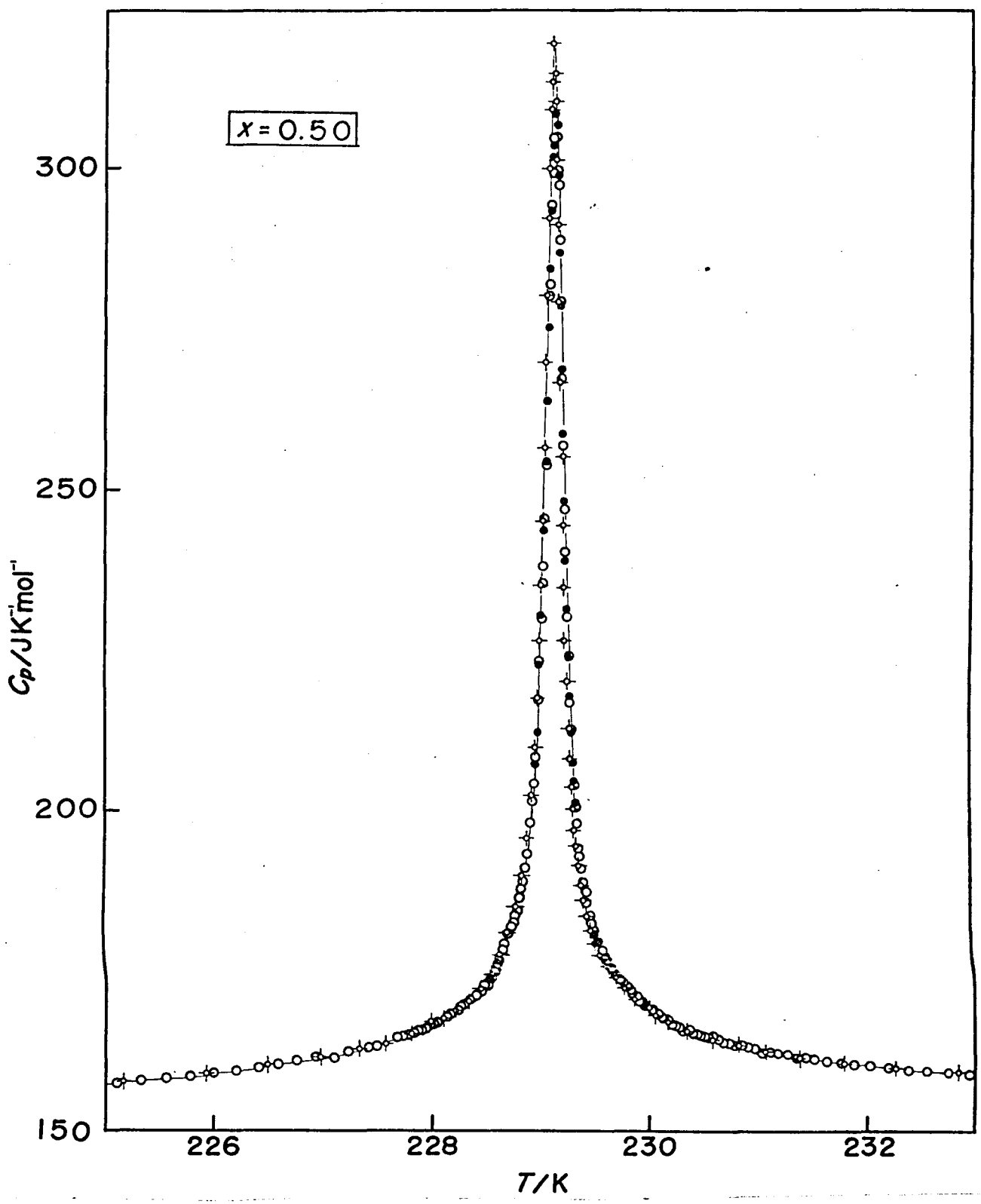

Fig.20. Annealing effect on heat capacity of x=0.50. ○,● first measurement; -○- measurement for annealed crystal.

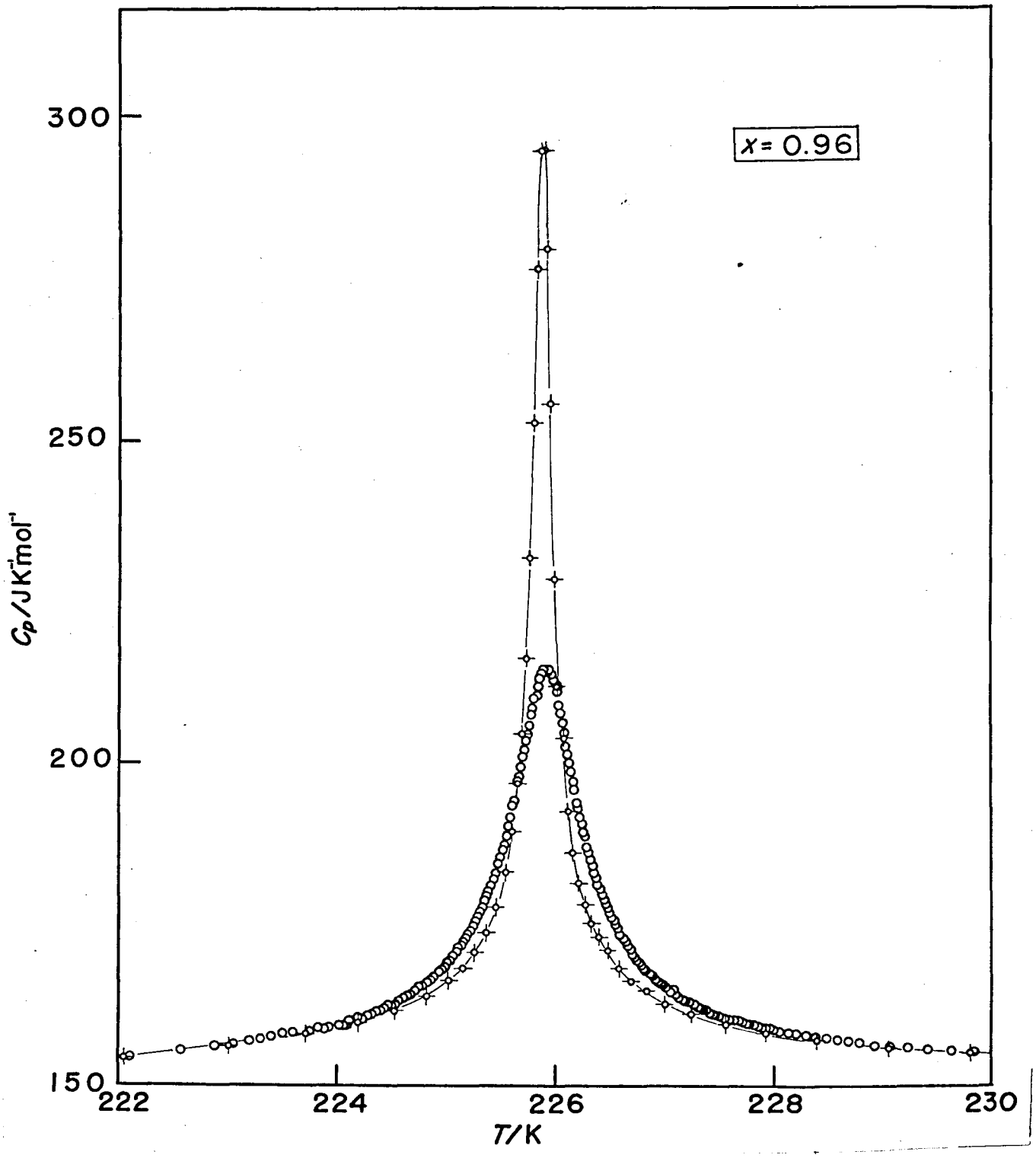

Fig.21. Annealing effect on heat capacity of x=0.96.

○ : first measurement

⊹ : second measurement.

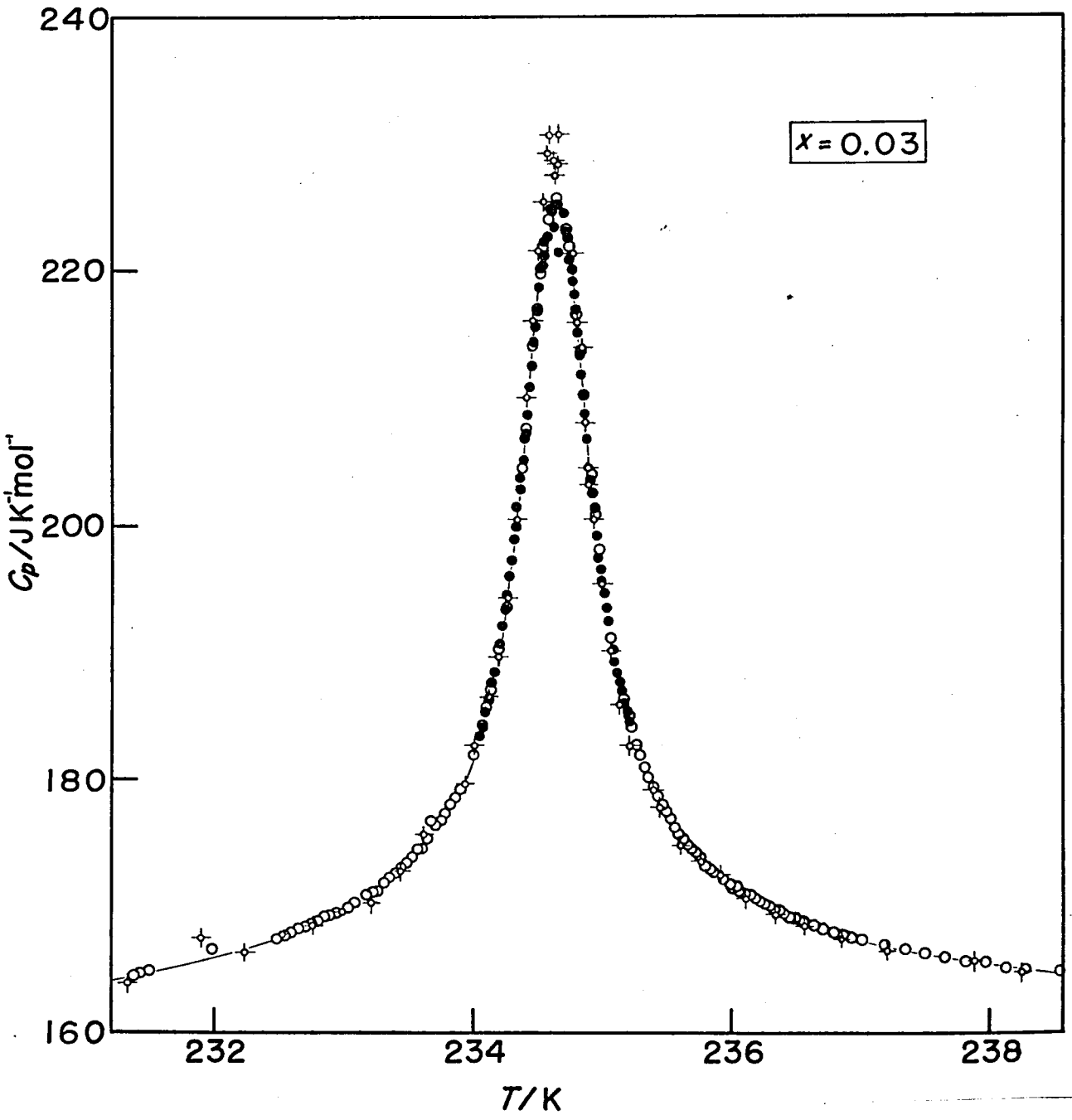

Fig.22. Annealing effect on heat capacity of x=0.03.

○ ● : first measurement

⊹ : second measurement

interfacial angles. The oriented SCD crystal was cooled by a home-made dewar of the cold finger type, which is coupled to a Raman spectrometer. The temperature of the crystal was varied by liquid N_2 together with a heater. The temperature of the crystal was measured by a copper-constantan thermocouple, and was accurate to ± 1 K. The Raman spectra were obtained using the 514.5 nm excitation line of an argon ion laser. The spectrometer used was Nihonbunko Model R 750, with a photon counting system for detection. The Raman spectra in the 0 - 300 cm^{-1} region for anhydrous, monohydrated and dihydrated stannous chloride powdered samples at room temperature are shown in Fig. 23. Spectral lines common in the anhydrous and monohydrated $SnCl_2$ samples are at 67, 85, 97, 129, 163 and 193 cm^{-1}. These are associated with the various types of the Sn-Cl vibrations and lattice vibrations in the crystalline state. Note that the intensities of these lines are remarkably affected by hydration. Most strikingly, the lines at 163 and 193 cm^{-1}, which is strong in anhydrous $SnCl_2$, become weak in $SnCl_2H_2O$ and substantially weaker in $SnCl_2 \cdot 2H_2O$. Although the previously reported Raman spectra of SCD agree in general with the present one, the information provided by polycrystalline or powdered samples is limited. We have thus studied polarized Raman spectra of SCD single crystals. The spectra obtained using the c(a*a*)b, c(a*c)b, b(cc)a*, and b(cb)a* geometries at several temperatures above and below T_c are shown in Fig. 24, 25, 26 and 27. Here a*, b and c denote three mutually orthogonal unit vectors. The vectors b and c correspond to the crystal axes of the unit cell. While, the vector a* does not correspond to the a-axis of the crystal, but is at an

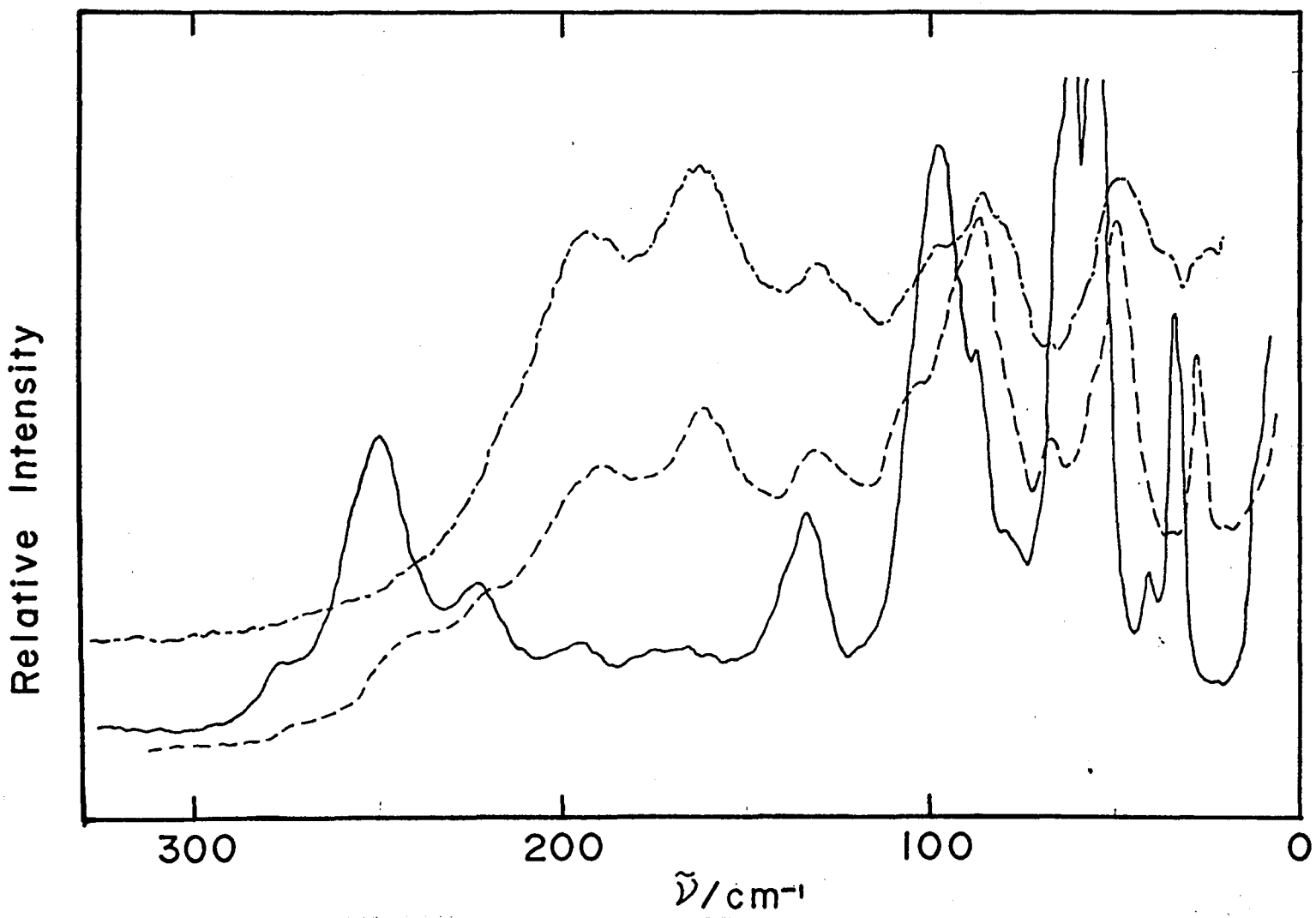

Fig.23. The Raman spectra in the 0–300 cm^{-1} region for anhydrous(-·-·), monohydrated(- - -), and dihydrated(——) stannous chloride.

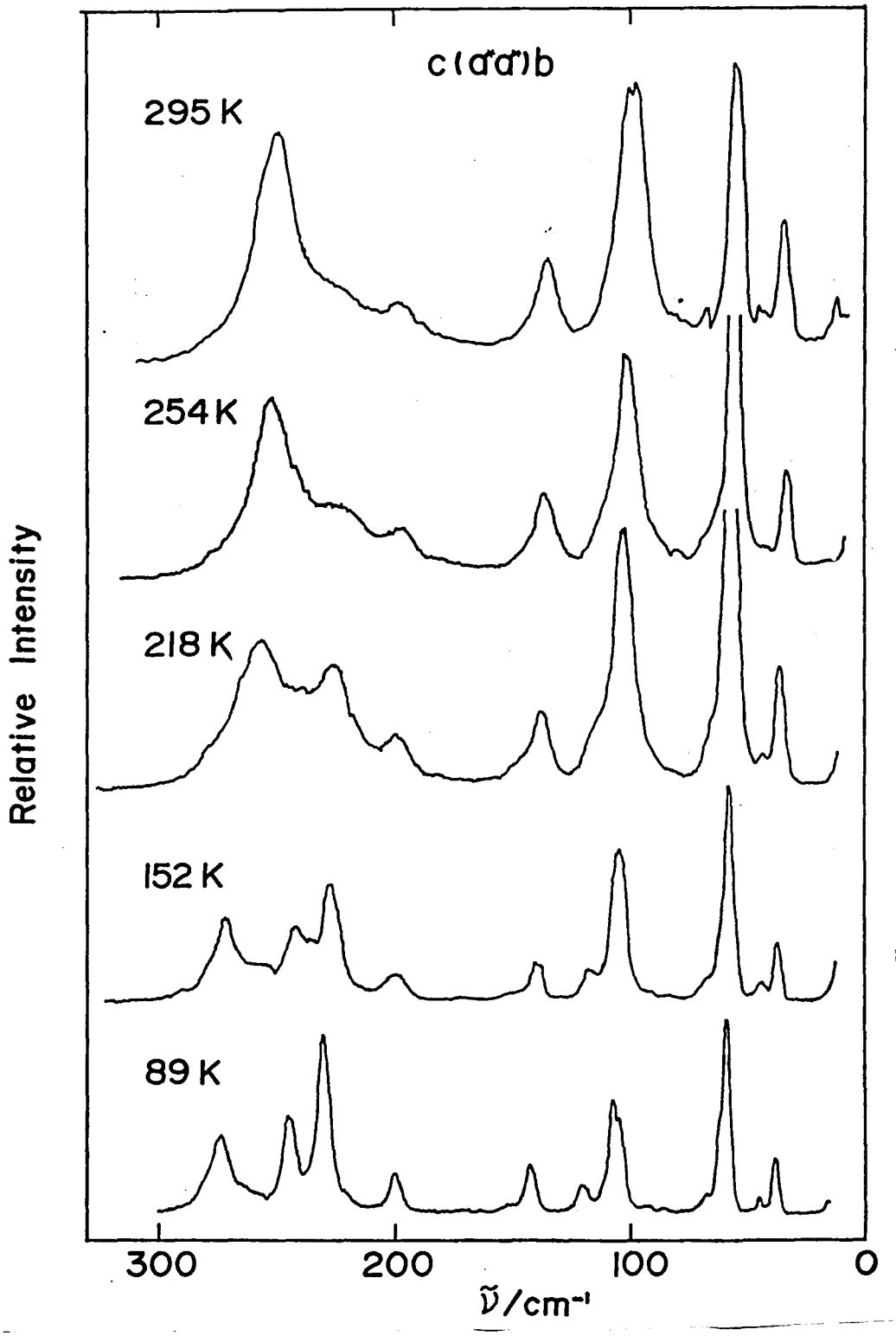

Fig.24. The c(a*a*)b Raman spectra at several temperatures above and below T_c.

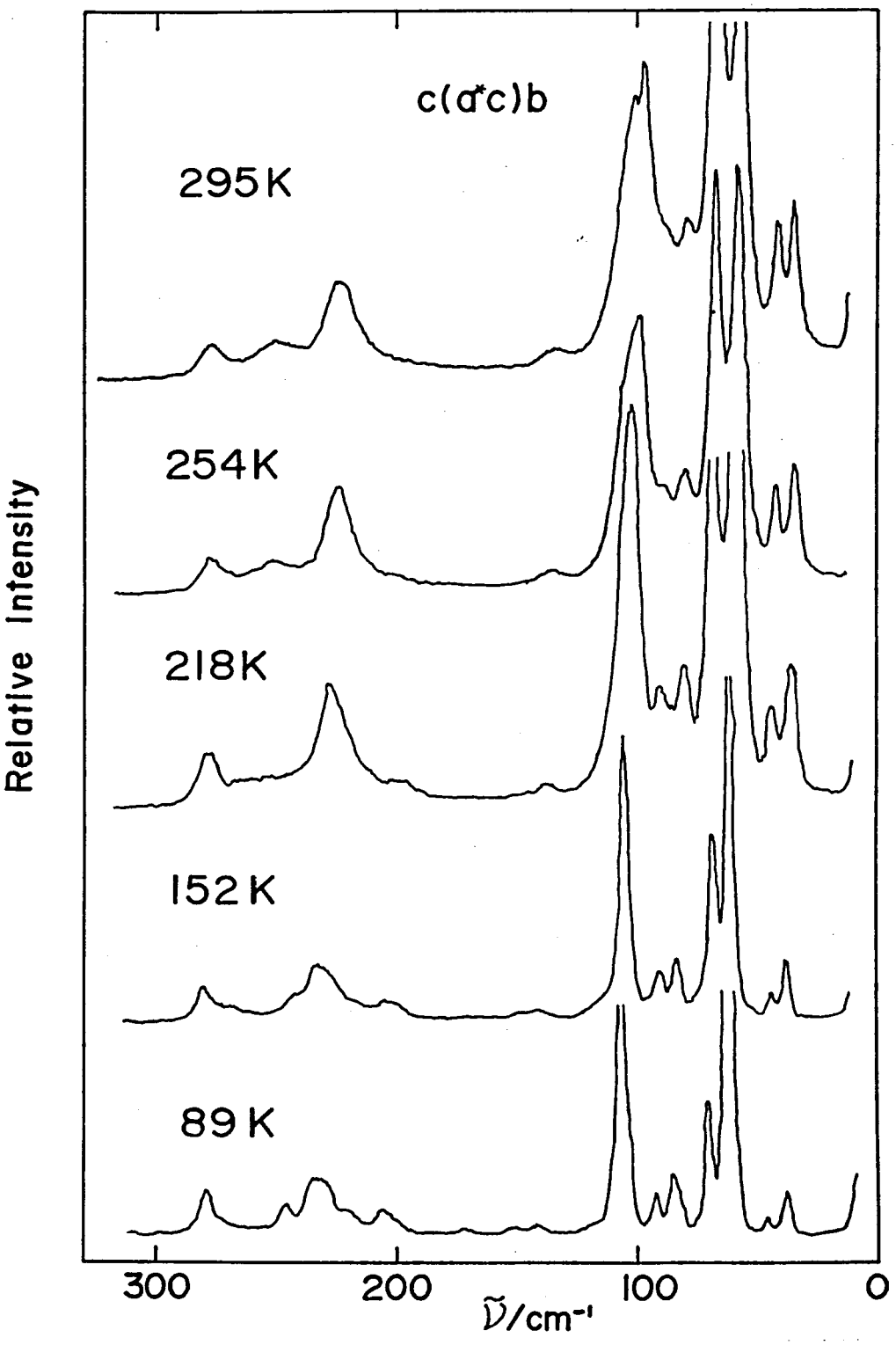

Fig.25. The c(a*c)b Raman spectra at several temperatures above and below T_c.

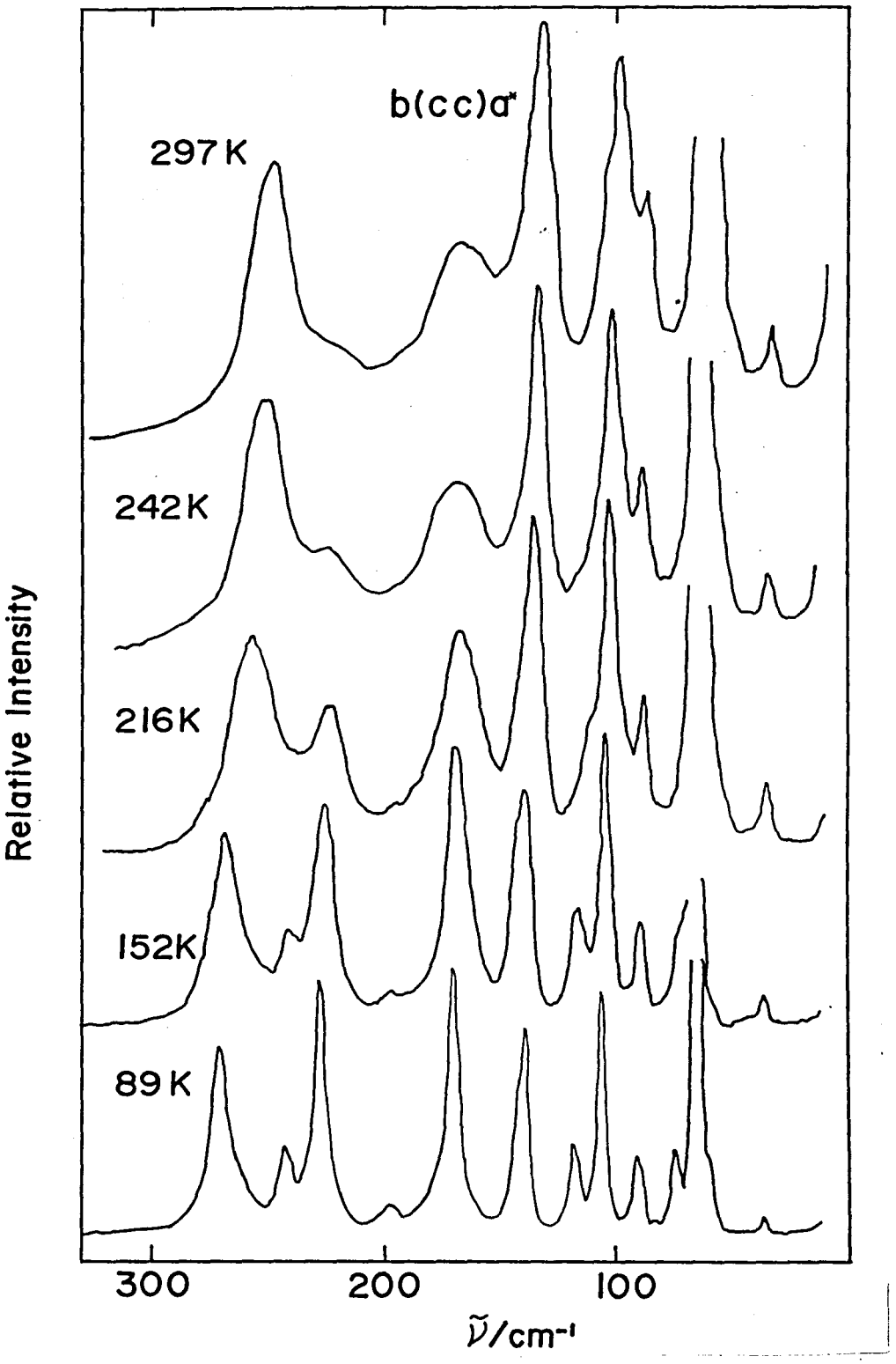

Fig.26. The b(c c)a* Raman spectra at several temperatures above and below *Tc*.

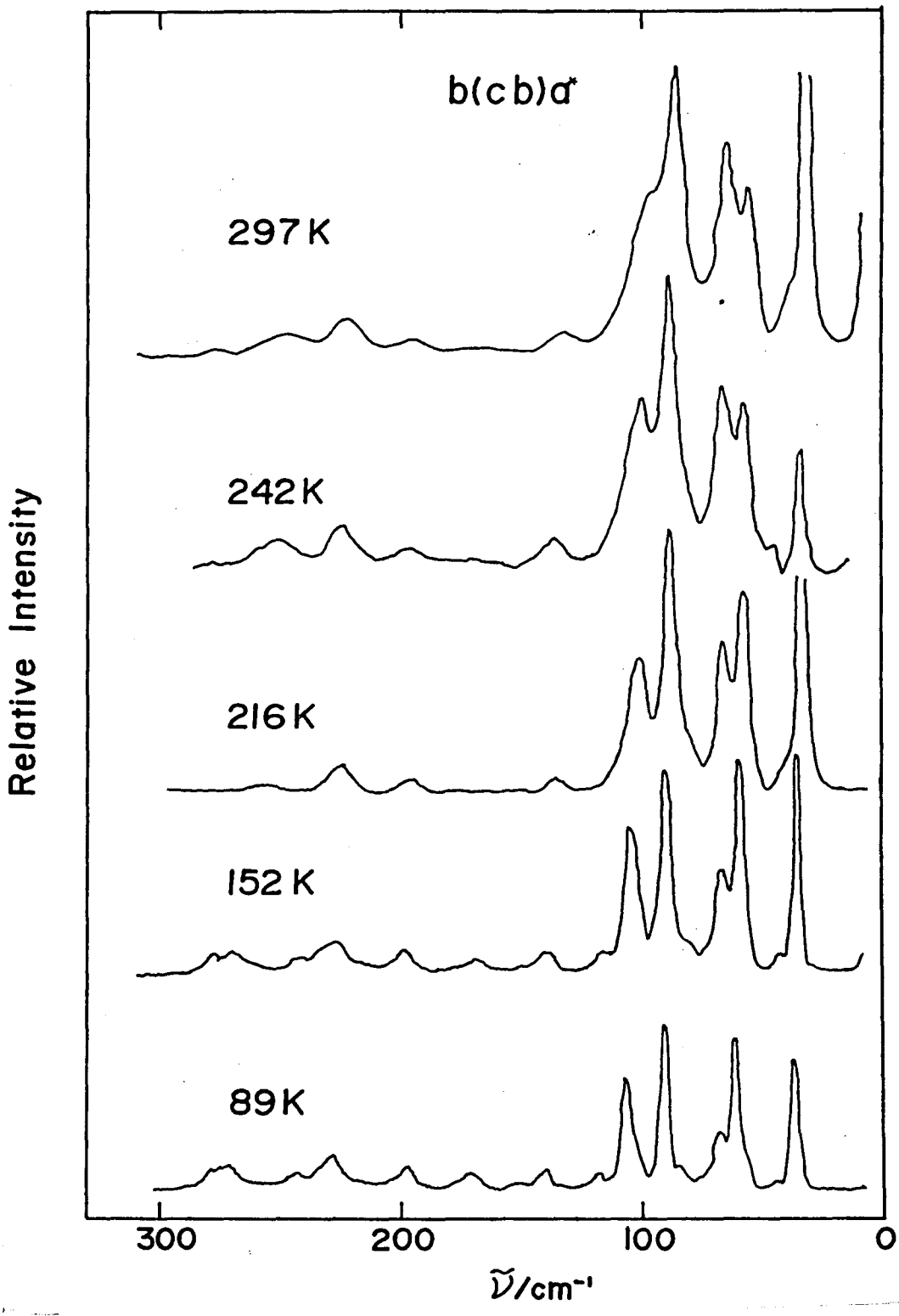

Fig.27. The b(c b)a* Raman spectra at several temperatures above and below T_c.

angle about 25° from the a-axis. The notation used for the scattering is conventional, with the letters before and after the parenthesis indicating the propagation directions of the incident and scattered radiation, respectively. The first and second letters inside the parenthesis correspond to the polarization directions of the incident and scattered radiation, respectively. The most pronounced feature above 200 cm^{-1} is the peak at 250 cm^{-1}. At room temperature the shape of this band is asymmetrical, with additional scattering intensity at its low frequency wing. As the temperature of the crystal is lowered, the 250 cm^{-1} peak shifts to high frequency accompanied by a gradual reduction in the integrated intensity. Moreover, the scattering intensity at the low frequency wing is enhanced and then splits into two peaks. They appear most pronouncedly in the polarized scattering configuration.

3.3. Data analysis and discussion

3.3.1. Dependence of transition temperatures upon the compositions of solid solutions

The isotope effect on the transition temperature of the present substance(T_c^D/T_c^H = 1.076) is of the same order of magnitude as that of a group of hydrogen-bonded ferro- and antiferroelectrics including $Cu(HCO_2)_2 \cdot 4H_2O$[71], $K_4Fe(CN)_6 \cdot 3H_2O$[72], TGS[73], TGSe[74], Rochelle salt[42], etc. The relatively small change in T_c suggests that the transition is associated with the ordering of the protonic position but is not related to the tunneling motion as in KDP[75]. Figure 28 shows a de-

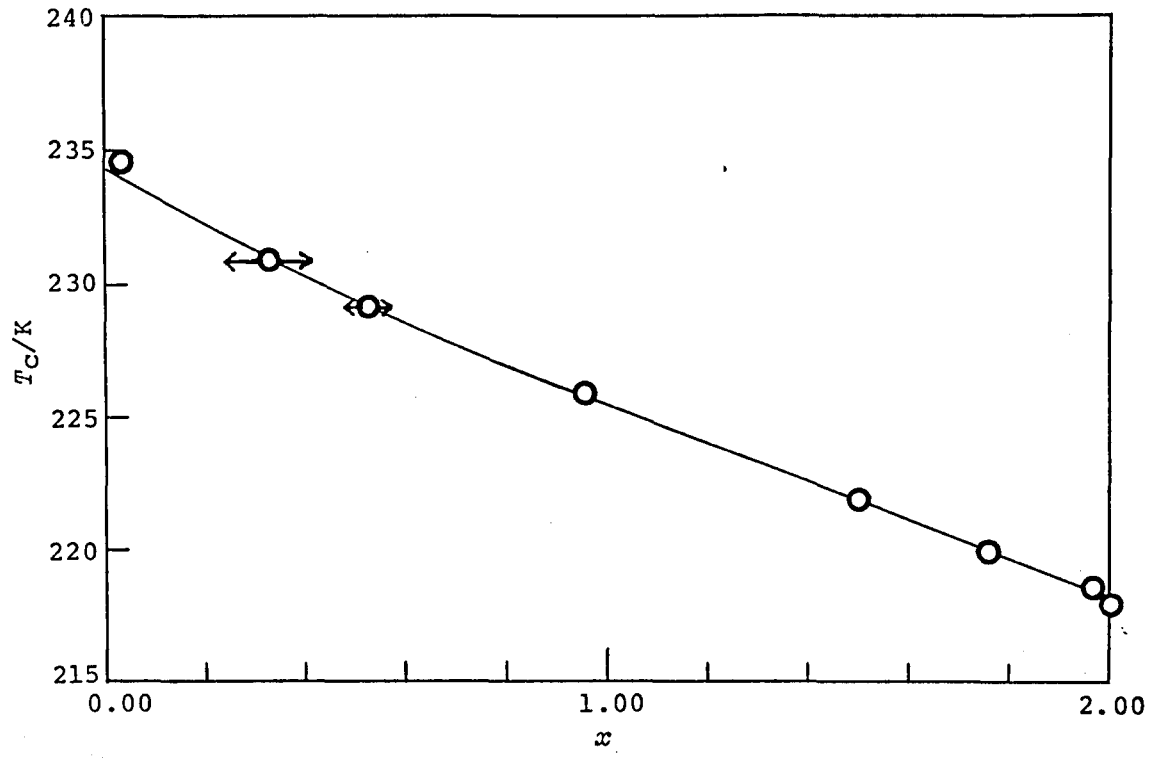

Fig.28. Transition temperature vs. composition. The horizontal arrows indicate the ambiguity due to addition of hydrochloric acid.

pendence of transition temperature upon the composition of solid solutions. The observed behavior of T_c against x for present system is similar to that reported for TGS-DTGS[73] and TGSe-DTGSe systems[74], where the transtion temperature monotonously increases with increasing x.

3.3.2. Determination of critical parameters

Critical exponents characterize the behavior of various physical properties in the vicinity of critical point T_c and they are one of the most important physical quantities to be compared with theory. These exponents are generally defined as follows[27]. If a positive function $f(x)$ varies as x^{λ} when x approaches zero from positive, the exponent can be determined by $\lim \{\ln f(x)/\ln x\} = \lambda$.

As for the heat capacity, its asymptotic form near the critical point is given by,

$$C = (A/\alpha)(|t|^{-\alpha}-1)(1+D|t|^{x}) + B + Et, \qquad \text{Eq. (1)}$$

where $t = (T-T_c)/T_c$ is the reduced temperature and the parameters are allowed to take different values above and below T_c. In the latter case, as has become customary, the primed parameters are employed. The term $(A/\alpha)|t|^{-\alpha}$ represents the leading contribution to the singularity of C. The positive values of α correspond to a heat capacity diverging to infinity at critical point. The smaller the magnitude of α, the sharper the heat capacity becomes and it is called weaker divergence. Negative values of α correspond to a cusped singularity where the heat capacity curve has an infinite slope but remains finite. In the case of $\alpha=0$, there are two types

of singularity. One is the logarithmic divergence and the other the finite jump.

$D|t|^{x}$ is the correction term which represents a singular contribution to C and vanishes at T_c and this term was first estimated experimentally for the superfluid density of liquid ^{4}He[76]. The renormalization group theory predicted that in the case of heat capacity, $B = B'$ and $x = x' = 0.5$(and also pointed out that such terms must be generally considered in the data analysis). The lattice contribution to the heat capacity is expressed by the last two terms, $B + Et$, where the constant B may contain a contribution associated with the phase transition. It is difficult to separate lattice heat capacity from one due to phase transition, especially in the case of the dielectric transition where the interaction causing the phase transition is correlated intimately to the lattice vibration.

There is another difficulty, in fitting the experimental data to Eq. (1). In the case of small values of α and $\alpha'(\simeq 0)$, as the heat capacity exhibits a sharp peak and the temperature range expressed by Eq. (1) is very small, the measurements must be carried out in the region very close to the critical point. However the approach to the critical point is limited by rounding effect in many cases. There always remains the question: where can an experimentalist say for certain that he has reached the critical region? An exacting colleague can always observe that you may not be near enough to critical point to allow the use of the asymptotic expression. Griffiths[77] commented amusingly that the only way out is to invite the

critic to spend a night in your laboratory measurements. There is, however, a semiquantitative definition of the critical region. According to Ginzburg[78] the critical region can be defined as the region where the fluctuations of the order parameter within a correlation length are equal to or greater than the value of the order parameter itself. For example, it was qualitatively predicted for the Ising-model-heat-capacity that it was $|1 - T/T_c| < 10^{-1}$ or 10^{-2} for $T > T_c$ and $|1 - T/T_c| < 10^{-4}$ for $T < T_c$[79]. For the critical range of KDP, it estimated 0.0007 K($|1 - T/T_c| < 5.8 \times 10^{-5}$), however this region could not be completely covered even by excellent high resolution measurement(Reese and May)[28]. In the present case, the larger critical exponents (0.4∿0.8) of the heat capacity make it easier to determine their values than in many magnetic or fluid systems. We calculated the critical exponents from the experimental data in the range of $|t| < 10^{-2}$ and excluded the first order phase transition regions as well as the rounding regions from the fitting range. Though the present phase transition has a small 1st order component, it appears in the limited range near the transition temperature so that we can consider that the phase transition is higher-order character except in the 1st order region. Therefore we can calculate the critical exponent in the higher order region. To simplify the fitting procedure, several constraints were imposed to Eq. (1). It is assumed that the singular higher order corrections to the leading singularity are negligible, *i.e.* $D = D' = 0$. The lattice contribution in Eq. (1) is assumed to be smooth through the tran-

sition temperature. This assumption should be more legitimate for this crystal than is usual because there is no significant change in the crystal structure as far as viewed by the X-ray diffraction[62]. Therefore we assumed that $E = E'$ and $B = B'$ and also that B includes the quantity of $-A/\alpha$. Thus the final asymptotic form employed in the present analysis consists of five unknown parameters as below.

$$C = (A/\alpha)\,|(T - T_c)/T_c|^{-\alpha} + B + ET.$$

The values of E are determined on the basis of the lattice heat capacities by using of the spectroscopic data and the exact solution of the dimer model for SCD[67]. The detail of the calculation will be given in sec 3.3.8. The small error (±1 $JK^{-1}mol^{-1}$) in determination of this value gives little effect (±2%) on other parameters, because this error does not significantly affect the value of $\log(C - B - ET)$ in the region of large heat capacity and fitting region is narrow. The $\log |C_p - (ET + B)|$ is plotted as a function of $\log|(T - T_c)/T_c|$ for various values of T_c and B. The values of T_c and B were altered step by step so as to fit to a straight line in wider range. This procedure is easily performed owing to the property of logarithm, *i.e.* the small variation of T_c does not affect this plot in the region of large $|t|$ but drastically changes the value of $\log|t|$ in the region of small $|t|$ or vice versa for B. The values of B are determined so as to be the same in both sides of the transition temperature. By this method the critical exponents α are determined within ±5%. The results for the various parameters are given in Table 11 and the log-log plots for each crystals are shown in Figs. 29∿36 where we

Table 11. Summary of critical parameters.

	T_c/K	α'	α	α'/α	$\frac{A'}{JK^{-1}mol^{-1}}$	$\frac{A}{JK^{-1}mol^{-1}}$	A'/A	$\frac{C_{p\,max}}{JK^{-1}mol^{-1}}$
x=2.00	218.01	0.492	0.492	1.000	0.568	0.565	1.005	∞
x=1.97	218.22	0.434	0.451	0.962	0.793	0.720	1.101	∞
x=1.75	219.96	0.573	0.579	0.990	0.389	0.354	1.099	∞
x=1.50	221.88	0.731	0.757	0.966	0.200	0.168	1.192	571
x=0.96	225.92	0.720	0.765	0.941	0.287	0.233	1.228	214
x=0.96(II)	225.89	0.696	0.733	0.950	0.238	0.194	1.225	295
x=0.50	229.15	0.747	0.785	0.952	0.165	0.134	1.230	306
x=0.50(II)	229.14	—	—	—	—	—	—	316
x=0.25	230.92	0.753	0.754	0.999	0.168	0.134	1.251	269
x=0.03	234.64	0.730	0.778	0.938	0.228	0.170	1.341	226
x=0.03(II)	234.64	—	—	—	—	—	—	231

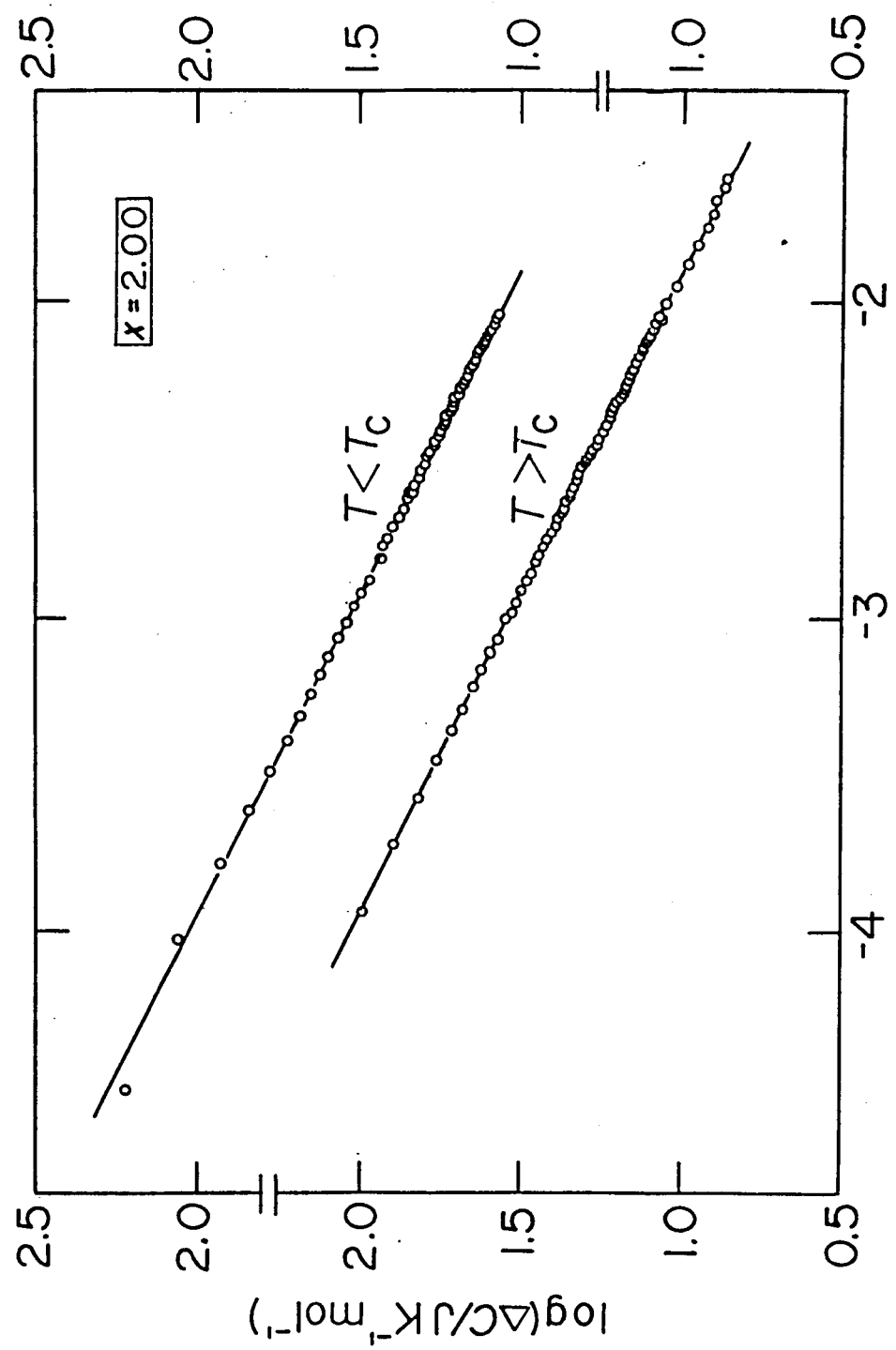

Fig.29. Logarithmic plot of the anomalous part of the heat capacity of x=2.00.

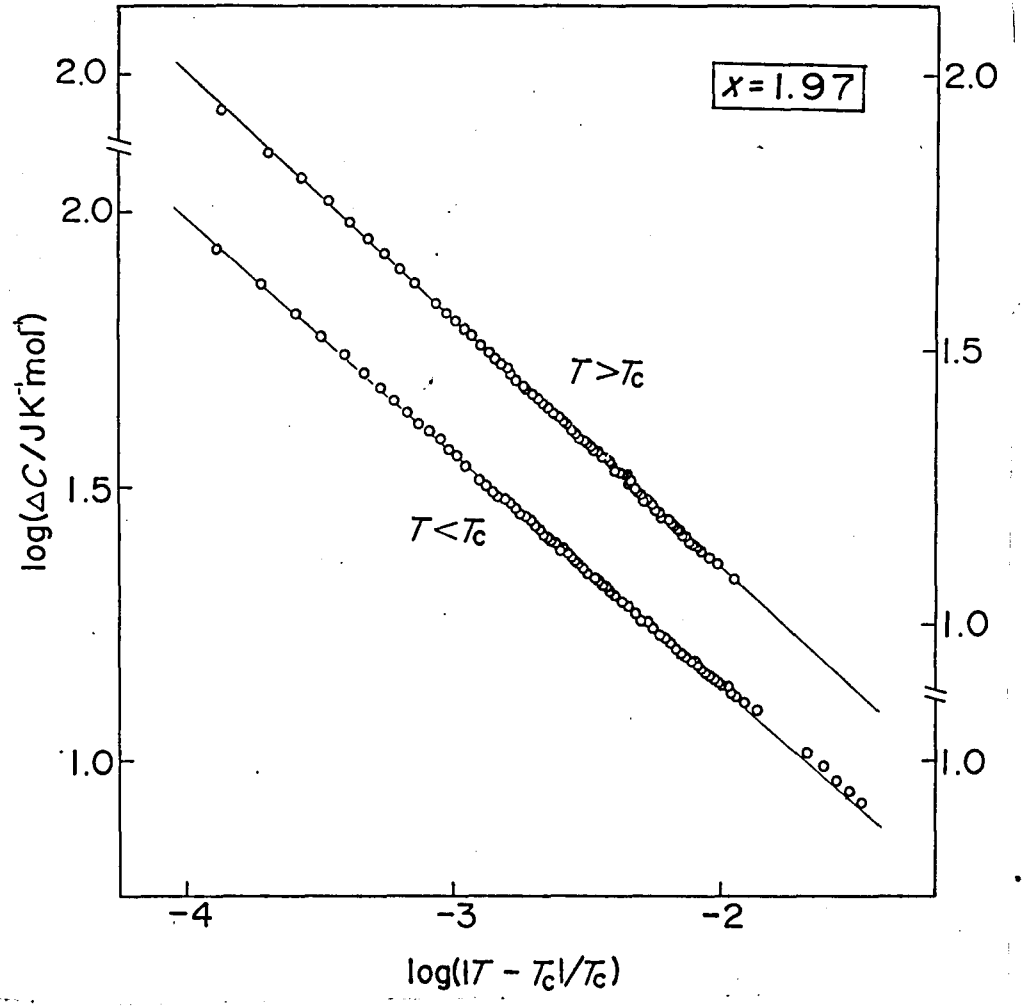

Fig.30. Logarithmic plot of the anomalous part of the heat capacity of x=1.97.

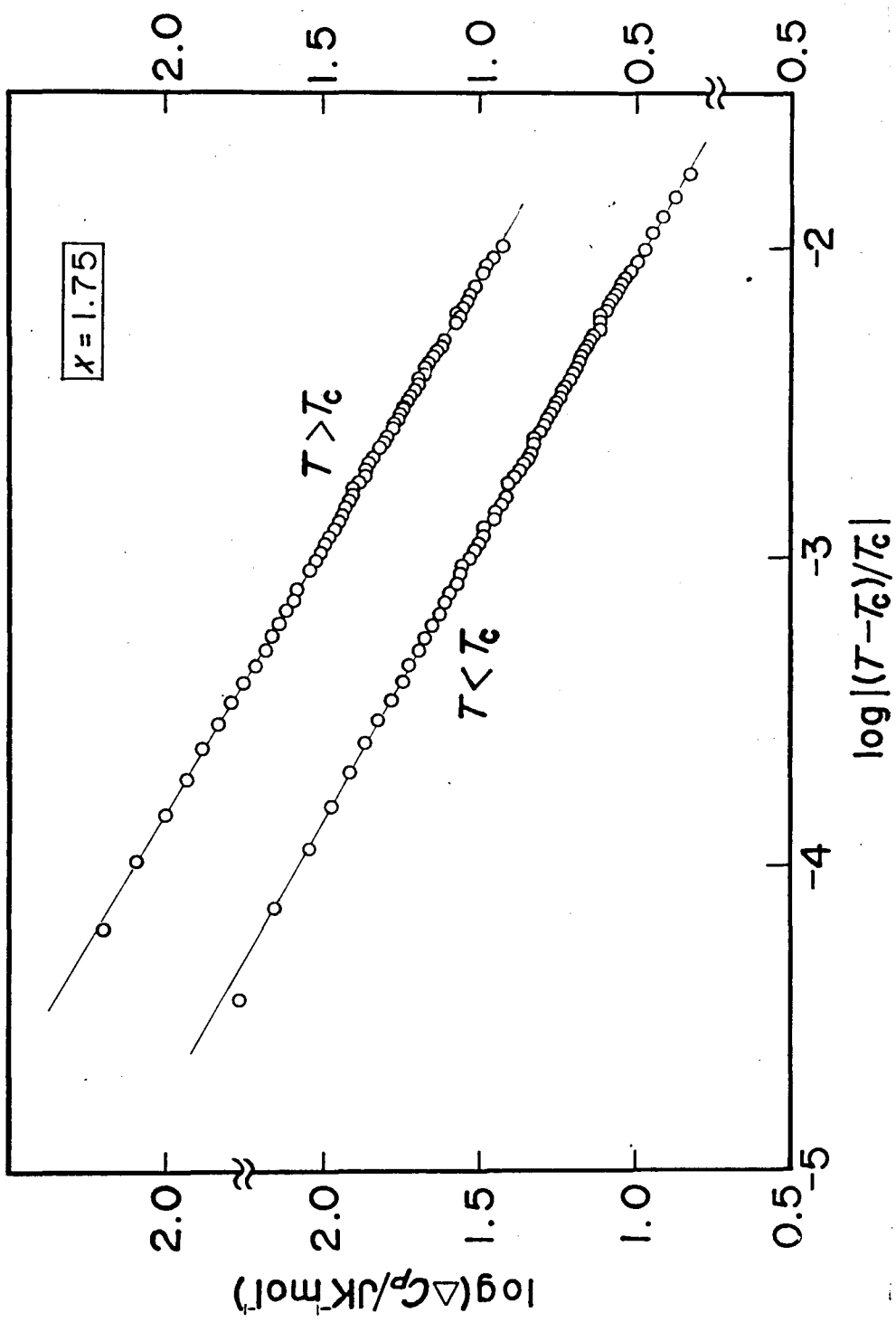

Fig.31. Logarithmic plot of the anomalous part of the heat capacity of x=1.75.

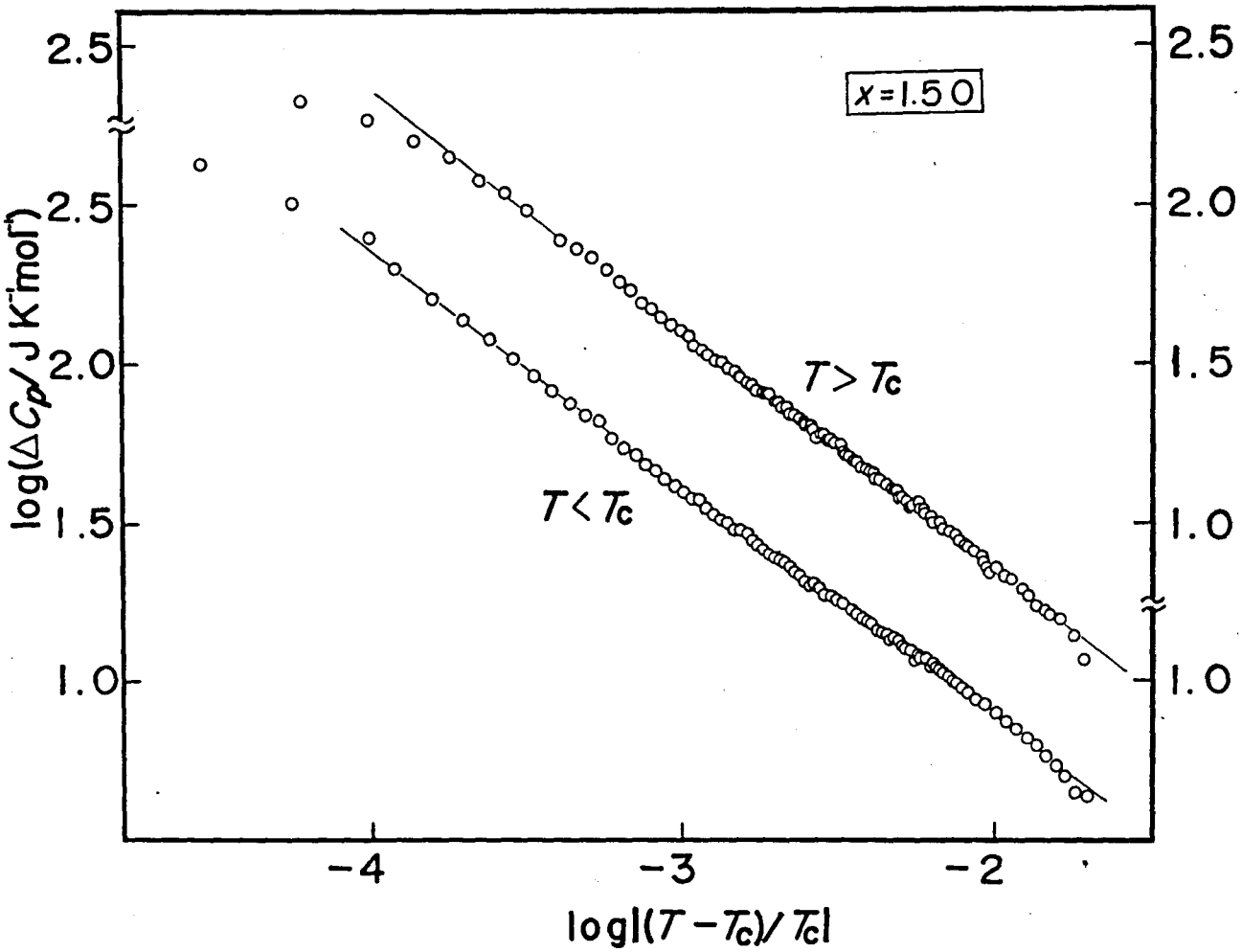

Fig.32. Logarithmic plot of the anomalous part of the heat capacity of x=1.50.

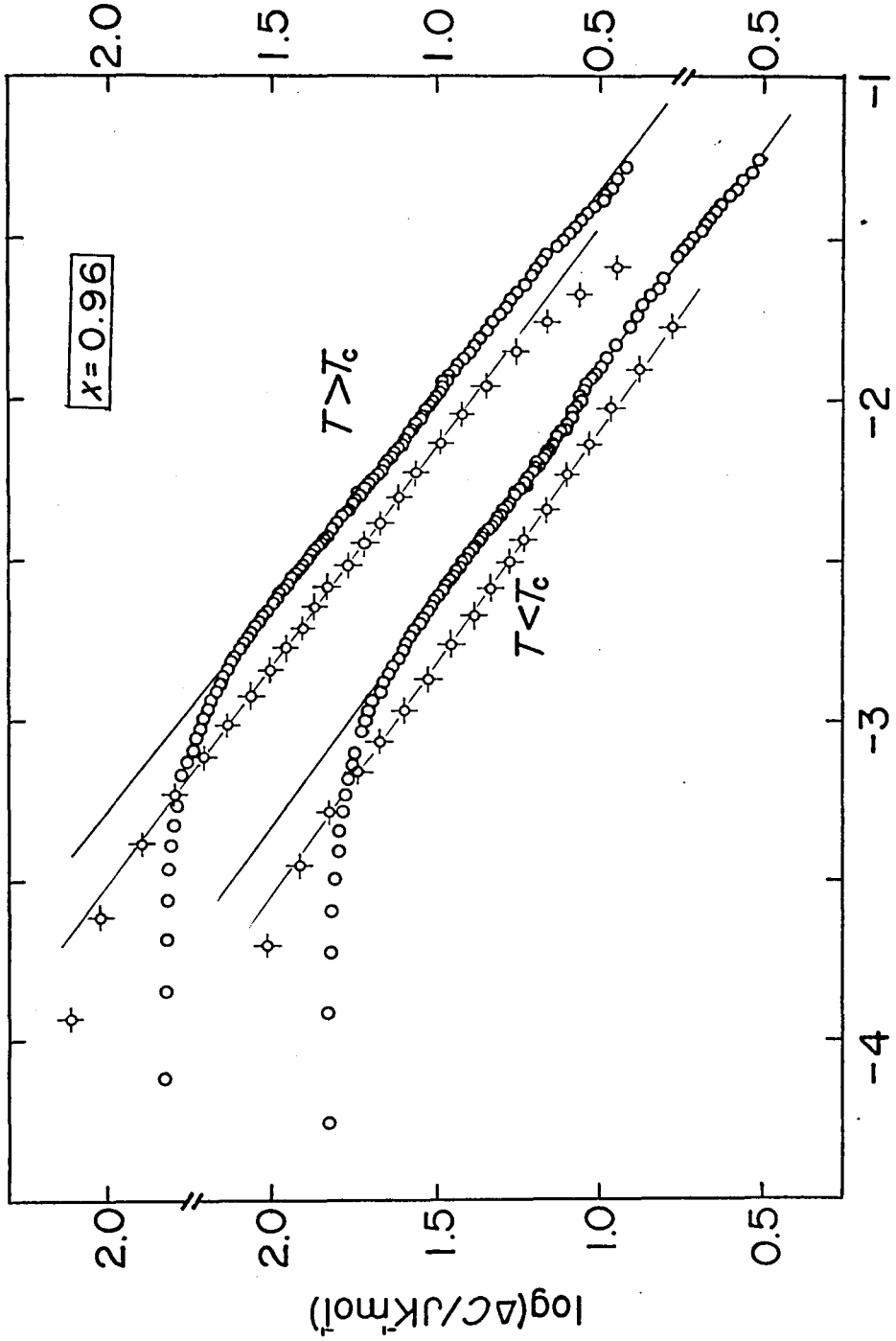

Fig.33. Logarithmic plot of the anomalous part of the heat capacity of x=0.96. O : x=0.96, ⊕ : x=0.96(II).

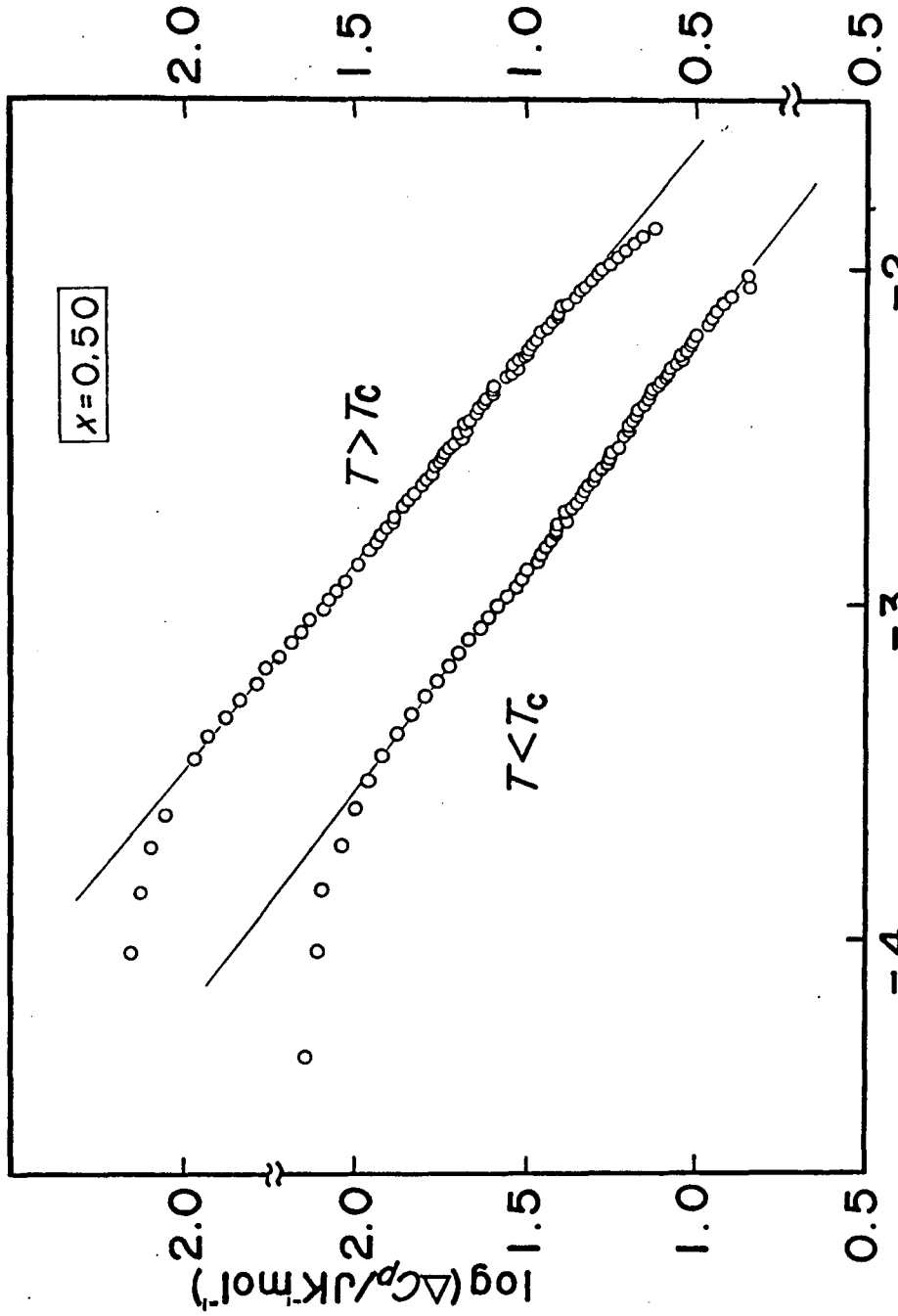

Fig.34. Logarithmic plot of the anomalous heat capacity of x=0.50.

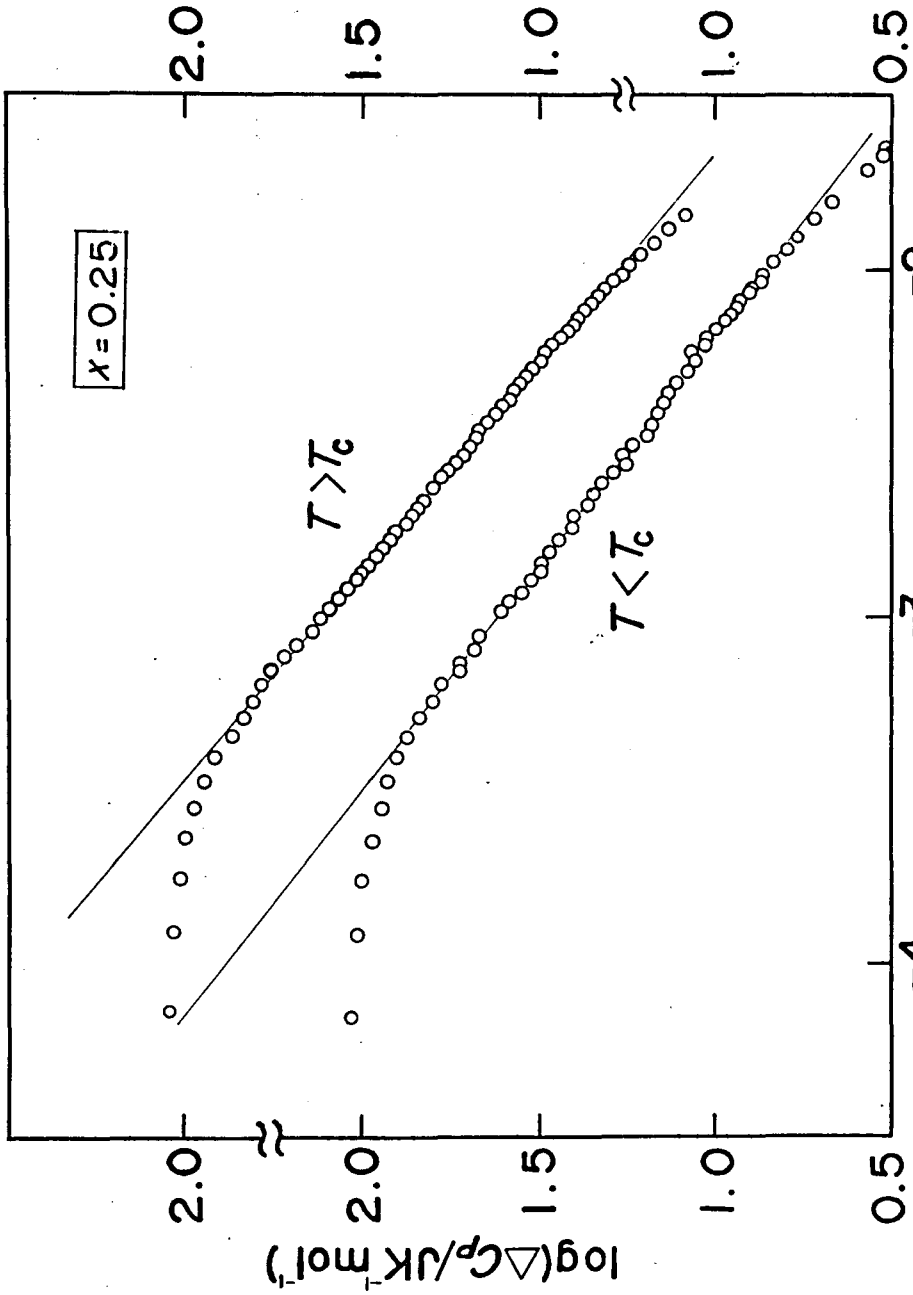

Fig.35. Logarithmic plot of the anomalous part of the heat capacity of x=0.25.

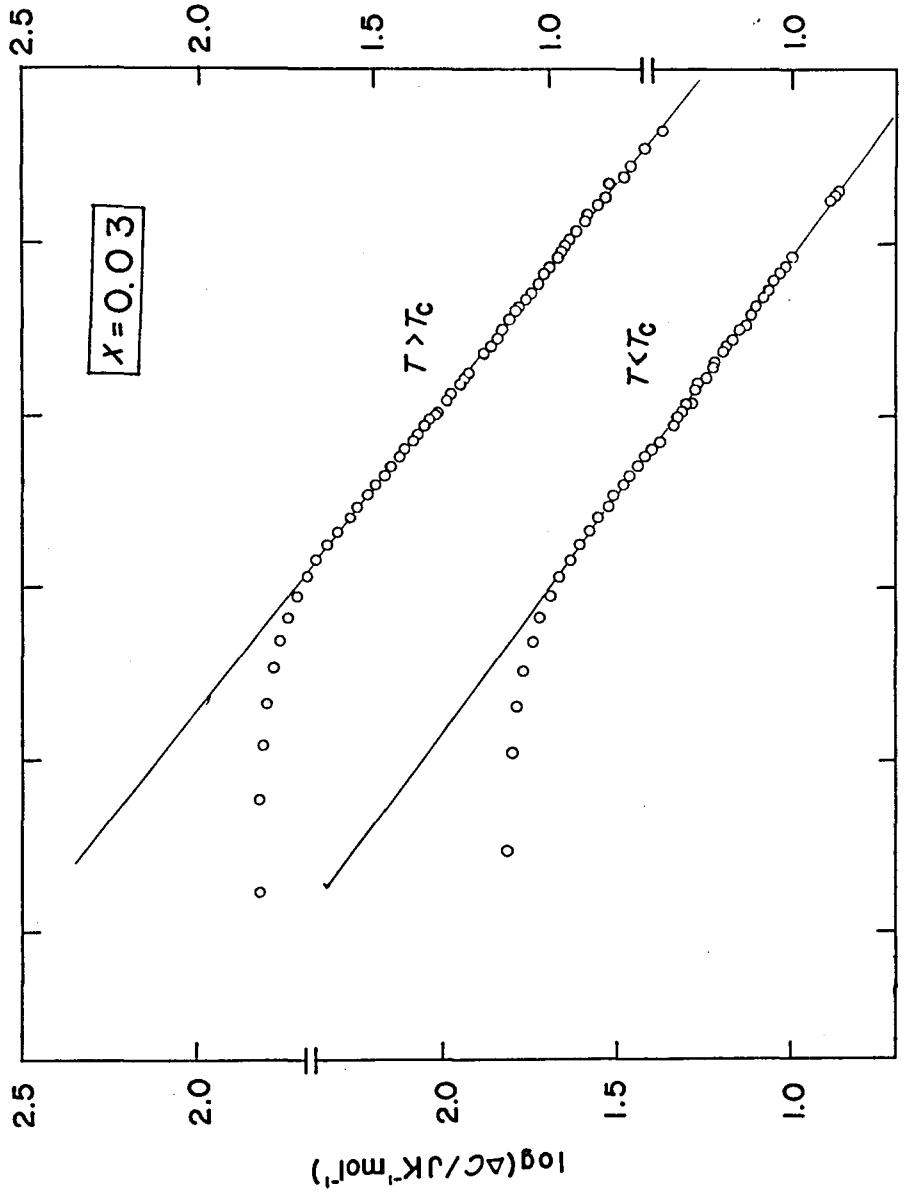

Fig.36. Logarithmic plot of the anomalous heat capacity of x=0.03.

also give the result for x=2.00 and x=0.03. (For x=0.96 the log-log plot of the second measurement is also shown in Fig. 33, and this result of annealed crystal is used in the subsequent discussion.) Outside $|t|<10^{-2}$ the data deviate systematically from Eq. (2). This may imply that contribution from the higher order correction term of Eq. (1) is significant or that the approximation to the lattice heat capacity deviates systematically from the actual one in this region. The rounding effects appear in the crystals, x=1.50, x=0.96, x=0.50 and x=0.25 x=0.03. The regions of the first and the last crystals are smaller ($|t|<10^{-4}$) and larger ($|t|<10^{-3}$) respectively, than those of the remainder which are rounding in the same region of $|t|<3\times10^{-4}$. Experimental results in many magnetic systems show the larger rounding region below than above T_c. Heller pointed out that it might be an intrinsic effect associated with the presence of a domain structure[2]. The rounding in the present crystals onsets in the same region below and above the transition point, which is not in conflict with the above statements because the crystals are free from domain structure below T_c as well as above. Recently it was suggested from the dielectric measurement parallel to the hydrogen bonded layers that SCD showed the crossover phenomenon between two and three dimension around t=10^{-3} below T_c[80, 81]. However, we cannot find the inflection point due to the crossover in our log-log plot. Figure 37 shows the ΔC_p ($=C_p-ET-B$) vs. T/T_c in the region fitted to Eq. (2) for comparison of the degree of sharpness (or divergence) in heat capacity with the magnitude of critical exponents. The crystals x=1.50, x=0.96, x=0.50 and x=0.25,

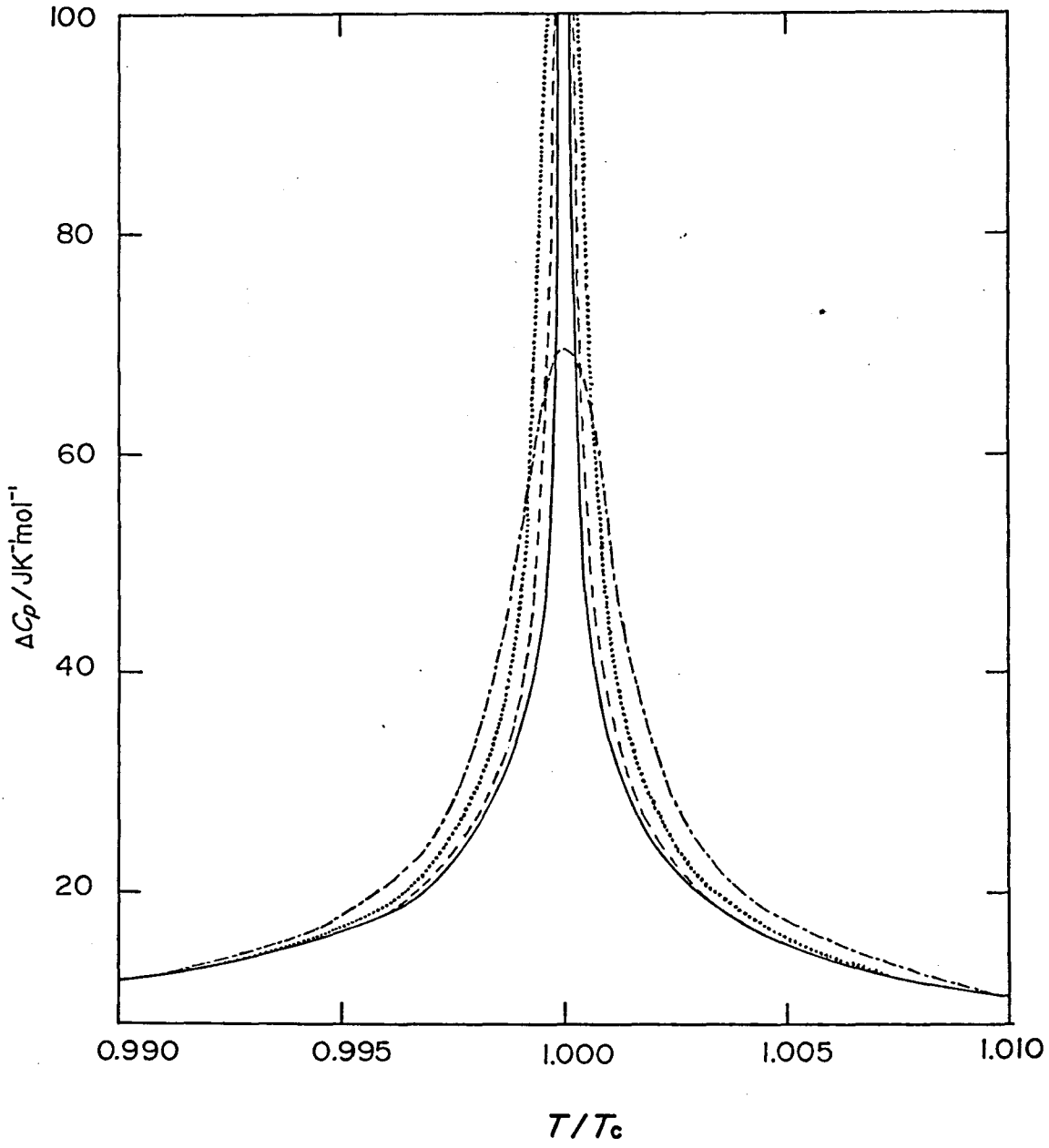

Fig.37. ΔC_p vs. reduced temperature(T/T_c).
—— : x=2.00, x=1.97, --- : x=1.75,
··· : x=1.50, x=o.96, x=0.50,
x=0.25, -·-· : x =0.03.

have approximately the same α and lie on the same smooth curve in the reduced plot (dotted line in the figure). It should be noted that the heat capacity with smaller critical exponent exhibits sharper peak than those with larger one. The critical exponents have approximately same values below and above T_c, as expected from these highly symmetrical curves of the ΔC_p's. They are in the range between 0.49 and 0.8. Although such large positive values have been rarely observed in the magnetic and fluid systems, they are found in some systems such as KDP, DKDP, NH_4Cl, NH_4Br[82], $NaNO_2$[83] etc. Small 1st order components were found in KDP and DKDP near the critical temperatures and the critical exponents were calculated below transition temperature. In the region $10^{-2}>t>3\times10^{-4}$ the heat capacity of KDP was proportional to $t^{-0.5}$, which could be fitted to the Landau theory and in the region inside about $t=2\times10^{-4}$ the singularity showed a logarithmic divergence. Very similar behavior was observed for DKDP but the transition in KDP was much more nearly of higher order than in DKDP. These behaviors in KDP and DKDP resemble those in $x=2.00$ and $x=1.97$ which have also small 1st order components and critical exponents of 0.49 and 0.44. However, the present substances does not exhibit logarithmic singularities near the critical temperatures. This difference seems to arise from that the long-range(dipole-dipole) interactions play an important role in the ferroelectric transition of KDP but that such an interaction is not found in SCD. Landau theory($\alpha=\frac{1}{2}$) was successfully applied to the phase transitions with small 1st order component in other systems of $NaNO_2$ and TlH_2PO_4[84]. Larger critical exponents were reported

for NH_4Cl *i.e.* $\alpha'=0.673$ and $\alpha=0.826$ and smaller values($\alpha'=0.18$, $\alpha=0.38$) for antiferroelectric-paraelectric transition of $NaNO_2$. The ratios(α'/α) in these crystals(0.815, 0.474) are smaller than in SCD systems(0.93∿1.00), which may reflect the fact that the former have three dimensional interactions while the latter have mainly two dimensional one. Theoretically critical exponents are calculated for various models by use of various techniques and some of them can successfully reproduce the experimental results especially for the magnetic or fluid systems. For SCD Salinus and Nagle[67] proposed the planar dimer model on the basis of the ice condition. Their exact solution gives the logarithmic divergence($\alpha=0$) of the heat capacity. They calculated also the critical exponents in the region of experimental interest based on their model, but it was about four times smaller than the experimental one. Figure 38 shows the parameters, α, α', A and A' as a function of the isotopic composition. These parameters remain practically constant up to $x=1.50$, and α, α' decrease and A, A' start to increase remarkably in the region $x=1.75$. The systematic variation is known hitherto only for ^3He-^4He mixtures. This behavior in Fig. 38 might be qualitatively explained by applying the vertex model. Several vertex models have been considered for two dimensional hydrogen bonded crystals. These generalized models of the ice or KDP model consist of a square lattice of N vertices with one hydrogen atom per lattice edge and there are sixteen possible vertex configurations. Figure 39 shows the eight of them where the constraints (*e.q.* ice condition) for the configuration are relaxed in turn from ice

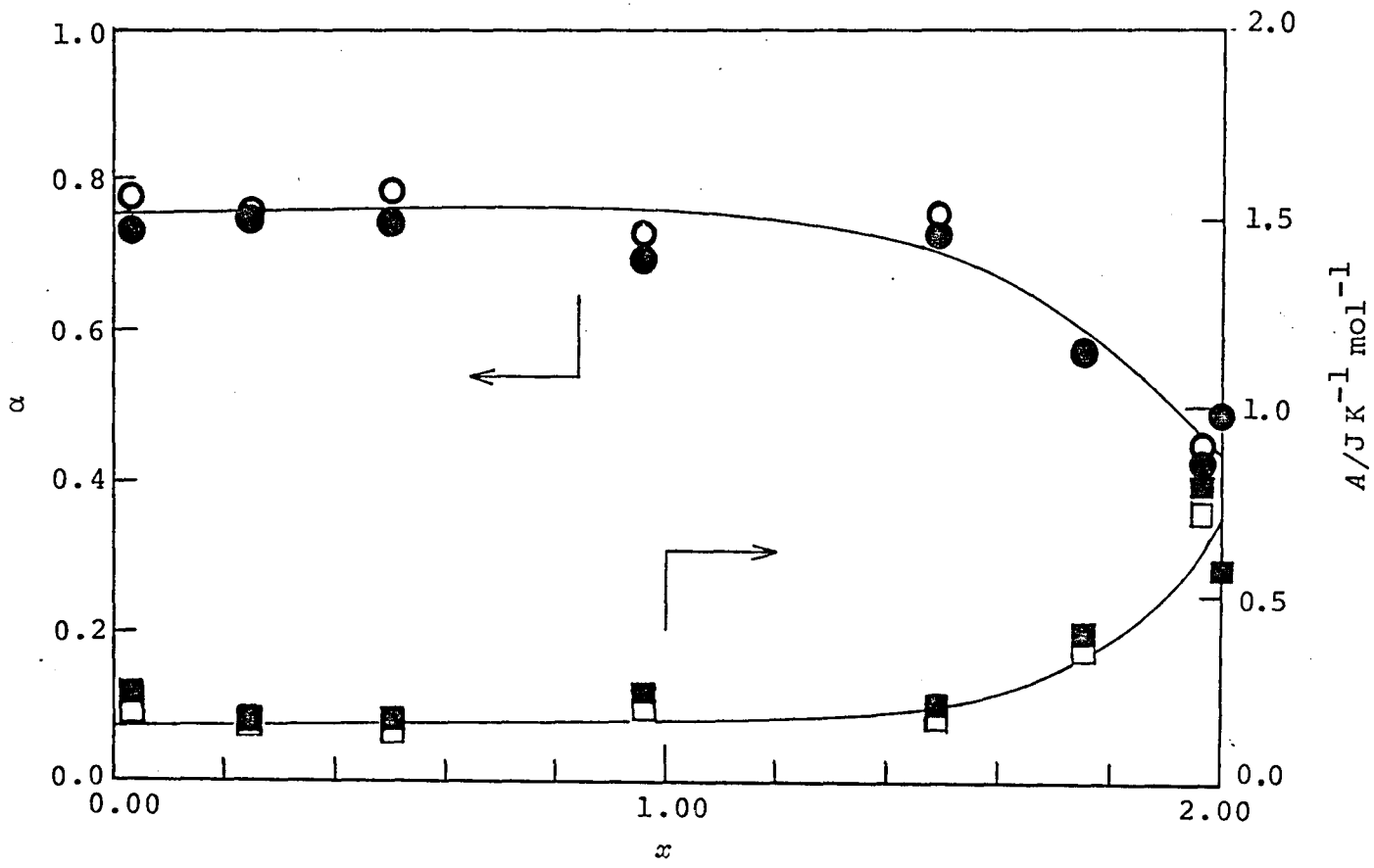

Fig.38. Composition dependence of critical parameter.

● : α', ○ : α, ■ : A', □ : A.

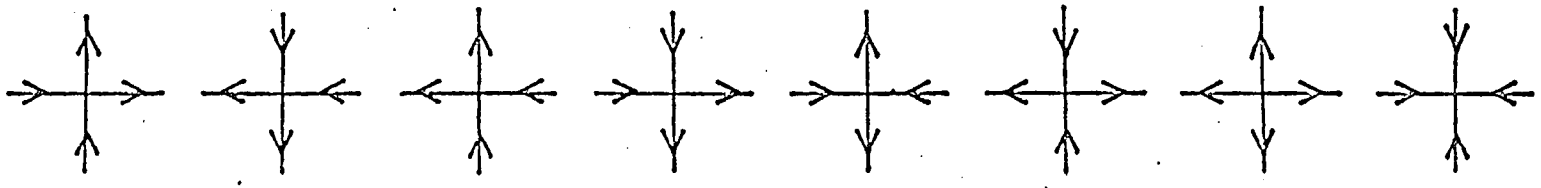

MODELS	ENERGIES							
ICE	0	0	0	0	0	0	∞	∞
KDP	0	0	ϵ	ϵ	ϵ	ϵ	∞	∞
F	ϵ	ϵ	ϵ	ϵ	0	0	∞	∞
8v	ϵ_1	ϵ_1	ϵ_2	ϵ_2	ϵ_3	ϵ_3	ϵ_4	ϵ_4
Staggered 6v	ϵ_1	ϵ_1	ϵ_2	ϵ_2	$\epsilon_3 \pm s$	$\epsilon_3 \mp s$	∞	∞

Fig.39. Eight of the sixteen possible vertex configurations on a square lattice. (quated from Ref. [6]).

model to staggered eight vertex model(8V). The staggered 6V model has been related to the SCD dimer model by Wu and Lin[18]. Vaxter gave the exact solution for the 8V model[20] which allowed the formation of ionic species(vertices) such as O^{2-} or H_4O^{2+} (breaking the ice condition). This model shows that the critical exponents of the heat capacity depend smoothly on the vertex energy ε_1, ε_2, ε_3, ε_4 and that $\alpha=\alpha'$. It might be reasonable to consider that the staggered 8V model can be applied to our system, though we cannot assign the configurations in SCD to each vertex. This suggestion is supported by the observed DC conductivity[61] due to proton transfer.

3.3.3. Universality and scaling law

Let us consider now our results from the view points of universality and scaling law. It is expected that critical exponents and certain other parameters, will be universal in the sense that they are identical for apparently vastly different systems, proveided that the physical dimensionality and the number of degrees of freedom of the order parameter are the same, and also provided that the ranges of interaction are the same *i.e.* the interaction is either short range or long range[85]. This hypothesis has not been necessarily confirmed experimentally. For example a universality was not found in the superfluid transition of ^4He where the value of α depends on the pressure. Moldover however reported that a universal character was really observed in the ^3He-^4He mixtures with regard to variations of the composition. In our systems, the fundamental quantities described above seem to remain irre-

spective of the composition in solid solutions, so that each crystal can be expected to take the same critical exponent. However, the values of α continuously varied from 0.44 to 0.8 beyond their experimental errors(see Fig. 38). Similar destruction of universality hypothesis is also found in 8V model where the corresponding critical exponent changes continuously with the strength of the interaction.

Recently Suzuki[86] proposed a new concept of universality which included such an exception. It states that critical exponents defined through the inverse correlation length κ, instead of the variable $T-T_c$, should be universal, *i.e.* the reduced critical exponent $\hat{\phi}$ for a physical quantity Q is defined by $Q \simeq \kappa^{-\hat{\phi}}$ where $\kappa \simeq (T-T_c)^{\nu}$. In the case of heat capacity the critical exponent is defind as $\hat{\phi} = (2 - \alpha)/\nu$. The prediction is checked in the experimental results on the planar antiferromagnet K_2NiF_4. The 8V model is also confirmed to satisfy the universality with regard to the critical exponents. Therefore, it is expected that the critical exponent ν of the correlation length will be determined by measurement of neutron scattering in order to check the applicability of the new universality hypothesis to our system.

The scaling law[87] is based on the principle that free energy or equation of state depend only on order parameter or its conjugate field(h) scaled by $|(T - T_c)/T_c|^{x_t}$, *i.e.*

$$\Phi(h, t) = t^{d/x_t}\Phi(h/t^{x_h/x_t}, 1),$$

where d is a dimension of space and x_h, x_t are any positive powers. From this relation the various critical exponents are

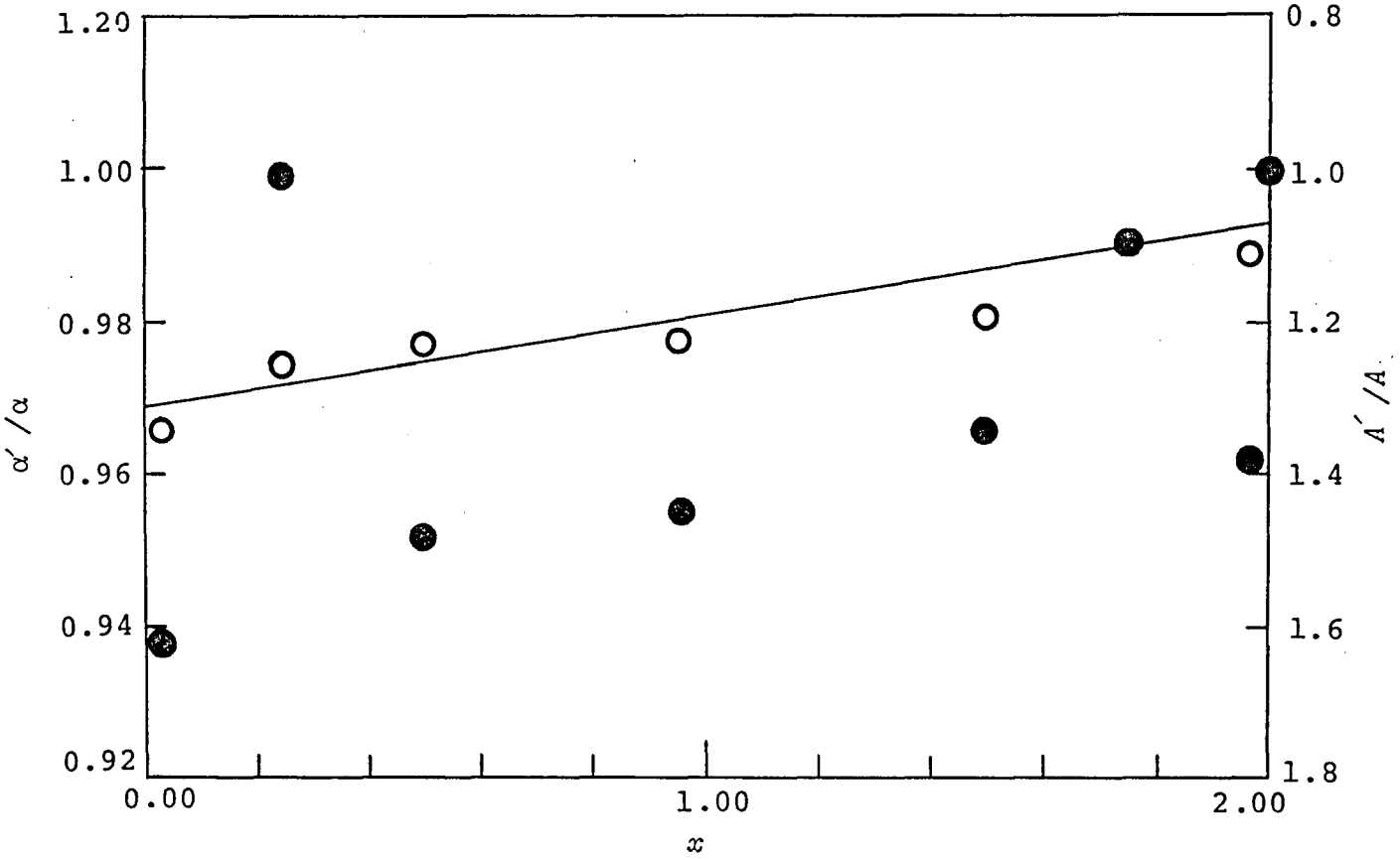

Fig.40. Ratio α'/α and A'/A vs. composition.

● : α'/α, ○ : A'/A.

determined by the two scaling parameters, x_h, x_t, and are related to each other. Some of them with respect to the critical exponent α of the heat capacity are given below.

$$\alpha = \alpha', \ \alpha' + 2\beta + \gamma' = 2, \ \alpha' + \beta(\delta + 1) = 2, \text{ etc.},$$

where the notations obey conventional terminology. The scaling predictions which we can attempt to test directly on the present data alone are $\alpha = \alpha'$. The relation was usually accepted as the constraint($\alpha=\alpha'$) by several authors[88, 89] when experimental data were fitted to Eq. (1). The ratios α'/α are located between 0.94 and 1.0, and its concentration dependence is shown in Fig. 40 where the ratios A'/A are also given for comparison. All crystals in our system satisfy the scaling relation, $\alpha=\alpha'$, within the error (±5%) and furthermore, the strict relation of $\alpha=\alpha'$ can be obtained by adjusting the other parameters(T_c, E, B), or fitting region and by introducing the correction term ($D|t|^x$). It is difficult to apply the second relation, $\alpha' + 2\beta + \gamma' = 2$, to SCD, because the order parameter cannot be found in SCD so that the critical exponent β of the order parameter cannot be obtained. The value of γ' was estimated to be larger than 2 from the dielectric measurement. Evidently the second relation fails in SCD, however these critical exponents satisfy the Rushbrooke inequality, $\alpha' + 2\beta + \gamma' \geq 2$, derived from the thermodynamics.

3.3.4. Effect of annealing

In general critical phenomenon is very sensitive to imperfection of crystalline sample, chemical impurity, inhomoge-

neity of external parameter, etc. The chemical or physical impurity leads to decrease the effective dimension of the sample through damping the correlation length and consequently give rise to change the heat capacity due to phase transition. The inhomogeneous distribution of impurities also causes the smearing of the singularity, that is, the maximum of the heat capacity has a smooth and broader top. Imperfect crystal containing impurities exhibits a different behavior from that of ideal crystal which obeys the asymptotic formula such as Eq. (1) and hence sometimes gives the erroneous results in determining the critical parameter or critical region. Since some of the imperfections can be removed from crystal by annealing, we carried out the high resolution heat capacity measurements on some annealed crystals(x=0.96, x=0.50 and x=0.03) in order to check the homogeneities in the distribution of isotopes. For this purpose the crystals were annealed in closed glass jars at room temperature for long time. The results are shown in Figs. 20, 21 and 22. The maximum and the shape of the heat capacity are affected only slightly by annealing in the sample x=0.50 but the remarkable changes are observed in the case of x=0.96. These facts suggest that the inhomogeneity of the isotopic composition or the strain in the crystal relax within about four months after the recrystallization from the melt, because the first measurements for x=0.96 and x=0.50 were performed after a month and four months, respectively. The results in x=0.03, which was annealed for *four years*, reproduced quite well those of the first crystal which was measured at one month after preparation. From the fact that the different

annealing effect were found in between x=0.96 and x=0.03, the annealing effects can be regarded as one due to concentration inhomogeneity among isotopes of water molecules(H_2O, D_2O), since the inhomogeneity of distribution between H_2O and D_2O in x=0.03 is expected to be much smaller than in x=0.96. A slight effect in x=0.03 will be caused by the relax of strains in the crystal. Two mechanisms can be considered for the process of redistribution between H_2O and D_2O in the crystal. One is the diffusion of the H_2O or D_2O molecules as known in ice[90]. The other will be due to the jump of proton or deuteron in the hydrogen bonded network. It was found from the study of NMR that a jump of proton occur per about 10^{-6} s with 180° flip motion and three-fold reorientation of water molecule. We attempt to calculate the time t in which completely localized protons or deuterons redistribute over the range of 7.5×10^{-1} mm^2(10^{12} unit cell) in the hydrogen bonded network of SCD. The time t was estimated to be 32 days at room temperature by the method of random walk. This calculated value corresponds to maximum value because the distribution of proton or deuteron is already almost homogeneous in the real sample employed for measurement.

3.3.5. Fitting to rounding curve

The rounding phenomena are observed in many systems by various experiments, although these must arise from different several reasons described in 2.3.4. The physical mechanism causing the rounding effect is still not clearly understood. The rounding phenomena are explained phenomenologically on the assumption that the crystal could behave as if it were composed

of microcrystals. In the case the crystal is subdivided into a number of microsystems which do not correlate each other. These homogeneous microsystems are assumed to have slightly different ordering temperature. The heat capacity of the entire system then would be given by,

$$C(T, T_c)=\sum_i C(T, T_{c_i}) f(T_c, T_{c_i}) / \sum_i f(T_c, T_{c_i}) \cdot \qquad \text{Eq. (3)},$$

where $C(T,T_{c_i})$ is the asymptotic heat capacity of microsystems at T and $f(T_c, T_{c_i})$ is the distribution function. This method of analysis was successfully applied to several magnetic systems. We have calculated the heat capacity of x=0.03, x=0.50 and x=0.96 using Eq. (3) and Gaussian distribution of transition temperature T_{c_i} with half-width d for $f(T_c, T_{c_i})$, *e.g.*

$$f(T_c, T_{c_i})=K \exp[-(T_c - T_{c_i})^2/2d^2]. \qquad \text{Eq. (4)}$$

The asymptotic heat capacity $C(T,T_{c_i})$ is assumed to be given by Eq. (2). *i.e.*

$$\begin{aligned} C(T, T_{c_i}) &= A\left|(T - T_{c_i})/T_{c_i}\right|^{-\alpha} + B \qquad T \geqq T_{c_i} \\ &= A'\left|(T - T_{c_i}/T_{c_i}\right|^{-\alpha'} + B' \qquad T \leqq T_{c_i} \end{aligned} \qquad \text{Eq. (5)}$$

The value of T_c is fixed to each peak temperatire. In x=0.03, two different sets of values (x=0.03 and x=2.00) are fed in critical parameters in Eq. (5). The values of the Gaussian half-width d is varied in order to produce the best fit to the data over the range of $|t| \leqq 5\times10^{-3}$, but we cannot obtain good agreement between the calculated heat capacity and the experimental data. The results are shown in Fig. 41(a) for

d=0.1, d=0.2 and d=0.5. In the case of x=0.96, if the rounding is due to the distribution of the microcrystals with different concentrations, the annealing effect might be accounted by the above method. We employ the parameters of the x=0.96(II) as those of microsystem. The result also is not satisfactory as shown in Fig.41(b). The heat capacity of x=0.50 couldn't be reproduced by this method. The same attempt in KDP system was also unsuccessful[28]. This is due to the fact that since in contrast with the magnetic system[91], interaction of electric dipole moment or ordering of proton, coupled strongly with lattice vibration, it is difficult to realize the isolated homogeneous microsystems in the crystal. The other possible origin of rounding will be considered on the basis of the intrinsic nature of crystals in 3.3.7.

3.3.6. Order of the phase transition and entropy change near the transition temperature

In this section we will discuss the order of the phase transition. The present system composed of the solid solutions showed the change from the first order to the higher order with the variation of the concentration. When phase transition accompanies a small first-order component, it is difficult to determine experimentally whether the transition is first order or higher one. From purely observational view, it is often noticed that thermal equilibrium in the calorimeter is attained very sluggishly at the first-order

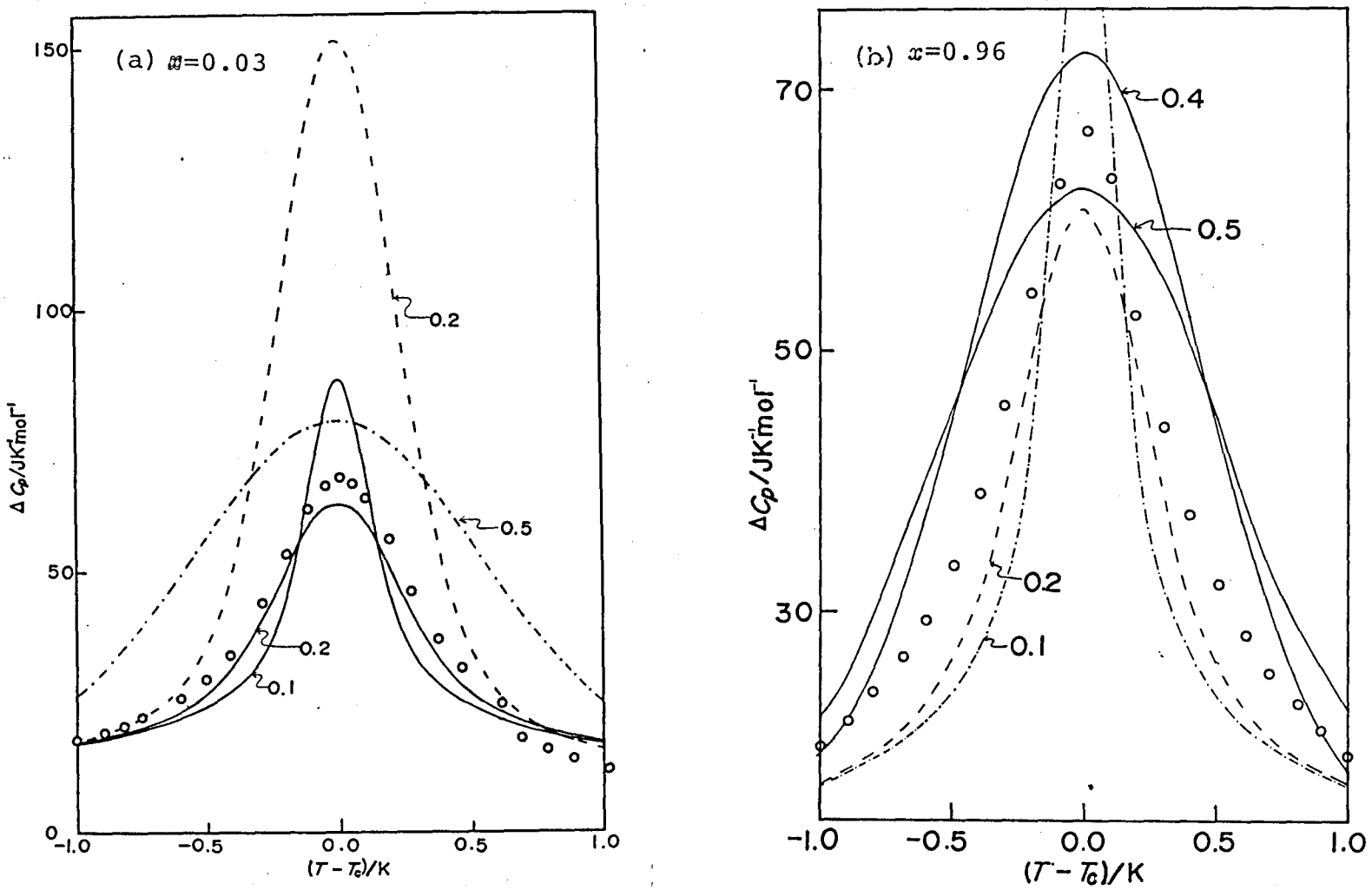

Fig.41. Experimental points compared with curve calculated from Eq.(3) by using of the critical parameters of x=2.00(——), x=0.03(---) in (a) and x=0.96(II)(——), x=2.00 in (b).

transition points. This is usually attributed to the slow progress of the first order transition. In the present case, slow equilibration was observed in the pure hydrate and H_2O-rich solid solutions. Namely at the transition temperatures of the crystals x=2.00, x=1.97, and x=1.75, the equilibration time amounted to 5 $\sim$ 7 times in comparison with that found in the normal temperature regions. This fact suggests the occurrence of first order transitions in the mixed crystals with these compositions. No such anomalous equilibration characteristics were observed through the transition regions of all the crystals x=0.96, x=0.50, x=0.25 and x=0.03. The crystal x=1.50 was the boundary case where the unusually long equilibration time was observed at only one point of observation located at the peak of the transition. A more quantitative evidence for the change of the character of the transition with the increase of the deuterium content is shown in the excess entropy vs. temperature diagram in Fig. 42, where the ordinate is the absolute entropy. These curves were calculated by integration of the excess heat capacity $\Delta C=C_{obs.}-C_l$ divided by the temperature, where the estimation of the lattice heat capacity C_l will be given in 3.3.8.

It should be noted that changes of the entropy at the T_c gradually diminish and that distinct jumps of entropy are found for x=2.00, x=1.97, and x=1.75. The amounts of the jump in the entropy are 0.15, 0.15, and 0.13 $J K^{-1} mol^{-1}$ and the corresponding enthalpy changes are 32.45, 33.12 and 29.24 $J mol^{-1}$ for x=2.00, x=1.97 and x=1.75, respectively. From these results we can conclude that x=2.00, x=1.97 and x=1.75 have first-order component

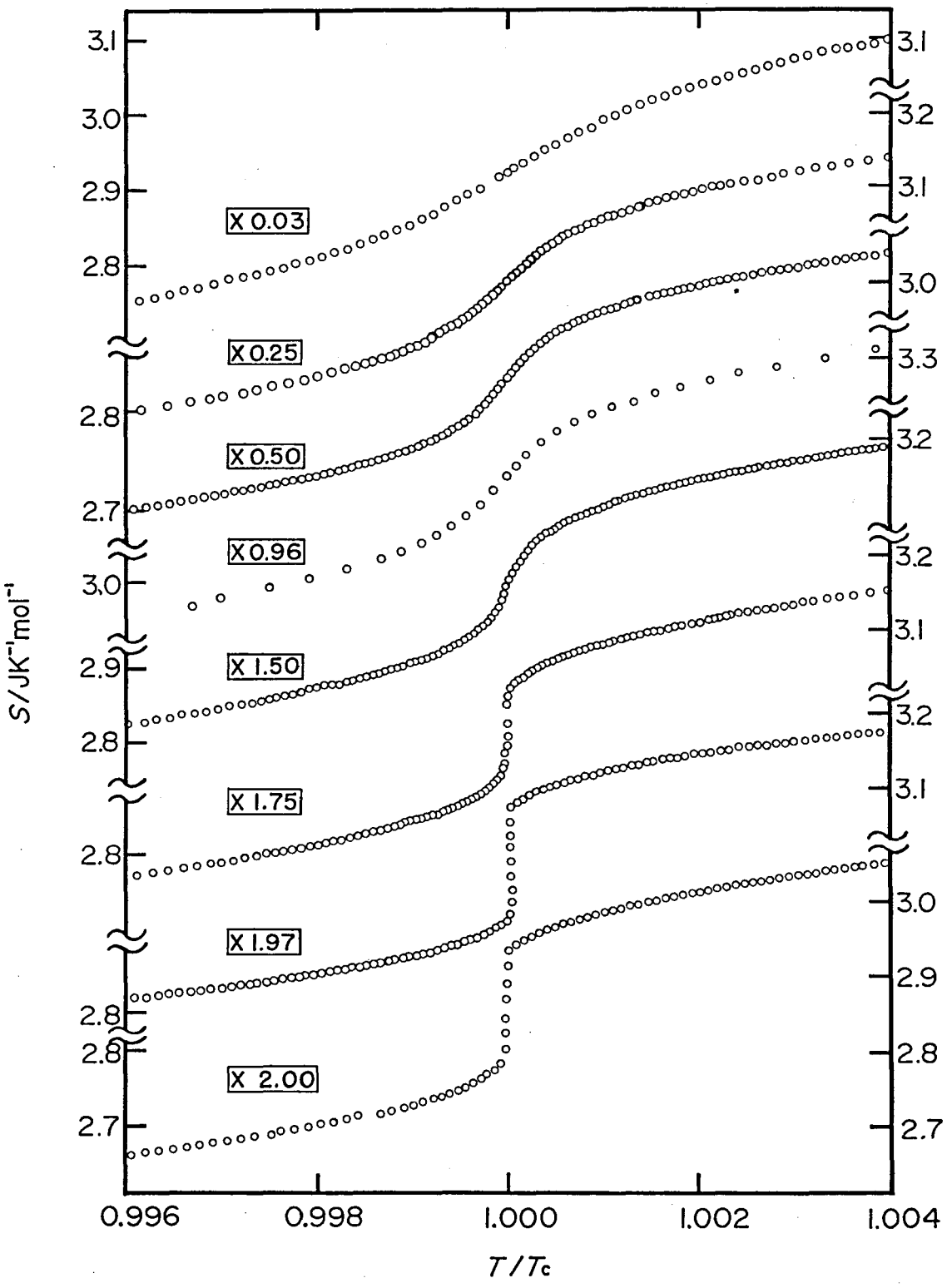

Fig.42. Transition entropy vs. reduced temperature. The ordinate indicates the absolute value.

and that the transitions are higher order in x=0.03, x=0.25, x=0.50 and x=0.96. The sample x=1.50 shows no distinct jump at T_c, but its temperature drift observed is similar to those for x=2.00, x=1.97 and x=1.75 as described above. This suggests that the phase transition in x=1.50 has a first-order character. Consequently, the nature of the phase transition in our system changes continuously from the first order to the higher order with the increase of the deuterium contents. There are some differences($\pm$0.12 $JK^{-1}mol^{-1}$) in the absolute values of entropy at T_c(S_c), which are due to the uncertainty($\pm$1 $JK^{-1}mol^{-1}$) in estimating the lattice heat capacity. The experimental entropies are minimum values because the lattice heat capacity employed above is probably upper limit(see 3.3.8.). The experimental entropy at T_c and T/T_c = 2.0 are 3.0 $\pm$ 0.12 and 3.94 $\pm$ 0.23 $JK^{-1}mol^{-1}$ and they are larger than the theoretical values, S_c= 2.34 and S_∞= 3.02 $JK^{-1}mol^{-1}$ which are calculated by Salinus and Nagle based on their dimer model. These differences exceeds the uncertainty of the estimation and appears mainly around the transition temperature as shown in Fig. 43. These differences in entropy are caused by the fact that the dimer model dose not allow the creation of the ionic species of water molecules, and hence the transition entropy is less than the experimental one. Accordingly the 8V model(described in 2.3.2.) seems to be more suitable to the case of SCD.

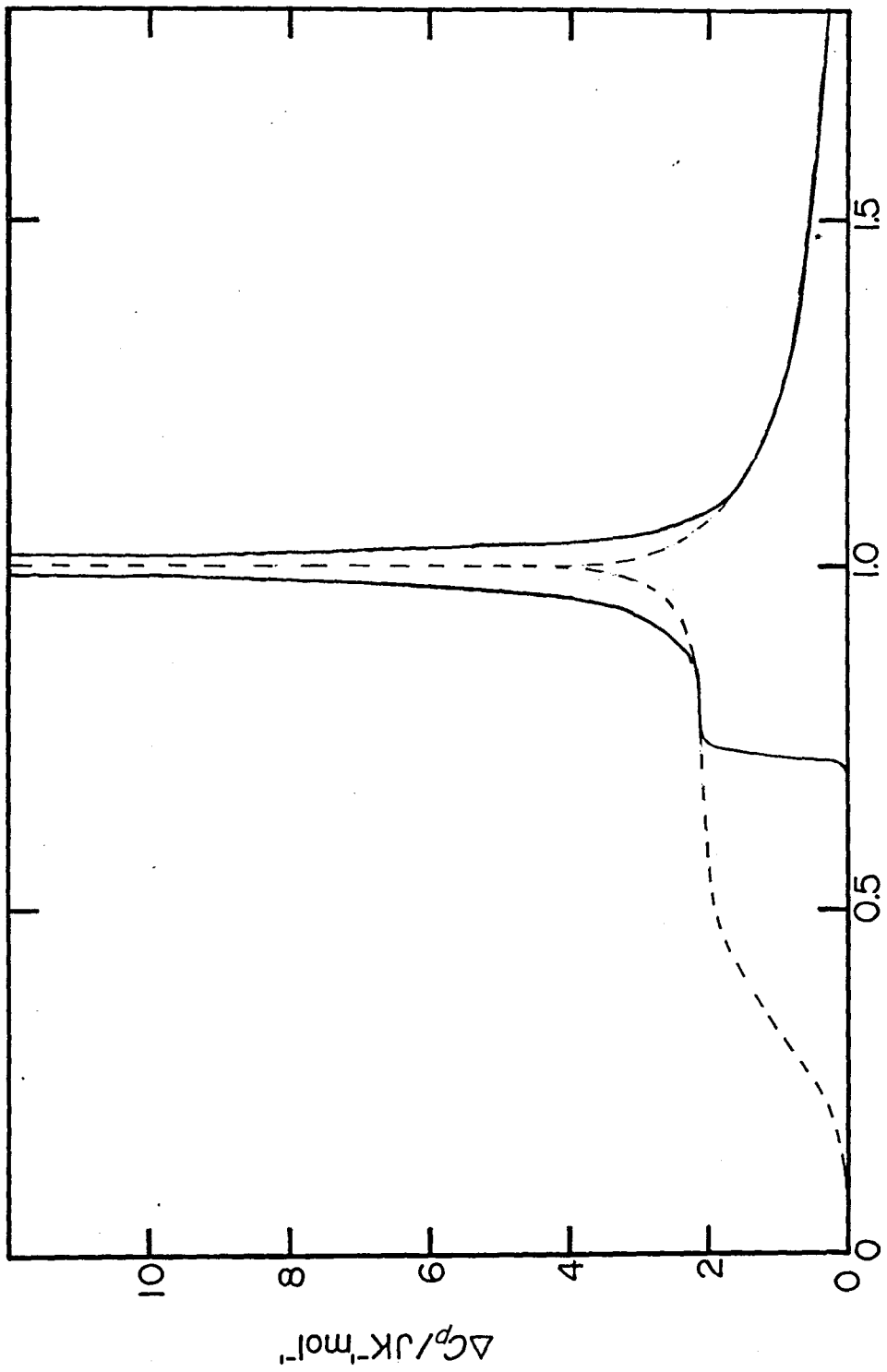

Fig.43. Comparison of the experimental heat capacity of x=2.00 (solid line) with the theoretical one calculated from dimer model(broken line).

3.3.7. Problem of tricritical or supercritical phenomenon

We will now consider our results on the basis of the phase diagram. In general a coexistence surface (CXS) or a first-order phase transition surface may terminate in the field space in the following ways[92]. i)The CXS intersects another CXS in a triple line at which three phases are in equilibrium. ii) The CXS passes into another hypersurface which continues to separate two phases but which has the property that all densities(extensive variables)are continuous at the hypersurfce. iii) The CXS may terminate in a line of critical point. In the two dimensional phase diagram these cases correspond to i)triple point, ii)tricritical point and iii)critical point. Our results correspond to the case of either ii) or iii).

a)Second case(tricritical point)

There has been recently considerable interest in tricritical phenomenon. The tricritical points have been observed in the ^3He-^4He mixtures, metamagnetic systems, NH_4Cl, ND_4Cl and NH_4Cl-NH_4Br solid solutions[93]. In addition to these systems, quite recently it has been also found in the cases of ferroelectrics and liquid crystals. Fig. 44(a) shows a phase diagram displaying a tricritical point, where ζ is a field *i.e.*, internal magnetic field, chemical potential or pressure, and η is a thermodynamic conjugate of order parameter such as staggered magnetic field. η is a fictious field unavailable in laboratory. A first-order coexistence surface at $\eta=0$ bifurcates into two coexistence surfaces or "wings" projecting in a symmetrical fashion into the regions $\eta>0$ and $\eta<0$. On the sur-

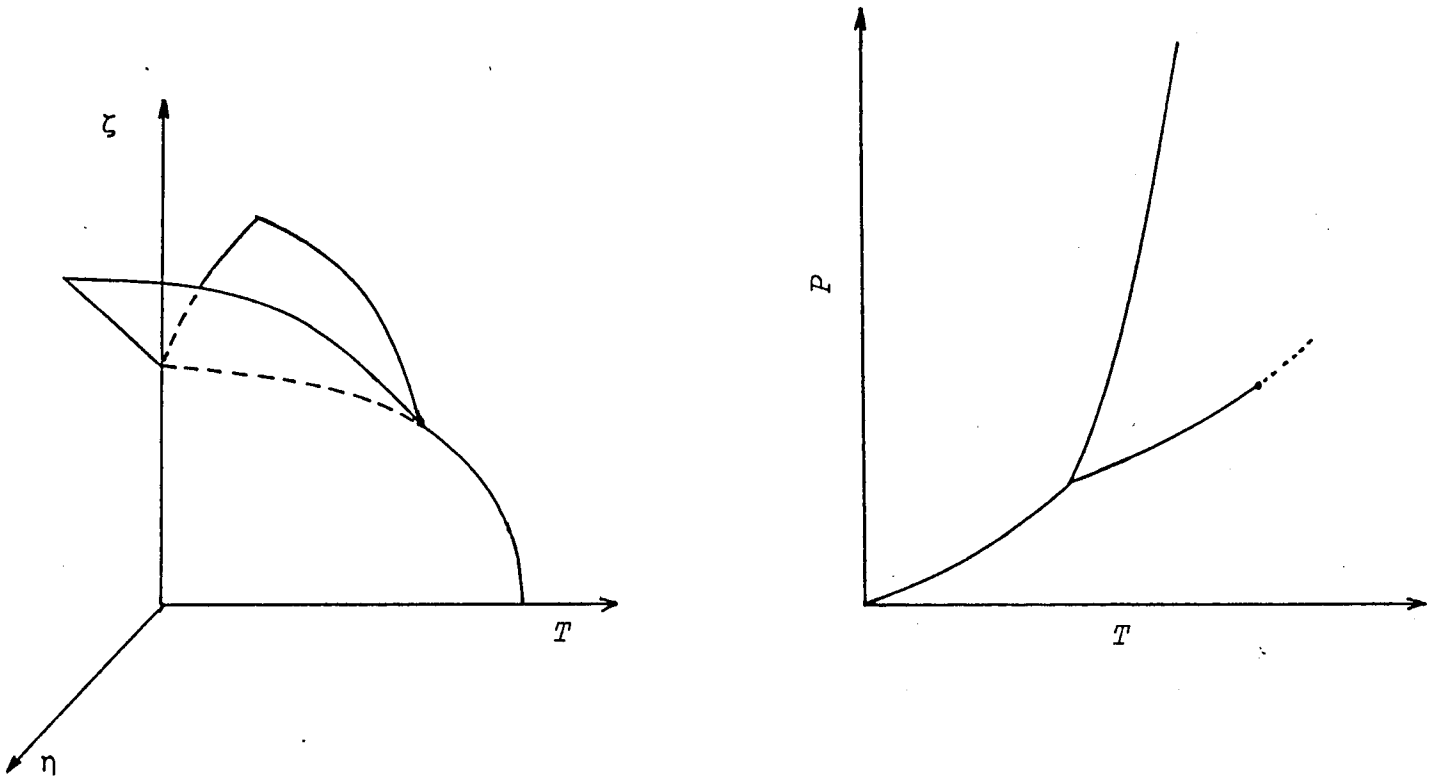

(a) (b)

Fig.44. Phase diagram displaying a tricritical point(a) and liquid-vapor phase diagram(b).

face at $\eta=0$ the order parameter changes discontinuously as η goes from positive to negative values. The discontinuity across the CXS goes continuously to zero upon approaching the critical line(or tricritical point) in such a fashion that at the critical line there is no longer any distinction between the previously separated phases. The first-order line in the surface $\eta=0$ is line of triple point. Our system, the solid solutions of SCD and DSCD, exhibits similar behavior described above except several points. The first-order components observed in proton rich side are continuously decrease as the deuterium concentration increased and completely disappears at the sample of $x=0.96$. Change of the critical exponents is found in the region between $x=1.75$ and $x=2.00$. However, there are some problems which cause us to hesitate about applying the tricritical phenomenon to our system. We cannot define the order parameter corresponding to thermodynamic conjugate of η in our system. Therefore, it is difficult to give the definite physical meaning to the first order coexistence surface, that is, we cannot define two kinds of state which coexist on this surface. The two kinds of state is possible to be defined in some other systems with tricritical point. For example in NH_4Cl system[94] there exist two ordered states of ammonium ion with different orientation in each sublattice. On the other hand we cannot conclude the existence of tricritical point in the present case on account of the reson described above.

b) third case(supercritical point)

In the solid this case can take place only if the symmetry does not change through the transition and this point is always found at liquid-vapor critical point. Such a transition found in solid state is called as an isomorphous transition where only the quantitative nature changes but the qualitative one (symmetry) remains unchanged. There are only two examples which have been observed for the γ-α transitions in Ce[95] and for the Mott transition in Cr-doped V_2O_3[96]. On the *P-T* phase diagram in Fig.44(b), first order phase transition occurs below the critical pressure and no phase transition occurs above the critical pressure(supercritical region). In the case of SCD it is reported by Kiriyama et al.[61] that the space group $P2_1/c$ is the same below and above the phase transition. In this respect we may take account another possibility, in addition to the case(a), that our system displays the vapor-liquid type phase diagram. In the α-γ transition of Ce, Jayaraman[95] performed the measurements of electrical resistance as a function of both pressure and temperature. The pressure-resistance isotherms indicated that the magnitude of the vertical drop in resistance progressively diminished with temperature up to the critical temperature where it became zero and that above the temperature the resistance smoothly varied with pressure. Similar changes are found in our system(see Fig.42), where one can see the smooth decrease of the transition entropy at the transition temperature from x=2.00 to x=0.03. However, it was difficult to observe the region

where the phase transition vanishes completely, even though x=0.03 shows only a minute change of entropy around the transition temperature. If our case corresponds to the case(b) the critical point is expected to exist around x=1.50. It is difficult to compare our result directly with the heat capacity in vapor-liquid system because the latter is usually measured at constant volume. Namely the C_V at $V=V_c$ diverges at T_c but the first order phase transition always occurs at both $V>V_c$ and $V<V_c$. However, we can guess from the P-V-T phase diagram in liquid-vapor that the change of the $C_{p_{max}}$ with pressure is similar to our result of $C_{p_{max}}$ vs. isotopic composition(see Fig.45). In the case(b) we can explain the change of the rounding effect and the $C_{p_{max}}$ with isotopic composition as below. The regions of the first-order phase transitions found in x=2.00, x=1.97 and x=1.75 spread over the interval of about 0.05 K most of which arises from the imperfection of crystals. The appearance of the first-order transition in such a narrow region suggests that there exist an inhomogeneous distribution of proton only to a few extent. The rounding in x=1.50 is caused by the same kind of imperfection and occurs in the same region(x>1.50) where the first-order transitions take place. The crystals x=0.96, x=0.50 and x=0.25 exhibit the rounding phenomena in the wider region(0.1 K). The degree of the imperfection of crystals and inhomogeneous distribution of proton are considered not to change significantly with the isotopic composition, since the preparations of the single crystals were carried out with the same procedure. These increases of round-

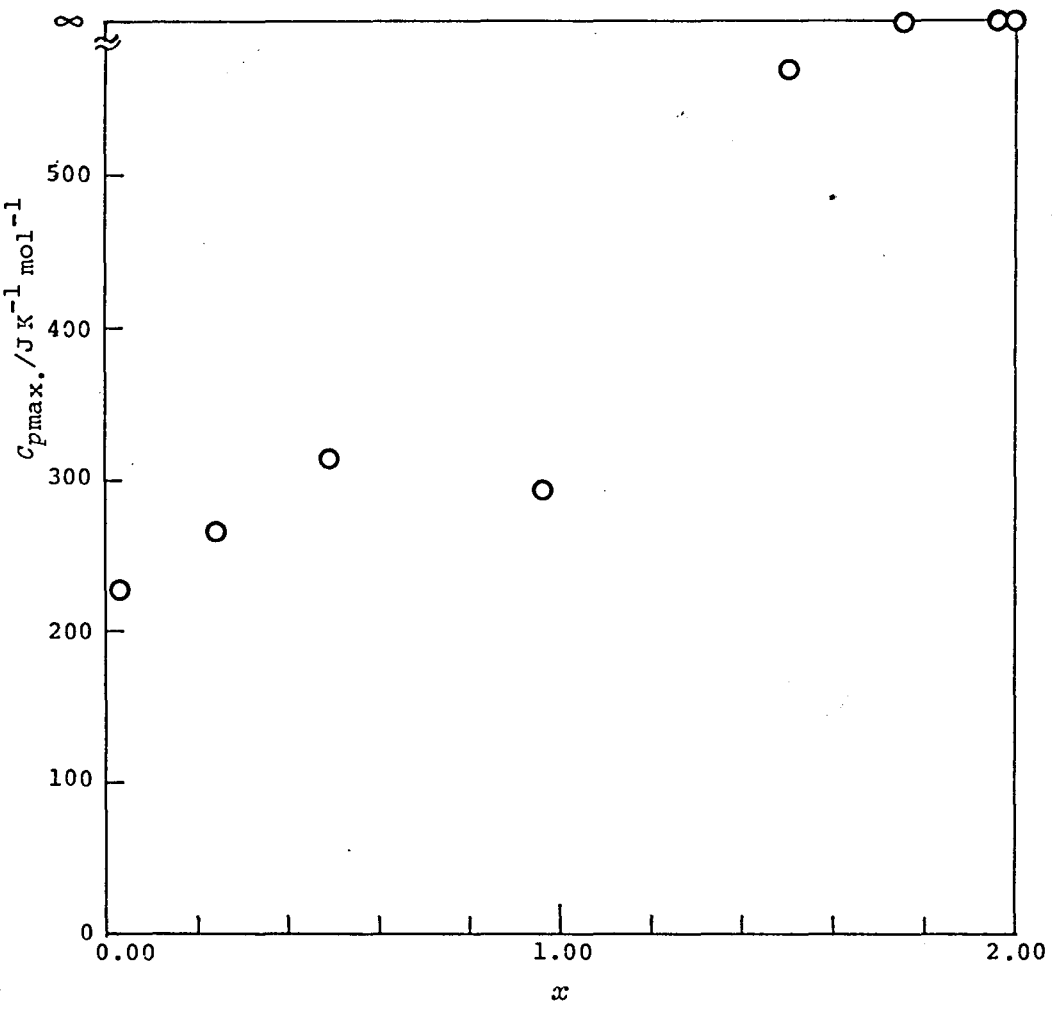

Fig.45. Composition dependence of maximum heat capacity($C_{pmax.}$).

ing regions reflect the fact that the phase transition of these crystals are in supercritical region. The rounding region may become wider as the isotopic composition deviates from critical composition(x=1.50). Therefore x=0.03 shows wider rounding region(0.2 K). Although we cannot definitely conclude which case (a) or (b) should be preferably applicable to our result, we consider that our system belongs to the case(b) at the present stage of our investigation. The measurement of critical scattering of neutron may be useful to answer this problem with the determination of the location of tricritical or critical point, *i.e.* whether the region between x=1.50 and x=0.03 is critical line or point.

3.3.8. Determination of lattice heat capacity

Below the glass transition temperature the heat capacity related to the phase transition does not contributes to the total heat capacity, since the hydrogen-bond configuration is frozen-in. Accordingly we can expect to find out the effect of composition on the change of the lattice vibration in this temperature region. The vibrational part is expressed in terms of the sum of the Debye and Einstein functions. The Debye characteristic temperature Θ_D is a useful parameter which reflects the mass effect and is sensitive to the small change of the heat capacity. The Debye temperatures are calculated from our heat capacity data on the solid solution in the following way. C_p was first converted to C_V according to the Nernst-Lindemann relation $C_p - C_V = AC_p^2T$,

where we determined the value of A ($=1\times10^{-7}$) so as to give the same order correction ($\frac{C_p - C_V}{C_p} \simeq 3\times10^{-3}\sim2\times10^{-2}$) as that of the copper formate tetrahydrate, and the same values were assumed for all mixed crystals. The internal mode vibrations contributing to the Einstein heat capacity were adopted from the results of the infrared absorption and the Raman scattering for SCD, DSCD and $SnCl_2(H_2O)(D_2O)$. These assignment is not complete but may be a possible one. We employed the following optical mode; intramolecular vibration of $H_2O(1)$ and $H_2O(2)$ (3125, 2975, 1545, 3505, 3375 and 1610 cm^{-1}), librational mode of water (945, 853, 542, 710, 486 and 415 cm^{-1}), intramolecular vibration of $SnCl_2(H_2O)$ (58, 67, 101, 134, 198 and 323 cm^{-1}), librational mode of $SnCl_2(H_2O)$ (111, 121 and 139 cm^{-1}) and translational mode (164, 250, and 254 cm^{-1}). As there was no spectroscopic data for the solid solutions, we assumed that there were only three vibrations (due to H_2O, HDO and D_2O molecules) for a given mode in the crystal with concentration x and that they contribute to the Einstein heat capacity C_E with the weight of $(x/2)^2$, $2\cdot(x/2)\cdot\{(2-x)/2\}$ and $\{(2-x)/2\}^2$, respectively. The Debye temperatures were calculated at each temperature from the Debye heat capacity which was equal to the C_V-C_E. $SnCl_22H_2O$ has twenty degrees of freedom per one molecule of which twenty four degrees are assigned to the Einstein mode and the remained three degrees are given to the degree of freedom in Debye function. Fig.46 shows the temperature dependence of Debye temperature where those of $x=2.00$ and $x=0.03$ are calculated from the data by Matsuo et al. Above

130 K the calculations were not carried out because of the existence of the glass transition region. Although Debye temperatures continuously decrease with the increase of the deuterium concentration, we cannot find any quantitative relation between them. The difference of the optical mode, especially of the librational mode of water molecule, explain the great part(80 %) of the differences among the heat capacities. The Einstein heat capacity increases in proportional to the concentration. The ratio of Θ_D for the SCD and DSCD can be described by the square root of the ratio of the molecular weight M for each crystal, *i.e.* $\Theta_D^H/\Theta_D^D = M_D/M_H$. But the ratio $\Theta_D^H/\Theta_D^D = 1.09$ is greater than $M_D/M_H = 1.009$, which is probably due to the incomplete assignment for optical mode. Generally it is difficult to discuss the Debye temperature by calorimetric study since the heat capacity is insensitive to the Debye temperature. The lattice heat capacity(C_l) above the glass transition could not be exactly determined by using the spectroscopic data, because the ambiguity of the $C_p - C_V$ correction and the effect of the anharmonicty gave large uncertainty. Therefore we estimated the C_l above 150 K for the calculation of the critical parameter and the entropy of transition in the following way. In the region from 150 to 190 K the lattice heat capacity was determined from the extrapolation of the heat capacity below the glass transition and from the exact solution of the dimer model. The heat capacity of the dimer model(ΔC) were numerically calculated and C_l was given by $C_p - \Delta C$. We assumed here that the heat capacity(ΔC) of the dimer model was valid in the region far from the transition temperature. This assumption

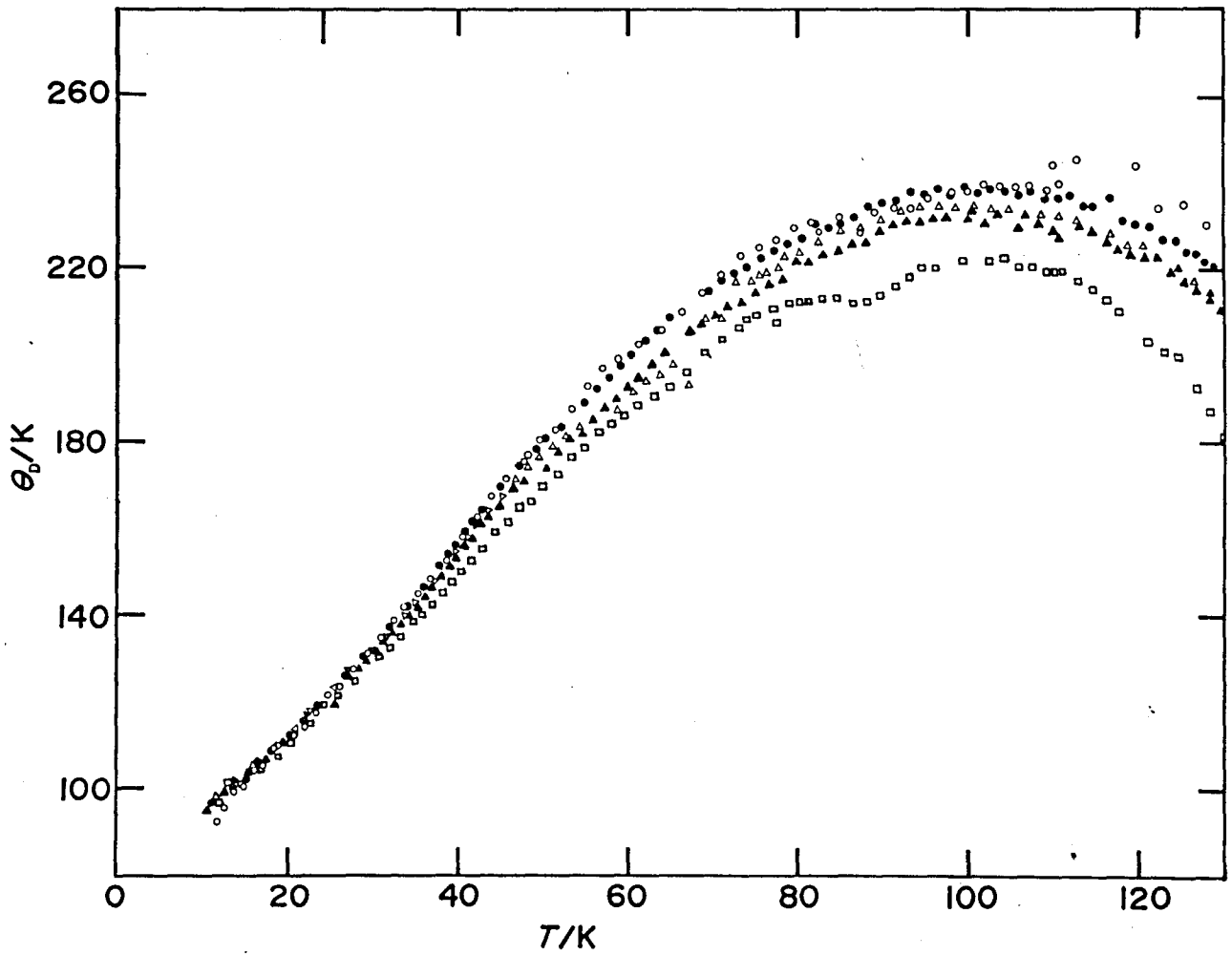

Fig.46. Calculated Debye temperatures from heat capacity and spectroscopic data. ○ : x=2.00, ◉ : x=1.50, △ : x=0.96, ▲ : x=0.50, □ : x=0.03.

was supported from the fact that ΔC reproduced the jump at the glass transition temperature. Figure 43. shows the heat capacity of the dimer model and experimental one for SCD(x=2.00) The dimer model was also employed above 250 K. In the intermediate region(190∿250 K) where the dimer model cannot reproduce the real heat capacity, the lattice heat capacity was estimated by intrapolating the lattice heat capacity determined above. These estimation was carried out with reference to the heat capacity calculated from spectroscopic data where the Debye heat capacity was assumed to be classical value($3R$).

3.3.9. Glass transition

Glass transition phenomena in stannous chloride dihydrate and its deuterate analogue were discussed in detail by Matsuo et al. Fig.47 shows the concentration dependence of the glass transition temperatures, which were defined as the temperature where the temperature drift changed from the exothermic to the endothermic. The relaxation times at each temperature were calculated according to the same manner as proposed in Ref[66]. The Arrhenius plots shown in Fig.48 where the results of x=2.00 and x=0.03 were quoted from Ref[66].

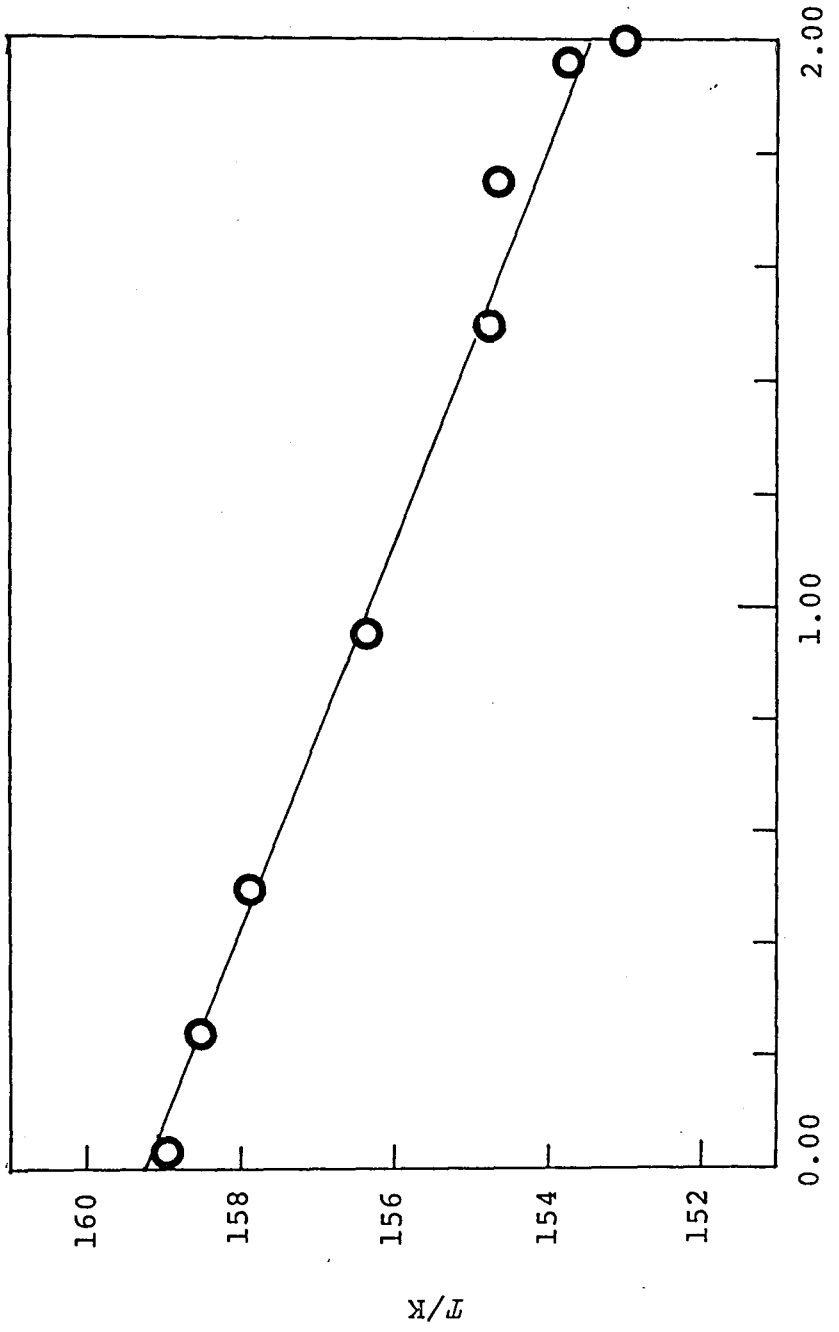

Fig.47. Glass transition temperature vs. composition.

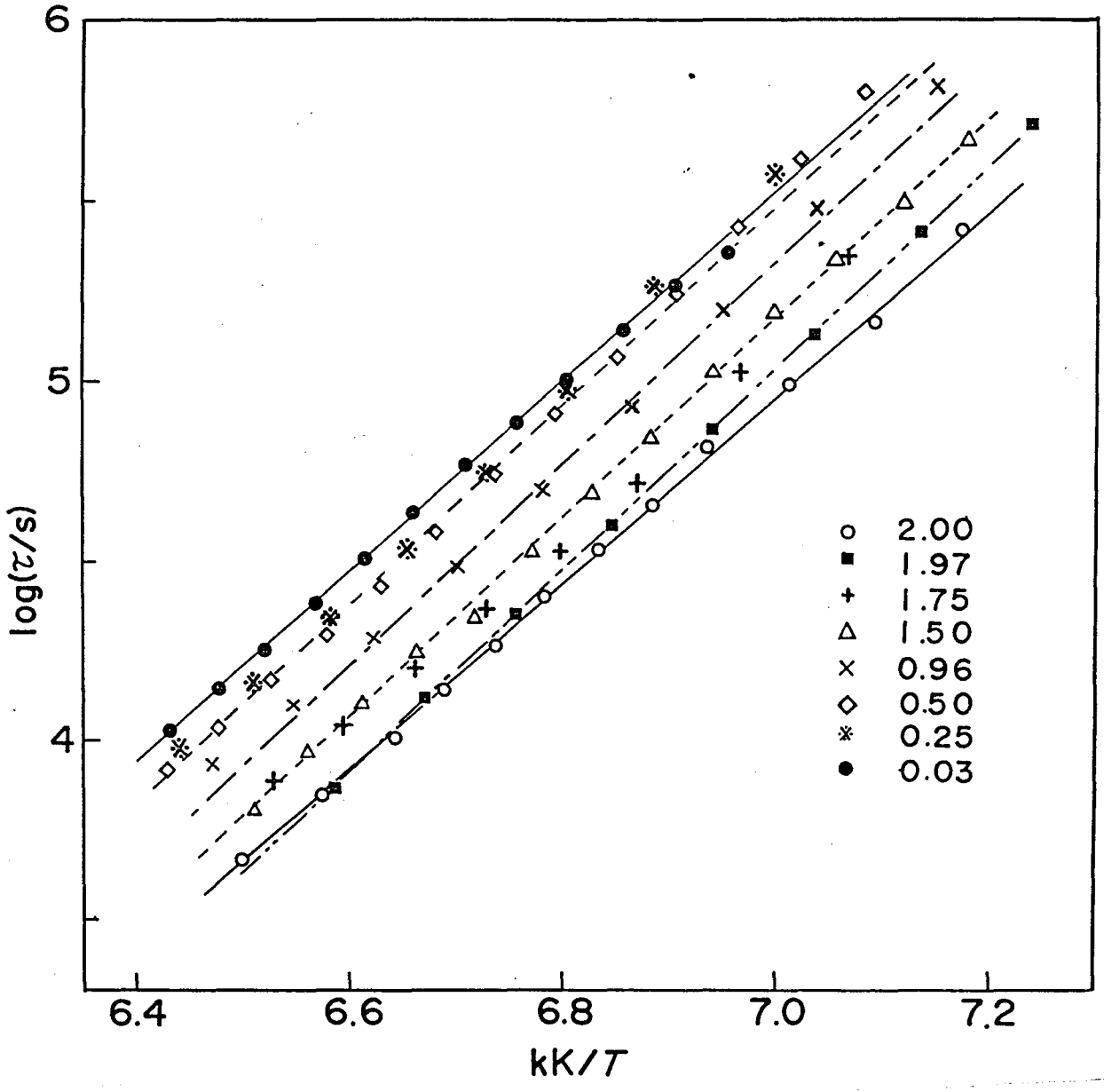

Fig.48. Arrhenius plot of the enthalpy relaxation time.

3.3.10. Raman scattering

The Raman spectra of monohydrated and anhydrous $SnCl_2$ solids makes possible a clear comparison of the different nature of the three types of solids and hence allow one to state definitely the important effect of the H_2O molecules on the Raman spectra of SCD. $SnCl_2$ in the solid state combines with other molecules and forms a triangle pyramid ($SnCl_3$). In the hydrated $SnCl_2$ solids(both $SnCl_2H_2O$ and SCD), one of the chlorine atoms in the pyramid is replaced by H_2O. The large intensity reduction of the lines at 163 and 193 cm^{-1} suggests that these lines are associated with the totally symmetric vibrations in the pyramid and not the lattice vibrations. The features at 223 and 248 cm^{-1} which appear only in SCD and not in $SnCl_2H_2O$ or in $SnCl_2$ can definitely be assigned as the hydrogen bond vibrations. These are the lattice modes as they are associated with the two non-equivalent H_2O molecules in the hydrogen bonded network(see Fig. 12(a)). Fig.23. shows a broad spectral distribution in this spectral region at room temperature due to the protonic motion. It should be pointed out that the assignment of the 223 cm^{-1} line to be the Sn-Cl stretching vibration made previously by Morisaki et al.[64] must be incorrect. However their assignment of the 250 cm^{-1} line to the OH···O hydrogen bond vibrations is consistent with the present result. The difference in the Raman spectra of $SnCl_2H_2O$ and SCD is doubtlessly due to the presence of the intervening layers of H_2O

molecules in SCD. In addition to the appearance of the new features at 223 and 248 cm^{-1}, the presence of the H_2O layers also causes frequency shifts and intensity variations in other spectral lines, *i.e.* the non-coordinated waters have also significant effects on the bonding character of the Sn-Cl bonds as discussed by Kiriyama et al. on the basis of their X-ray data[62]. The polarlized Raman spectra of the single crystal shown in Fig.24,25,26 and 27 can approximately be devided into two regions: one above 200 cm^{-1} and one below that. The features which appear above 200 cm^{-1} are due to the -O(1)···O(2)- hydrogen bond vibrations. These below 200 cm^{-1} are presumably associated with the different types of the Sn-Cl and Sn-O vibrations, some of which are perturbed by the hydrogen bonded vibrations. The spectral lines below 50 cm^{-1} are likely associated with the Sn-O vibrations they are also present in $SnCl_2H_2O$(but not in $SnCl_2$). Changing the SCD temperature has a significant effect on its Raman spectrum, particularly in the hydrogen-bond vibration region. As the temperature of SCD decreases, the rate of H_2O orientational fluctuations which result in hydrogen bond breaking and formation becomes slower, and the spectral resolution of these vibrations is expected. Thus, one should observe three Ag hydrogen bonded vibrations below T_c, which are Raman active under the inversion symmetry. This is indeed the case, as shown in from Fig.24 to 27. Below T_c the intensity in the 200-245 cm^{-1} spectal wing region into two peaks located clearly at 225 and 240 cm^{-1}. The intensities of these two spectral lines as a function of temperature are also shown in Fig.49.

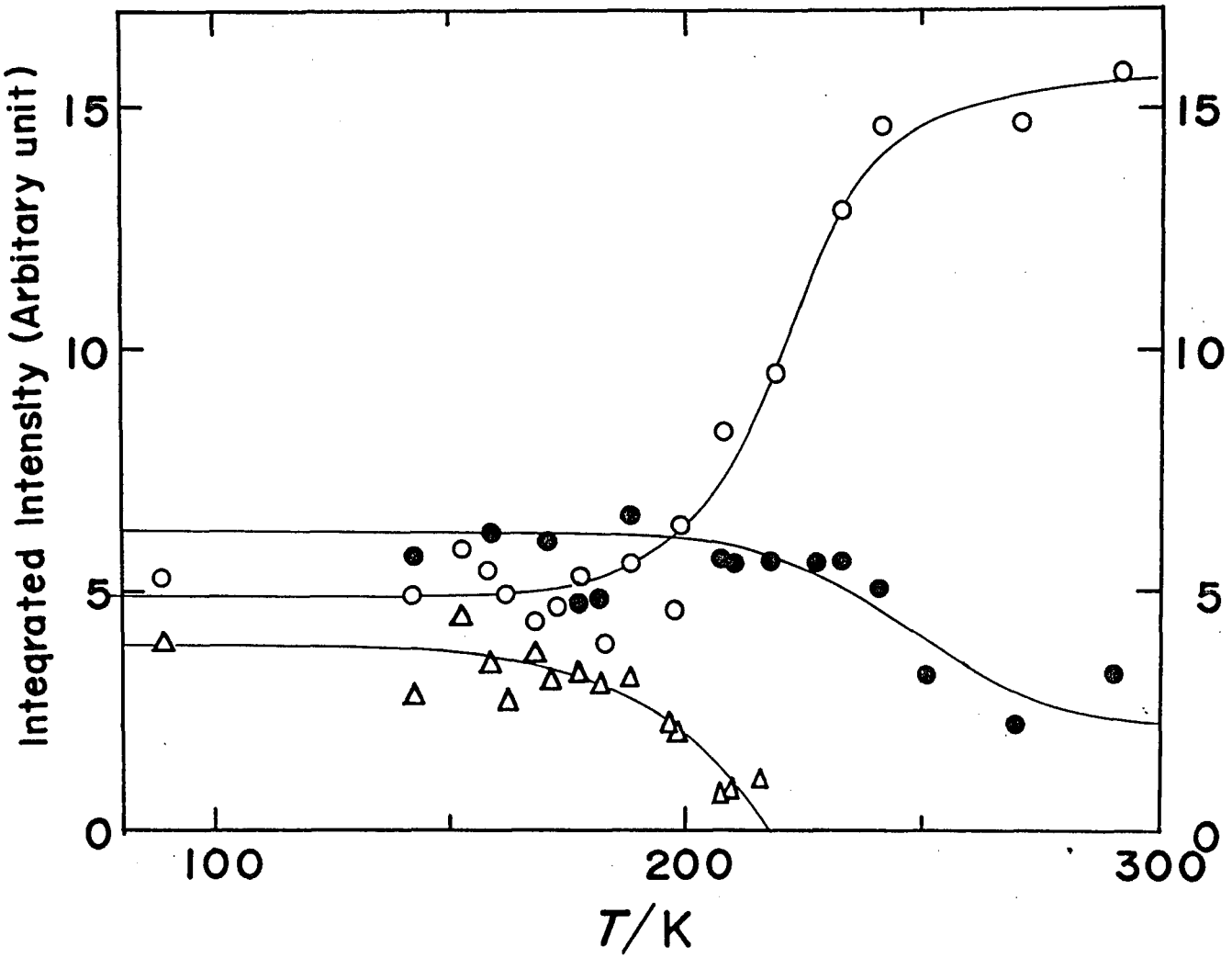

Fig.49. The integrated intensities of the three components above 200 cm^{-1} as a function of temperature.

It should be pointed out that, due to the band overlap, accurate intensity data is difficult to obtain in this region. The integrated intensity data plotted in Fig.49 were obtained by assuming symmetric bandshapes for the 225 and 250 cm^{-1} lines. Based on this approximation, the intensities of the 225 and 250 cm^{-1} lines can then be determined. The difference between the total spectral intensity over the 200 to 280 cm^{-1} region (with the contribution of the 198 cm^{-1} line subtracted off) and the sum of the intensities of the 225 and 250 cm^{-1} lines gives the integrated intensity of the 240 cm^{-1} line. The intensity data for the 225 and 240 cm^{-1} lines are subject to larger deviations than that for the 250 cm^{-1} line.

From Fig.49, one notes that on passing through T_c from above, the integrated intensity of the 225 cm^{-1} line increases slightly and remains constant thereafter. On the other hand, the intensity of the 240 cm^{-1} line increases rapidly from very small value at T_c to a constant value below T_c.

While all three hydrogen bonded vibrations are affected by the change of proton population at various sites, the highest frequency component at 250 cm^{-1} displays the most clear effect, due to its greater separation from the other two components. Experimental results such as the intensity, peak frequency and linewidth of this band can be more accurately obtained. Thus we now focus our discussion on the 250 cm^{-1} component.

Referring again to Fig.12, one notes that at room temperature the proton occupancy at D(6) is high. Fluctuations of the proton population at D(6) affect the intensity of the

hydrogen-bond vibration at 250 cm^{-1}. As the crystal becomes ordered the proton population at D(6) rapidly decreases to zero. This results in the intensity decrease of the 250 cm^{-1} line and a corresponding intensity increase at its low frequency spectral wing, due to the fact that a decrease in population at D(6) corresponds to an increase at D(5).

The idea about relating the intensity change of the hydrogen bonded vibrations to the proton population at the various sites is strengthened by comparing quantitatively the intensity data with the transition entropy $S(T)$ determined from the heat capacity measurements. The excess entropy associated with the phase transition gives a measure of local proton disorder in the whole hydrogen bonded system. As pointed above, although the excess entropy is affected by all sites, it is more significantly affected by the proton occupancy at sites D(1), D(3) and D(5) because of greater population fluctuations at these sites. In Fig.50, the integrated intensity data of the 250 cm^{-1} line are compared with the excess entropy. In spite of some scatter of the experimental data, the agreement between the Raman data and that of excess entropy is satisfactory.

If the 250 cm^{-1} line is indeed associated with the hydrogen bond vibration, then the behavior of the vibration is closely related to the phase transition in SCD. The temperature dependence of the peak frequency and the spectral linewidth at half maximum intensity of the 250 cm^{-1} line is given in Fig.51. The polycrystalline data of Morisaki et al. do not agree with the present single crystal data at high and low temperatures. The frequency and linewidth data may be understood

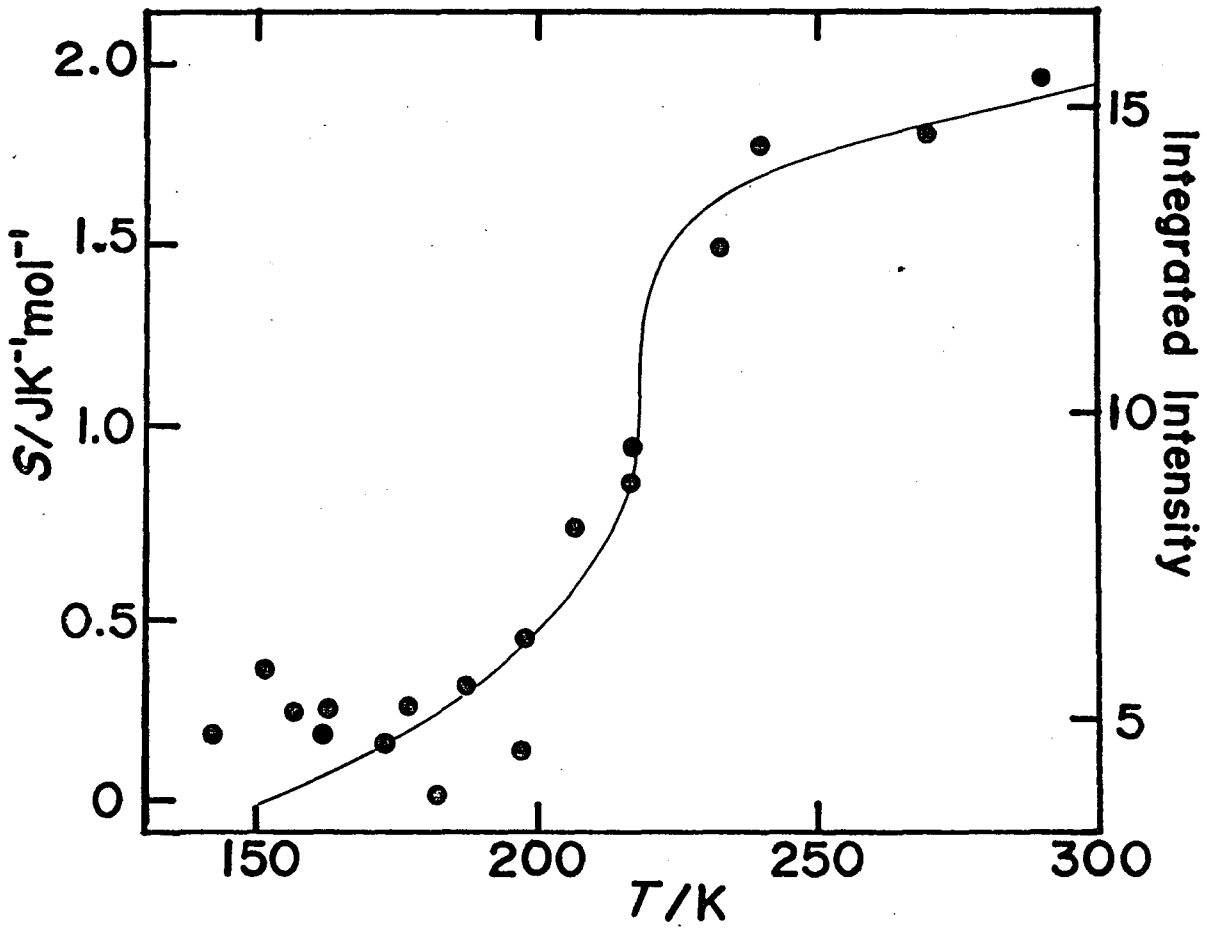

Fig.50. The integrated intensity data of the 250 cm^{-1} peak are compared with the transition entropy S obtained from the heat capacity measurement. S is indicated by the curve and solid circles are the integrated intensity.

qualitatively by considering the anharmonicity associated with the hydroben bond potential. According to the consideration of the damped harmonic oscillator, the peak frequency ω_m and linewidth are given by

$$\omega_m \simeq \omega_o - \frac{1}{2}\Delta \quad \text{and} \quad \omega_m\gamma, \text{ respectively,}$$

where ω_o is a frequency of the corresponding harmonic oscillator and Δ is the anharmonic correction to the oscillator frequency. Although both ω_o and Δ vary with temperature, the fact that the temperature dependence of Δ is greater as the variation of ω_o is due to mainly thermal expansion of the crystal, whereas the variation of Δ is affected by the protonic motion in the hydrogen bond which changes the anharmonicity in the potential significantly. If the frequency shift of the 250 cm^{-1} mode is considered to be due to the disorder of the protons in the hydrogen bond network, this is equivalent to saying that the occupational probability of protons at D(5) and D(6')(see Fig.12) must affect the hydrogen bond potential in a very significant way. As one sees in Fig.51, when the SCD temperature is increased from the ordered phase, the peak frequency shifts towards a lower values accompanied by linewidth increase, which is consistent with the nature of Δ and γ due to anharmonicity. For SCD, as the temperature of SCD is increased from below through T_c, many channels for protonic occupation open and the density of the final states increases rapidly. In this sense, we expect that the temperature dependent behavior of the peak frequency at 250 cm^{-1} should reflect the decrease of the proton population at D(5). The theoretical calculation of that at D(5) at several temperatures yields a curve whose shape is quite

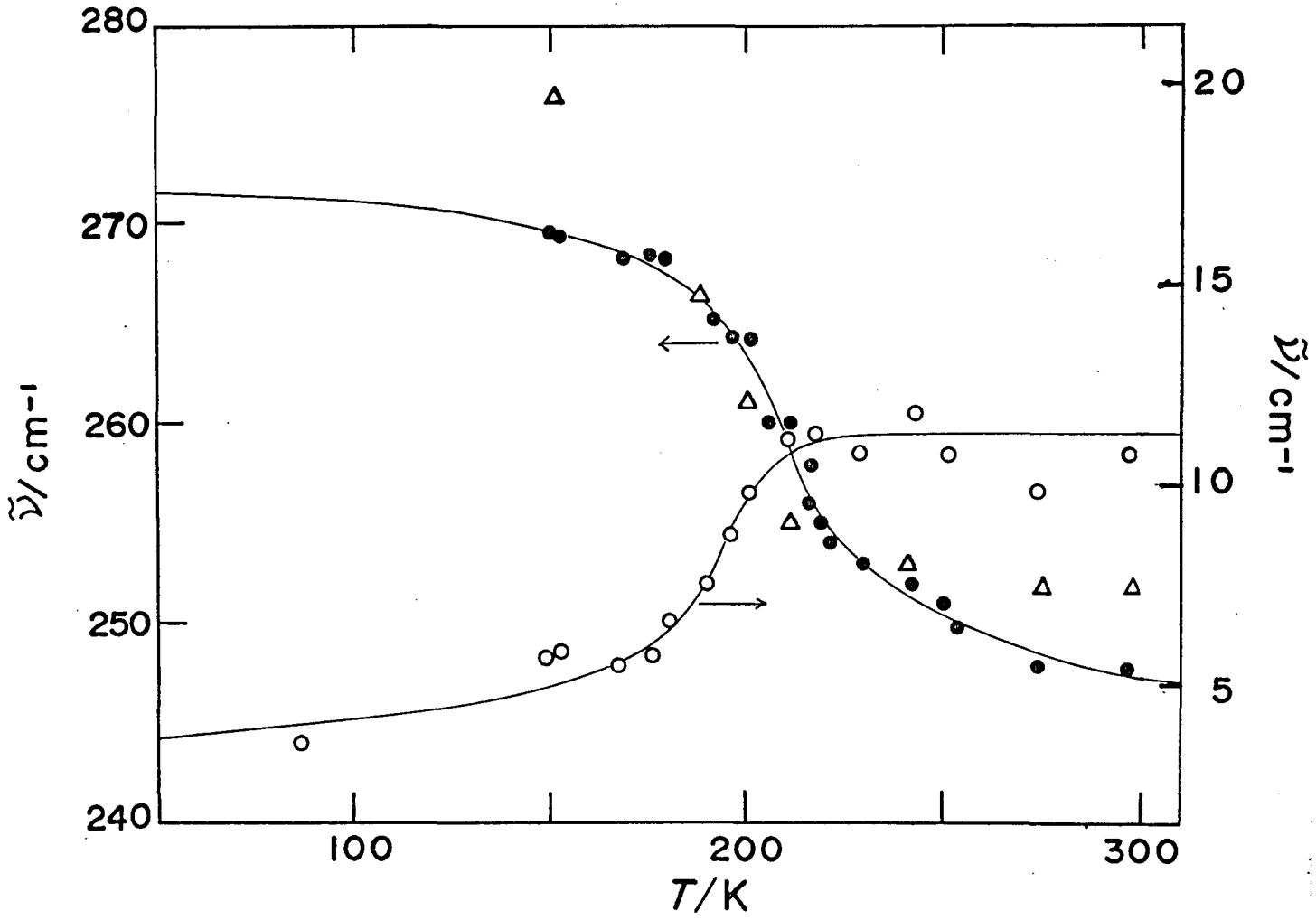

Fig.51. The temperature dependence of the peak frequency and the spectral linewidth of the 250 cm^{-1}.

O : This work, Δ : Morisaki et al[64].

similar to the ν versus T curve as given in Fig.51. Below 200 cm^{-1} the most interesting feature is the intensity variation pattern of the doublet at 58 cm^{-1} and 67 cm^{-1}. They do not show significant frequency shift or line broadening as the temperature of the crystal is increased from 89 to 210 K, however, their intensities alternate between high and low temperatures. The total intensity of the lines remain more or less fixed. The intensity ratio of them as well as the intensity of the individual line divided by the total intensity are shown as a function of temperature in Fig.52. As seen in Fig.23 the monohydrate $SnCl_2H_2O$ spectrum also show the features in this region, it is not unreasonable to speculate that the doublet is associated with some type of bending vibration of the Sn-O(1) bond in SCD. One expects the protonic motion to affect these bending vibrations significantly, as the shape of the intensity versus temperature appears rather similar to the ν-T curve as given in Fig.51. The intensity behavior of the 57 cm^{-1} line is probably associated with the decrease of proton population at D(6) as the temperature is increased. The Raman scattering data suggest that the phase transition in SCD on approaching T_c from below or from above appears to be a higher order phase transition.

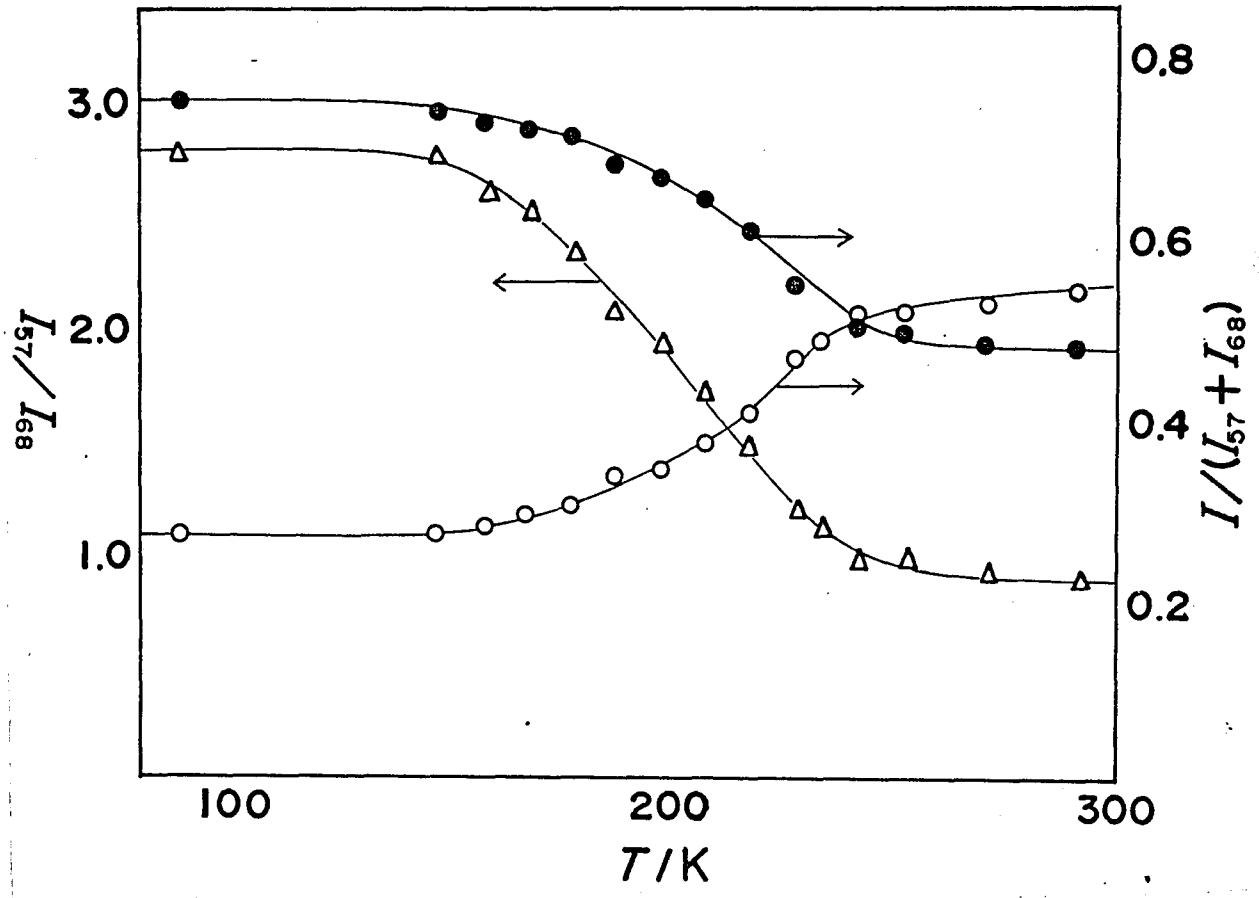

Fig.52. The intensity ratio of the doublet lines as well as the intensity of the individual line divided by the total intensity as a function of temperature.

3.4. Conclusion

Heat capacity measurements were performed on the single crystals of solid solution between SCD and DSCD (x=1.97, x=1.75, x=1.50, x=0.96, x=0.50, x=0.25) in the temperature range from 13 to 300 K. All crystals exhibited the anomalous heat capacity in two temperature regions. One was around 220∿230 K region and was due to the order-disorder transition in the hydrogen bonding network. The other was a relaxational anomaly found around 150 K which is due to an equilibrium-nonequilibrium change in the ordering process of the hydrogen bonding network. The high resolution heat capacity measurements were carried out with the temperature step of 3/100∿5/1000 K in the vicinity of the transition temperatures. Moreover, in order to study any effect of aging of the crystals, we repeated high resolution measurements for the samples of x=0.96, x=0.50 and x=0.03 near the transition temperature. In addition to these calorimetric studies, we measured the Raman spectra of anhydrous, monohydrated and dihydrated stannous chloride crystals. We also obtained polarized Raman spectra of SCD at several scattering geometries and at several temperatures above and below T_c.

The following conclusions can be drawn from the present investigation:

(1) The transition temperatures of phase transition and glass transition changed smoothly from 218.01 to 234.64 K and from 152.93 to 158.82 K, respectively, with the variation of isotopic composition.

(2) The heat capacities of every crystals exhibited highly symmetrical peaks at T_c, which was the trade mark of the two-dimensional phase transition. The critical parameter were calculated from the results of high resolution measurements and found to vary with composition. The critical exponents α and A took values of $0.47\sim0.79$ and $0.79\sim0.13$ $JK^{-1}mol^{-1}$ respectively. These large values of α could not be reproduced by the dimer model. However, the eight-vertex model or its modified model was considered to be a candidate to explain such large values and their change with composition. The scaling law $\alpha=\alpha'$ was found to hold for the present substances.

(3) The measurements on annealed crystals showed that the inhomogeneities almost vanished by annealing the samples more than three months, though the mixed crystals had slightly inhomogenous distributions of proton and deuteron for about one month after the preparation of the single crystals.

(4) The phenomena of small quasi-isothermal heat absorption were observed during the process of phase transition for the samples of $x=2.00$, $x=1.97$ and $x=1.75$. From the entropy change and the behavior of the temperature drift, we confirmed that the samples $x=2.00$, $x=1.97$ and $x=1.75$ showed the first-order phase transitions and that the sample $x=1.50$, $x=0.96$, $x=0.50$, $x=0.25$ and $x=0.03$ exhibited the higher-order one.

(5) Since the phase transitions in the present specimens were all isomorphous transitions in which the symmetry did not change, we considered that the phase diagram in the present system of solid solution was compared to that of liquid-vapor.

(6) The rounding phenomenon, which could not be reproduced by Gaussian distribution of the transition temperature, was explained on the basis of the phase diagram.

(7) Debye temperature for each crystal was calculated from the low temperature heat capacity as well as from the results of the Raman scattering and the infrared absorption.

CONCLUDING REMARKS

The study of critical phenomenon or phase transition accompanied with small excess heat capacity requires the measurement with high precision and high accuracy as well as the sample with high purity. Our calorimeter was constructed to accord with this purpose and equipped with two kinds of thermometer, platinum resistance and thermister thermometers, and we can perform heat capacity measurement within the inaccuracy of 0.1 % and within imprecision of 0.05 %. Furthermore we employed the single crystal for the measurement. This matter aided the improvement of the sampling procedure in order to reduce the contamination of the specimens. By these refinements on the construction of calorimeter and the procedure we found that our calorimeter is satisfactory enough to perform the high resolution measurement.

In the present work we performed the study of the heat capacity on two hydrogen bonded dielectrics. Rochelle salt exhibits the only slight anomalous heat capacity at the lower and upper Curie temperatures in parallel with the other electrical quantities. Although many calorimetrists have tried to find the excess heat capacity of this sample for about forty years, their apparatuses were insufficient in the point of precision and their results were in conflict with each other. By use of our sophisticated calorimeter mentioned above, we performed the high resolution measurements on Rochelle salt with the temperature interval of 0.1 K around the both Curie temperatures. The positive excess heat capacities were found to be 1.2 $JK^{-1}mol^{-1}$ at lower Curie temperature and 1.0 $JK^{-1}mol^{-1}$ at

the upper Curie temperature. They are 0.2∿0.3 % of the total heat capacity, which corresponds to the imprecision of the ordinary resolution measurement. The magnitude of the excess heat capacities are consistent with the values calculated from the results of thermal expansion, electrocaloric effect and piezocaloric effect. Another interest of the present work is to study the critical phenomenon. The study of critical phenomena were first developed on magnetic and fluid system and one of new attentions was directed toward the phase transitions of dielectric systems such as hydrogen-bonded crystals. We also studied the critical phenomena of the solid solutions between SCD and DSCD by high resolution heat capacity measurements. SCD, which shows an interesting feature, has layer structure with hydrogen bonded network and exhibits the highly symmetrical excess heat capacity around the phase transition temperature. Another feature is that the crystal symmetry does not change through the phase transition. Eight high resolution measurements were performed on eight samples which were kept for about one to seven months after their preparation and in addition four measurements on different samples annealed further for about one months to four years. The critical phenomenon is sensitive to the crystal imperfection, temperature fluctuation and inhomogeneity of other external parameters. Therefore we carried out heat capacity measurements under highly stabilized temperature control and checked the homogeneity of distribution of proton by reinvestigating the annealed crystals. In particular case we reinvestigated the sample annealed for about

four years. We found from these measurements that the solid solutions studied had nearly homogeneous distributions. The critical exponents were found to be large values(0.47∿0.79) and varied with isotope composition. These values and their change with the compositions were expected to be explained by vertex model. The small first-order components were observed in the pure hydrate and H_2O-rich solid solutions. Such a finding of the first order component which were also found in KDP, NH_4Cl and $NaNO_2$ is important for characterizing the phase transition. We considered on the basis of the crystal symmetry that the present system belonged to the liquid-vapor type phase transition rather than the tricritical phenomenon. In general, the determination of the critical exponents is important to characterize and systematize the phase transition of various substances. However it is also important that critical phenomenon of a substance should be studied from the measurements on various physical quantities which are performed with high precision and accuracy on the sample with highly characterized purity.

REFERENCES

[1] L. P. Kadahoff, W. Götze, D. Hamblen, R. Hecht, E. A. S. Lewis, V. V. Palciauskas, M. Rayl, J. Swift, D. Aspenes and J. Kane, Revs. Mod. Phys., 39, 395 (1967).

[2] P. Heller, Rept. Progr. Phys., 30, 731 (1967).

[3] M. E. Fisher, *ibid*, 30, 615 (1967).

[4] H. E. Stanley, Introduction to Phase Transitions and Critical Phenomena, Oxford University Press, London (1971).

[5] T. Andrews, Phil. Trans. Roy. Soc., 159, 575 (1869).

[6] J. F. Nagle, Ann. Rev. Phys. Chem., 27, 291 (1976).

[7] T. S. Chang, A. Hankey and H. E. Stanley, Phys. Rev., B8, 346 (1973).

[8] G. Goellrer, R. Behringer and H. Meyer, J. Low Temp. Phys., 13, 113 (1973).

E. K. Riedel, H. Meyer and R. P. Behringer, J. Low Temp. Phys., 22, 369 (1976).

[9] F. M. Gasparni and M. R. Moldover, Phys. Rev., B12, 93 (1975).

[10] D. P. Landau, B. E. Keen, B. Shneider and W. P. Wolf, Phys. Rev., B3, 2310 (1971).

idem, ibid, B5, 4472 (1972).

[11] C. W. Garland and B. B. Weiner, Phys. Rev., B3, 1634 (1971).

idem, J. Chem. Phys., 56, 155 (1972).

[12] W. B. Yelon, D. E. Cox and P. J. Daniels, Phys. Rev., B9, 4843 (1974).

[13] T. J. Mckee and R. J. McColl, Phys. Rev. Letters, 34, 1076 (1975).

[14] V. H. Schmidt, A. B. Western and A. G. Baker, *ibid*, 37, 839 (1976).

[15] P. S. Peercy, *ibid*, 35, 1581 (1975).

[16] L. Pauling, J. Am. Chem. Soc., 57, 2680 (1935).

[17] J. C. Slater, J. Chem. Phys., 9, 16 (1941).

[18] F. J. Wu and K. Y. Lin, Phys. Rev., B12, 419 (1975).

[19] F. J. Wu, Phys. Rev., 183, 604 (1969).

[20] R. J. Baxter, Ann. Phys.(N. Y.), 70, 193 (1972).

[21] F. Y. Wu, Phys. Rev., B3, 3895 (1971).

[22] J. F. Nagle and G. R. Allen, J. Chem. Phys., 55, 2708 (1971).

[23] S. R. Salinas, Ph. D. thesis Carnegie-Mellon University, (1973).

[24] G. R. Allen, J. Chem. Phys., 60, 3299 (1974).

[25] M. J. Buckingham and W. M. Fairbank, "Progress in Low Temperature Physics", Vol. 13 ed. by C. J. Gorter, North Holland, Amsterdom (1961) p. 80.

[26] A. V. Voronel, "Phase Transitions and Critical Phenomena", Vol. 5B, London, New York Academic Press. (1976) p. 343.

[27] A. Kornblit and G. Ahler, Phys. Rev., B8, 5163 (1973). *idem, ibid*, B11, 2678 (1975).

[28] W. Reese and L. F. May, Phys. Rev., 162, 510 (1967); *ibid*, 167, 504 (1968); 181, 905 (1969).

[29] P. Schwartz, Phys. Rev., B4, 920 (1971).

[30] J. J. White, H. I. Song, J. E. Reves and D. P. Landau, Phys. Rev., B4, 4605 (1971).

[31] F. Grϕnvold, Pure & Appl. Chem., 47, 251 (1976).

[32] M. Tatsumi, T. Matsuo, H. Suga and S. Seki, Bull. Chem. Soc. Japan, 48, 3060 (1975).

[33] E. F. Westrum Jr., G. T. Furukawa and J. P. McCullough, in Experimental Thermodynamics, Vol. 1, ch. 5., J. P. McCullough and D. W. Scott, editors. Butterworths, London. 1968.

[34] R. A. Robie and B. S. Hemingway, Geological Survey Professional Paper 755, United States Government Printing Office, Washington (1972).

[35] G. T. Furukawa, R. E. McCosky and G. J. King, J. Res. Nat. Bur. Stand., 47, 256 (1951).

[36] A. G. Cole, J. O. Hutchens, R. A. Robie and J. W. Stout, J. Amer. Chem. Soc., 82, 4807 (1960).

[37] The International Practical Temperature Scale of 1968, Metrologia, 5, 35 (1969).

[38] V. E. Gorburov and V. A. Palkin, Zh. Fiz. Khim., 46, 1625 (1972).

[39] J. Valasek, Phys. Rev., 15, 537 (1920).

[40] L. A. Beevers and W. Hughes, Proc. Ray. Soc.(London), A177, 251 (1941).

[41] F. Jona and G. Shirane, Ferroelectric Crystals, Pergamon Press, Oxford (1962).

[42] J. Habluetzel, Helv. Phys. Acta, 12, 489 (1939).

[43] G. G. Wiseman and K. Kuebler, Phys. Rev., 131, 2023 (1963).

[44] K. Imai, J. Phys. Soc. Japan, 39, 868 (1975).

[45] H. Mueller, Phys. Rev., 57, 829 (1940); 58, 565, 805 (1940).

[46] W. P. Mason, Phys. Rev., 72, 854 (1947).

[47] H. Takahashi, Busseiron-Kenkyu, 22, 1 (1950).

[48] A. F. Devonshire, Phil. Mag., 2, 1027 (1957).

[49] T. Mitsui, Phys. Rev., 111, 1259 (1958).

[50] B. Žekš, B. C. Shukla and R. Blinc, Phys. Rev., B3, 2306 (1971), R. Blinc and B. Žekš, Phys. Letters, 39A, 167 (1972).

[51] B. C. Frazer, M. McKeown and Pepinsky, Phys. Rev., 94, 1435 (1954).

[52] A. A. Rusterholz, Helv. Phys. Acta, 8, 39 (1935).

[53] J. F. G. Hicks and J. G. Hooley, J. Am. Chem. Soc., 60, 2994 (1938).

[54] A. J. C. Wilson, Phys. Rev., 54, 1103 (1938).

[55] K. Hirakawa and M. Furukawa, Japan. J. Appl. Phys., 9, 971 (1970).

[56] W. Reese and L. F. May., Ferroelectrics, 4, 65 (1972).

[57] J. Helwig, Ferroelectrics, 7, 225 (1974); *idem, ibid*, 11, 471 (1976).

[58] E. F. Ushatkin, V. V. Meriakri and U. M. Poplavkov, Piśma. Zh. Exper. Teor. Fiz., 19, 557 (1974).

[59] P. P. Kobeko and J. G. Nelidow, Phys. Z. Sowjetunion, 1, 382 (1932).

[60] K. Imai, J. Phys. Soc. Japan, 41, 2005 (1976).

[61] H. Kiriyama and R. Kiriyama, J. Phys. Soc. Japan, 28, Suppl., 114 (1970).

[62] H. Kiriyama, K. Kitahama, O. Nakamura and R. Kiriyama, Bull. Chem. Soc. Japan, 46, 1389 (1973).

[63] R. Kiriyama, H. Kiriyama, K. Kitahama and O. Nakamura, Chem. Lett., 1105 (1973).

[64] H. Morisaki, H. Kiriyama and R. Kiriyama, Chem. Lett., 1061 (1973).

[65] H. Kiriyama, O. Nakamura and R. Kiriyama, Chem. Lett., 689 (1976).

[66] T. Matsuo, M. Oguni, H. Suga and S. Seki, Bull. Chem. Soc. Japan, 47, 57 (1974).

[67] S. R. Salinas and J. F. Nagle, Phys. Rev., B9, 4920 (1974).

[68] T. Matsuo, M. Tatsumi, H. Suga and S. Seki, Solid State Commun., 13, 1829 (1973).

[69] B. Kamenar and D. Gredenic, J. Chem. Soc., 3957 (1961).

[70] M. Tatsumi, Master's Thesis; Osaka University (1974).

[71] T. Matsuo, Y. Kume, H. Suga and S. Seki, J. Phys. Chem. Solids, 37, 499 (1976).

[72] M. Oguni, T. Matsuo, H. Suga and S. Seki, Bull. Chem. Soc. Japan, 48, 379 (1975).

[73] B. Brezina and F. Smutny, Czech, J. Phys., B18, 393 (1968).

[74] K. Gesi, J. Phys. Soc. Japan, 41, 565 (1976).

[75] B. A. Strukov, A. Baddur, V. A. Koptsik and I. A. Velichko, Sov. Phys. -Solid State, 14, 885 (1972).

[76] G. Ahlers, Phys. Rev., A8, 530 (1973).

[77] R. B. Griffiths, Ferroelectrics, 7, 71 (1974).

[78] V. L. Ginzburg, Sov. Phys. -Solid State, 2, 1824 (1960).

[79] D. S. Gaunt and C. Domb, J. Phys. Chem., 1, 1038 (1968).

[80] E. R. Mognaschi and A. Rigamonti, Phys. Rev., B14, 2005 (1976).

[81] S. R. Salinas and J. F. Nagle, J. Phys. Soc. Japan, 41, 1643 (1976).

[82] E. N. Konstina and G. A. Mil'ner, Sov. Phys. -Solid State, 14, 2923 (1973).

[83] I. Hatta and A. Ikushima, J. Phys. Chem. Solids, 34, 57 (1973).

[84] T. Matsuo and H. Suga, Solid State Commun., 13, 1829 (1973).

[85] G. Ahlers and A. Kornblit, Phys. Rev., B12, 1938 (1975).

[86] M. Suzuki, Prog. Theor. Phys., 51, 1992 (1974).

[87] F. J. Wegner, Phys. Rev., B5, 4529 (1972).

[88] M. Barmatz, P. C. Hohenberg and A. Kornblit, Phys. Rev., B12, 1947 (1975).

[89] F. L. Lederman, M. B. Salamon, L. W. Shacklette, Phys. Rev., B9, 2981 (1974).

[90] K. Itagaki, J. Phys. Soc. Japan, 19, 1081 (1964); C. Haas, Phys. Letters, 3, 126 (1962).

[91] T. Yamamota, O. Tanimota, Y. Yasuda and K. Okada, "Critical Phenomena", Proceedings of a Conference (Natl. Bur. Stds. Misc. Publication, No. 273, Washington, D. C., 1966, p. 86; E. A. S. Lewis, Phys. Rev., B1, 4368 (1970).

[92] R. B. Griffiths and J. C. Wheeler, Phys. Rev., A2, 1047 (1970).

[93] I. R. Jahn and E. Neumann, Solid State Commun., 12, 721 (1973).

[94] A. Hüller, Z. Physik, 270, 343 (1974).

[95] A. Jayaraman, Phys. Rev., 137, A179 (1965).

[96] A. Jayaraman, D. B. McWhan, J. P. Remeika and P. D. Dernier, Phys. Rev., B2, 3751 (1970).

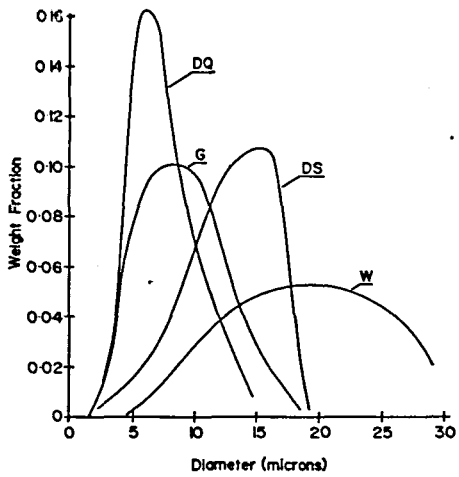

Fig. 2. Weight fraction of droplets of radius between r and $r+1\,\mu$ as a function of r. DS and DQ, dispersions in silicone oil; G and W, dispersions in glycerol and Welch pump oil respectively.

−194 C. Although this evidence is tenuous, the formation of those phases which on warming transform to the δ phase appears to be favoured in small droplets.

Acknowledgements—These studies were supported by operating grants from the National Research Council of Canada. One of us (SLS) thanks the Science Research council of Britain and the University of Geneva for their financial support during part of this work. We would also like to thank E. F. W. Seymour and J. Boocock for informing us of their DTA and nmr results on Ga dispersions, and the Mettler Instrument Co. and the Stanton Redcroft Ltd. for their assistance in preliminary thermal analyses.

Department of Chemistry,
Department of Physics,
Queen's University,
Kingston, Ontario, Canada

R. D. HEYDING
W. KEENEY
S. L. SEGEL

REFERENCES

1. BRIDGEMAN P. W. *Phys. Rev.* **48**, 893 (1935).
2. JAYARAMAN A., KLEMENT W., NEWTON R. C. and KENNEDY G. *J. Phys. Chem. Solids* **24**, 7 (1963).
3. BOSIO L., DEFRAIN A., EPELBOIN I. and VEDAL J. *J. Chim. Phys.* **65**, 719 (1968).
4. BOSIO L. *Comptes Rendu* **270B**, 1453 (1970).
5. BOSIO L., DEFRAIN A., CURIEN H. and RIMSKY A. *Acta crystallogr.* **B25**, 995 (1969).
6. BOSIO L., DEFRAIN A. and DUPONT M. *J. Chim. Phys.* **68**, 542 (1971).
7. SEGEL S. L., HEYDING R. D. and SEYMOUR E. F. W. *Phys. Rev. Lett.* **28**, 970 (1972).
8. TURNBULL D., *J. chem. Phys.* **18**, 769 (1950).
9. SUZUKI K. and UEMURA O. *J. Phys. Chem. Solids* **32**, 1801 (1971).
10. TURNBULL D. *J. appl. Phys.* **21**, 1022 (1950).

J. Phys. Chem. Solids, 1973, Vol. 34, pp. 136–138.

Phase transition and far i.r. spectrum of hexammine cobaltous chloride crystal

(*Received* 27 *April* 1972)

HEXAMMINE metal halide crystals exhibit interesting phase transitions. All halides studied so far, which include the chloride, bromide or iodide of nickel, cobalt, manganese and other metals, show one anomaly between the liquid helium and room temperatures in their thermal properties[1–3]. The entropy change accompanying this anomaly was reported to amount 35 J K^{-1} mol^{-1} (= Rln 64) in some cases, but no satisfactory explanation seems to have been advanced for the values. Magnetic resonance studies by Palma-Vittorelli *et al.*[4], Aiello *et al.*[5] and Trapp and Shyr[6] emphasized the importance of the role played in the transition phenomena by the protons of the coordinated ammonia molecules. On the basis of this observation, Bates and Stevens[7] and Bates[8] have calculated the interaction energy between the protons and other atoms in the crystal, with the result that the phase transition turned out to be all the more intriguing, because the calculation revealed that the ammonia motion has to be treated quantum mechanically. Importance of the quantum effect was also indicated in the low temperature heat capacities measured by van Kempen *et al.*[9] and Suga *et al.*[10].

At present, however, informations on the structural aspect of the transition seem to be lacking. In this note, we report the discovery of another example of phase transition of similar type in hexammine cobaltous chloride

by use of the differential thermal analysis (DTA) and the far i.r. absorption. The latter method gave some insights into the symmetry change of the crystal at the transition point. A preliminary result of the heat capacity measurement will also be touched briefly.

The sample was prepared in the wet method in accordance with the prescription by Clark *et al.*[11]. Care was taken to minimize exposure of the material to air when in solution or wet. The crystal was dried in ammonia atmosphere over sodium hydroxide in a desiccator. The chemical analysis for the metal showed the purity to be about 98 per cent. The rather poor value is probably due to the instability of the compound against oxidation. The low temperature DTA apparatus used was described elsewhere[12]. In loading the sample tube with the crystal, care was taken to handle it in ammonia atmosphere, so as to prevent the material from decomposing to the lower amine complexes. Figure 1 reproduces the DTA trace obtained in a heating run, the heating rate being 2 K min^{-1}. The temperature at which the curve departs significantly from the base line is 93 K and the peak temperature 99 K. In the cooling run, which is not shown, a corresponding exothermic peak was observed at the approximately same temperature.

Far i.r. spectrum was taken with a HITACHI FIS-3 spectrometer and a low temperature cell. The sample crystal was mulled in low melting paraffin and spread over a silicon cold window. The temperature was controlled by adjusting the amount of liquid nitrogen introduced into the coolant chamber and was monitored with a copper-constantan thermocouple attached to the center of the silicon disk. The thermocouple was fine enough not to interfere the passage of the i.r. radiation. The spectrum obtained is shown in Fig. 2. In addition to the absorption line given here, two other bands were observed at 190 cm^{-1} and at 110 cm^{-1}. These two were rather broad and at low temperature the former one had unresolved structures. The violet shift on cooling of the 330 cm^{-1} band shown in Fig. 2 and its splitting at the lowest temperature were completely reproducible even after keeping the mulled sample in the low pressure chamber for a day at room temperature: decomposition to the lower ammine complexes seems to take place only slowly, if it does at

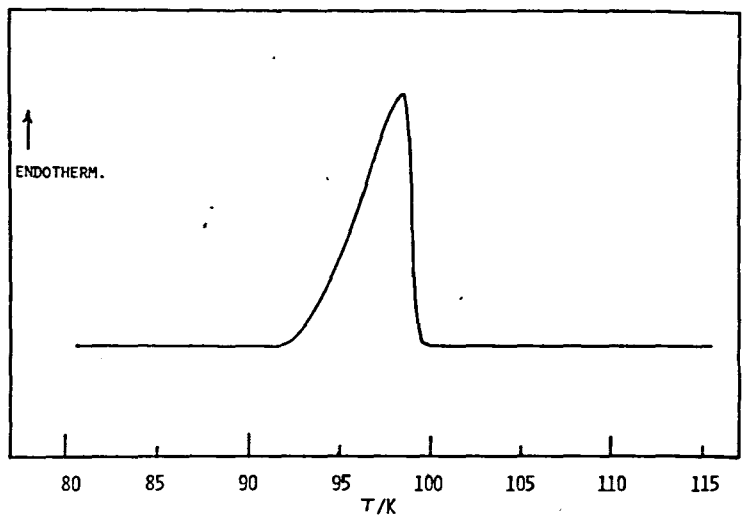

Fig. 1. Differential thermogram of hexammine cobaltous chloride. The heating rate was 2 K min^{-1}.

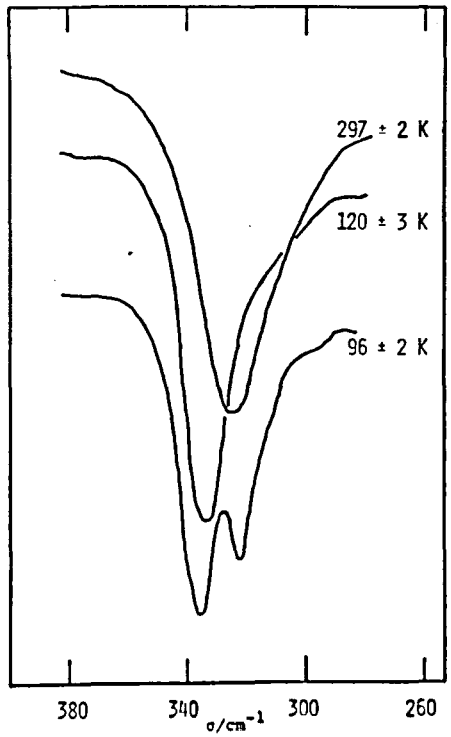

Fig. 2. Far i.r. absorption spectrum of hexammine cobaltous chloride at various temperatures.

all, when the crystal is mulled in paraffin. The splitting of the band occurred suddenly when cooled to 96 K and is not a result of gradual emergence of structure on cooling. One can, therefore, regard it as a characteristic feature of the modification stable below the transition temperature.

Now, if the ammonia molecule is treated as a single entity, the complex ion can be regarded as possessing the O_h symmetry at room temperature[13]. The spectrum of the complex ion has been analysed in accordance with this ionic symmetry[14, 15]. The 330 cm^{-1} absorption was assigned to the mainly metal-ammonia stretching vibration of F_{2u} species. The observed splitting can be explained if the symmetry of the ion is lowered to D_{3d} or D_{4h}. The intensity ratio of the component lines, approximately 1:2, indicates that the triply degenerate level split into a non-degenerate and a doubly-degenerate ones. Still lower symmetries possessing the two-dimensional irreducible representations are compatible with the spectrum, although the D_{3d} symmetry is the most probable one in view of the calculation by Bates[7, 8].

Finally, the heat capacity measurement, which will be reported in a separate publication, showed occurrence of a pronounced peak centered at 97 K. The entropy change was approximately equal to 35 J K^{-1} mol^{-1}, which is almost the same as that observed in the nickel salt[3]. Interpretation of the value will require careful investigation of the molecular interaction in the crystal.

Department of Chemistry, Faculty of Science, Osaka University, Toyonaka, Osaka, Japan

T. MATSUO
M. TATSUMI
H. SUGA
S. SEKI

REFERENCES

1. ELGSAETER A. and SVARE I., *J. Phys. Chem. Solids* **31**, 1405 (1970).
2. KLAAIJSEN F. W., SUGA H. and DOKOUPIL Z., *Physica* **51**, 630 (1971).
3. MATSUO T., SUGA H. and SEKI S., *Bull. Chem. Soc. Japan* **44**, 1171 (1971).
4. PALMA-VITTORELLI M. B., PALMA M. U., DREWES G. and KOERTS W., *Physica* **26**, 922 (1960).
5. AIELLO G., PALMA M. U. and PERSICO F., *Phys. Lett.* **11**, 117 (1964).
6. TRAPP C. and SHYR C-I., *J. chem. Phys.* **54**, 196 (1971).
7. BATES A. R. and STEVENS K. W. H., *J. Phys. C (Solid St. Phys.)* **2**, 1573 (1969).
8. BATES A. R., *J. Phys. C (Solid St. Phys.)* **3**, 1825 (1971).
9. Van KEMPEN H., GAROFANO T., MIEDEMA A. R. and HUISKAMP W. J., *Physica* **31**, 1096 (1965).
10. SUGA H., LAGENDIJK E. and HUISKAMP W. J., *Phys. Lett.* **32A**, 297 (1970).
11. CLARK G. L., QUICK A. J. and HAWKINS W. D., *J. Am. Chem. Soc.* **42**, 2488 (1920).
12. SUGA H., CHIHARA H. and SEKI S., *Nihon Kagaku Zasshi* **82**, 24 (1961).
13. BØDKER-NAESS G. and HASSEL O., *Z. anorg. allgem. Chem.* **211**, 21 (1933).
14. SACCONI L., SABATINI A. and GANS P., *Inorg. Chem.* **3**, 1772 (1964).
15. NAKAGAWA I. and SHIMANOUCHI T., *Spectrochim. Acta* **22**, 1707 (1965).